L2A+

Enhanced Aeolus L2A for depolarizing targets and impact on aerosol research and NWP

-

Requirements Baseline Document
Deliverable Item 01
[DI01]
(Version 1.0)

Submitted to: Christian Retscher (ESA)

	Name	Function	Date
Prepared by:	E. Proestakis	WP1000 – NOA	01/2023
	A. Gkikas	WP3000 – NOA	01/2023
	K. Rizos	WP3000 – NOA	01/2023
	A. Georgiou	WP4000 – NOA	01/2023
	A. Kampouri	WP4000/5000 – NOA	01/2023
	E. Drakaki	WP4000/5000 – NOA	01/2023
	P. Paschou	WP4000/5000 – NOA	01/2023
Approved by:	V. Amiridis	PI	01/2023

-

National Observatory of Athens (NOA)
Institute for Astronomy, Astrophysics, Space Applications & Remote Sensing (IAASARS)
Vas. Pavlou & I. Metaxa, 15236 Penteli, Greece
&
Leibniz Institute for Tropospheric Research (TROPOS), Leipzig, Germany
&
European Centre for Medium-Range Weather Forecasts
[ECMWF]
Reading, United Kingdom

[This page is intentionally left blank.]

Table of Contents

1. ESA-L2A+ DI01 – Overview.

This document consists the Deliverable Item 01 (DI01) – Version 1 (V1) submitted to the European Space Agency (ESA) by the consortium of the project "Enhanced Aeolus L2A for depolarizing targets and impact on aerosol research and NWP" (L2A+). DI01 reports on the activities performed in the framework of the L2A+ Work Package 1 (WP1000) – "Management, reporting and promotion" towards the L2A+ DI01, entitled "Requirements Baseline Document" (RBD), established on the basis of "ASKOS ground-based datasets in support of L2A+" (WP2000), "Development of the L2A+ aerosol product" (WP3000), "Assimilation of L2A/L2A+ and application of WRF-L experiments" (WP4000) and "Impact Studies" (PW5000). More specifically, DI01 aims to consolidate the preliminary scientific requirements for L2A+.

DI01 focuses on the following Sections:
1) Section 1: Provides review of (a) Aeolus L2A products (Flament et al., 2021; Ehlers et al., 2022), (b) AEL-FM and AEL-PRO (i.e., Dave Donovan), (c) CAMS aerosol assimilation techniques to the WRF regional model over L2A+ Region of Interest (RoI).
2) Section 2: Provides a survey of (a) satellite-based and (b) ground-based accessible datasets to be used for the framework of the developments and validation of L2A+ (WP3000/4000) and the evaluation of the model simulations, including the comparisons for the impact assessment of aerosol assimilation in NWP (WP5000). More specifically, this task includes the consolidation of the ESA-ASKOS/JATAC dataset for L2A+ needs, including observations on the (a) provision of pure-dust profiles from ground-based lidar measurements, (b) water-vapour profiles, (c) wind profiles, (d) radiosondes (i.e., launched at Sal Island), (e) airborne dropsonde datasets, and (f) radiation measurements (i.e., Tenerife) to be used for evaluation of the NWP runs and impact studies (WP4000/5000).
3) Section 3: Provides an overview of concluded and ongoing initiatives and projects related to the technical and scientific overarching objectives of L2A+ (i.e., ESA-ASKOS / eVe / NEWTON / DOMOS).
4) Section 4: Provides a consolidated risk analysis pointing out which risk areas could affect the final success of the project and proposed solutions.
5) Section 5: Overview of (a) L2A+ WorkLogic and (b) spatiotemporal focus.

On the basis of this analysis, DI01 – RBD provides a consolidated view of requirements associated with the ESA-L2A+ project. Moreover, DI01 provides technical and scientific overview for the methods and models to be applied. The current document provides the current status and aspects of Aeolus L2A for dust related studies. Based on L2A and these aspects, DI01 justifies the scientific importance of the proposed activities in the framework of the ESA-L2A+ project, to deliver innovative outcomes and to highlight the benefits and the necessity of Aeolus L2A enhancements towards enhancements on dust research.

2. Introduction.

The European Space Agency's (ESA) wind mission, Aeolus, hosts the first space-based Doppler Wind Lidar (DWL) world-wide. Its scientific objectives are to improve Numerical Weather Predictions (NWP) and to advance the understanding of atmospheric dynamics and its interaction with the atmospheric energy and water cycle. Aeolus primary data product consists of profiles of horizontally projected line-of-sight winds from the surface up to about 30 km, and spin-off products are profiles of cloud and aerosol optical properties (e.g., Straume-Lindner et al., 2021). The Aeolus optical properties spin-off product (L2A; Flamentet et al., 2021) has been used to study smoke emissions, e.g., from 2019 Californian wildfires (Baars et al., 2021) and the early 2020 Australian fires, enhancement of volcanic ash forecasting systems and the impact of the Tonga eruption on tropospheric and stratospheric loads (e.g., Kampouri et al., 2021), and has been successfully experimentally assimilated in Copernicus Atmosphere Monitoring Service (CAMS) model C-IFS.

While the L2A product has a reasonable quality (see Baars et al., 2021, GRL, Paschou et al. 2021), its full potential for aerosol and cloud studies and for further improving NWP, has not been exploited. This is mainly because L2A is not provided separately for aerosol and cloud targets. Furthermore, the product is underestimated in terms of backscatter because the instrument measures only the co-polar part of the atmospheric backscattered return of the circularly polarised emitted beam (Paschou et al., 2021; Ehlers et al., 2022). Hence, in the case of strongly depolarizing targets (mainly desert dust particles and ice crystals), the signal measured at the detectors is strongly reduced with respect to non-depolarizing targets. Additionally, the expected atmospheric return signal in orbit is a factor of 2.5 to 3 lower than expected before launch due to lower laser output energies than originally intended (45–72 mJ) and decreased instrument transmission by about 30%, which has caused a lower SNR since mission start (Reitebuch et al., 2020).

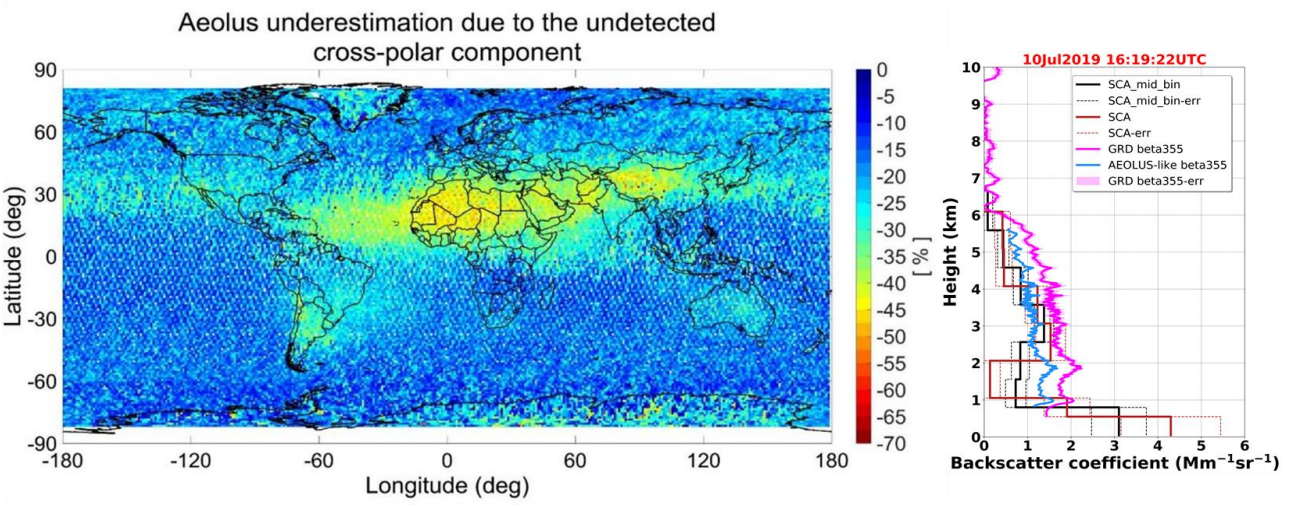

Figure 1: Aeolus underestimation due to the missing cross-polar channel (a:) theoretical calculation; (b) observational evidence.

There is a certain scope for delivering an enhanced L2A product based on a more detailed and robust classification, incorporating other data sources such as multi-sensor synergies or CAMS data. Furthermore, the potential of the extinction product should be further exploited as a constraint for the backscatter product for depolarizing targets, since the extinction is not affected by the missing cross-channel.

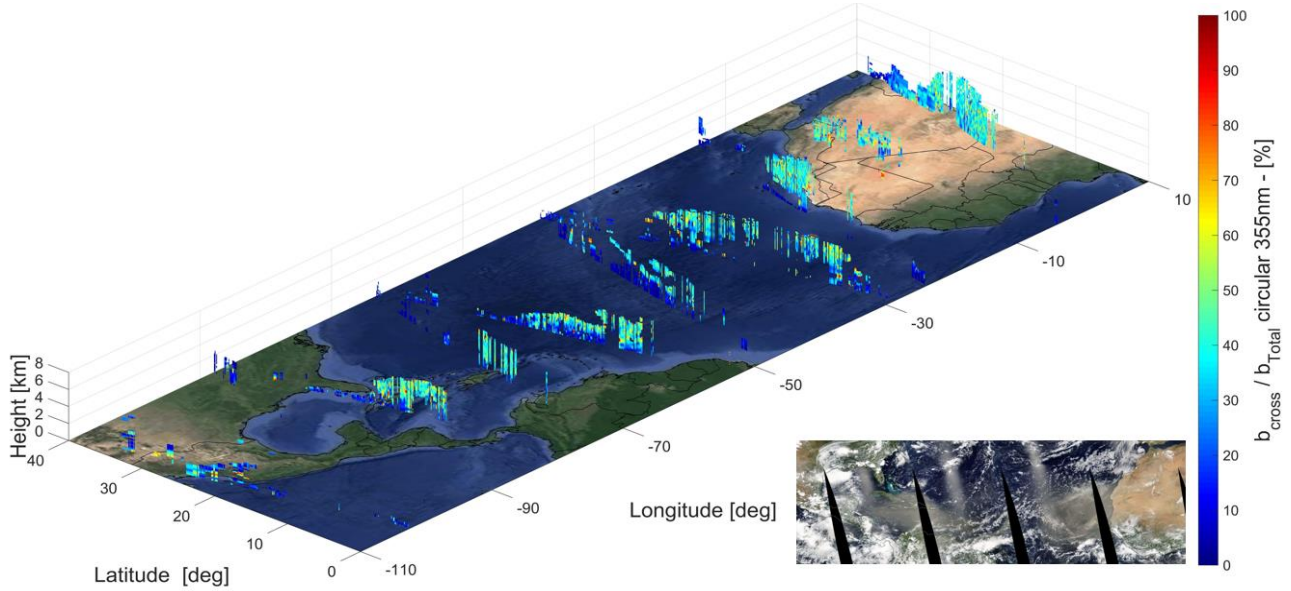

Figure 02: Estimates of Aeolus L2A underestimation due to the missing cross-channel using the Aeolus-like profiles retrieved based on CALIPSO for the trans-Atlantic Godzilla dust event on the 23rd of June, 2020.

ESA-L2A+ overarching objective includes the development of a refined Aeolus L2A aerosol product (L2A+), and accordingly test its applications for enhancing aerosol research, contributing to existing climate datasets. Furthermore, L2A+ aims at assessing the impact of the new product on aerosol assimilation towards improved dust transport modelling and for further enhancing NWP.
The following L2A+ individual objectives are identified:

1) Objective 1: To develop a refined Aeolus aerosol optical product (L2A+), based on AEL-FM/AEL-PRO algorithms, geostationary AOD products, CAMS, and new AOD retrievals from the Aeolus itself (WP3000). The product will be thoroughly compared with L2A and validated against quality-assured measurements from the ESA-ASKOS/JATAC experiment in Cabo Verde (WP2000).
2) Objective 2: To examine the impact of L2A and L2A+ on aerosol assimilation and dust transport models (WP4000). Constraining aerosol loads through Aeolus assimilation is expected to improve dust emission fluxes over the Sahara Desert and transport simulations of the full particle size range (from fine to giant dust particles).
3) Objective 3: To assess the impact of Aeolus on NWP, utilising L2A+ aerosol assimilation in an online coupled regional model driven by Aeolus wind-assimilated meteorological fields (WP5100).
4) Objective 4: To highlight the benefit of the Aeolus joint aerosol and wind assimilation for simulating dust deposition fields, and compare with CAMS reanalysis to assess the impact of L2A+ for ocean biogeochemistry studies (i.e., ESA-DOMOS study) (WP5200).
5) Objective 5: To compare the monthly averaged L2A+ product with the CALIPSO L3 product, to assess the climatological value of L2A+ for aerosol database of the ESA-LIVAS long-term climate dataset (WP5300).

On the basis of L2A+, DI01 – RBD provides a consolidated view of the requirements associated with the ESA-L2A+ overarching Objectives (1)-(5).

3. The L2A+ basis.

This DI01 Section provides an overview of the basis in terms of product of the ESA-L2A+ project, including (a) the Aeolus-ALADIN L2A products (Flament et al., 2021; Ehlers et al., 2022) and (b) the AEL-FM and AEL-PRO products (Dave Donovan).

3.1. Aeolus-ALADIN and L2A.

Since soon after its launch on 22 August 2018, the Aeolus mission (Stoffelen et al., 2005) is providing global coverage of horizontal projected Line-of-Sight (HLOS) wind and aerosol profiles. Aeolus, ESA's Doppler Wind Lidar (DWL) space mission, is designed to provide global profiles of the Horizontal Line-of-Sight (HLOS) wind component in the troposphere and the lower stratosphere (Dabas et al., 2010). This is made possible by the use of ALADIN (Reitebuch et al., 2009), a sophisticated DWL operating in the ultraviolet region of the spectrum (355 nm), implemented in a transceiver configuration and tilted 35° from nadir (Lolli et al., 2013).

Comprising a powerful laser, a large telescope and a very sensitive receiver, ALADIN is the first wind lidar in space. The laser system emits short powerful pulses of ultraviolet light down into the atmosphere. The telescope collects the light that is backscattered from air molecules, aerosols and clouds. The receiver analyses the Doppler shift of the backscattered signal to determine the wind speed at various altitudes below the satellite. Direct small-scale wind observations are well distributed over the globe in the present global observing system and this limits the ability to predict weather as well as the ability to understand fundamental processes that govern climate change.

Since ALADIN is also an HSRL (High Spectral Resolution Lidar; Shipley et al., 1983; Imaki et al., 2005), it is capable of deriving not only the HLOS wind component (Tan et al., 2008) but also aerosol and cloud optical parameters (Ansmann et al., 2007; Flamant et al., 2008) along the satellite's orbital path. Aeolus measurements enhance our current knowledge on aerosol and cloud by globally providing optical properties that include atmospheric backscatter and extinction coefficient profiles, lidar ratio profiles and scene classification.

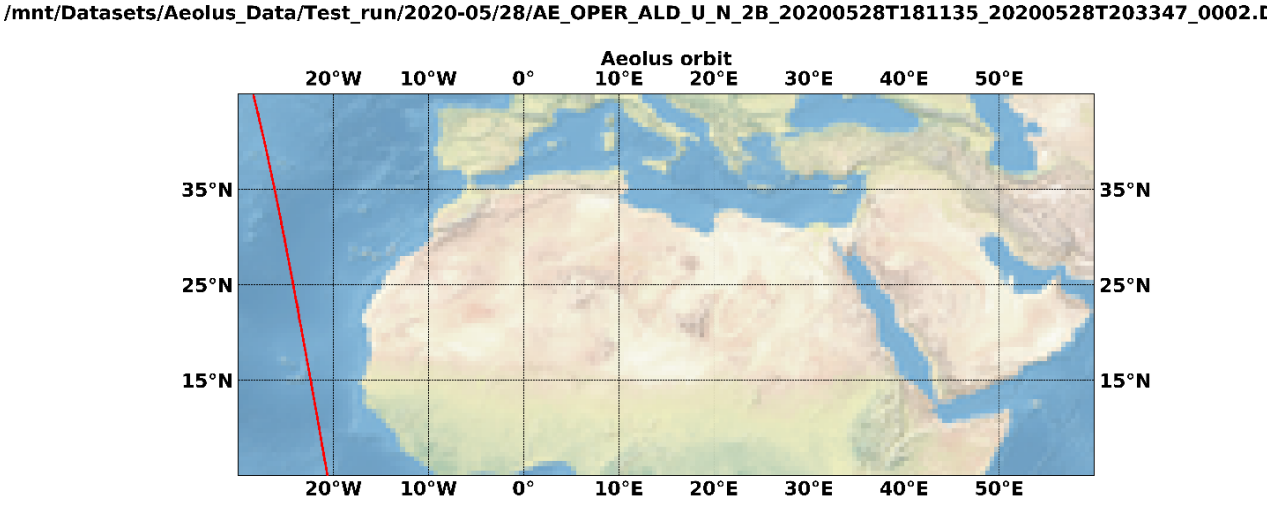

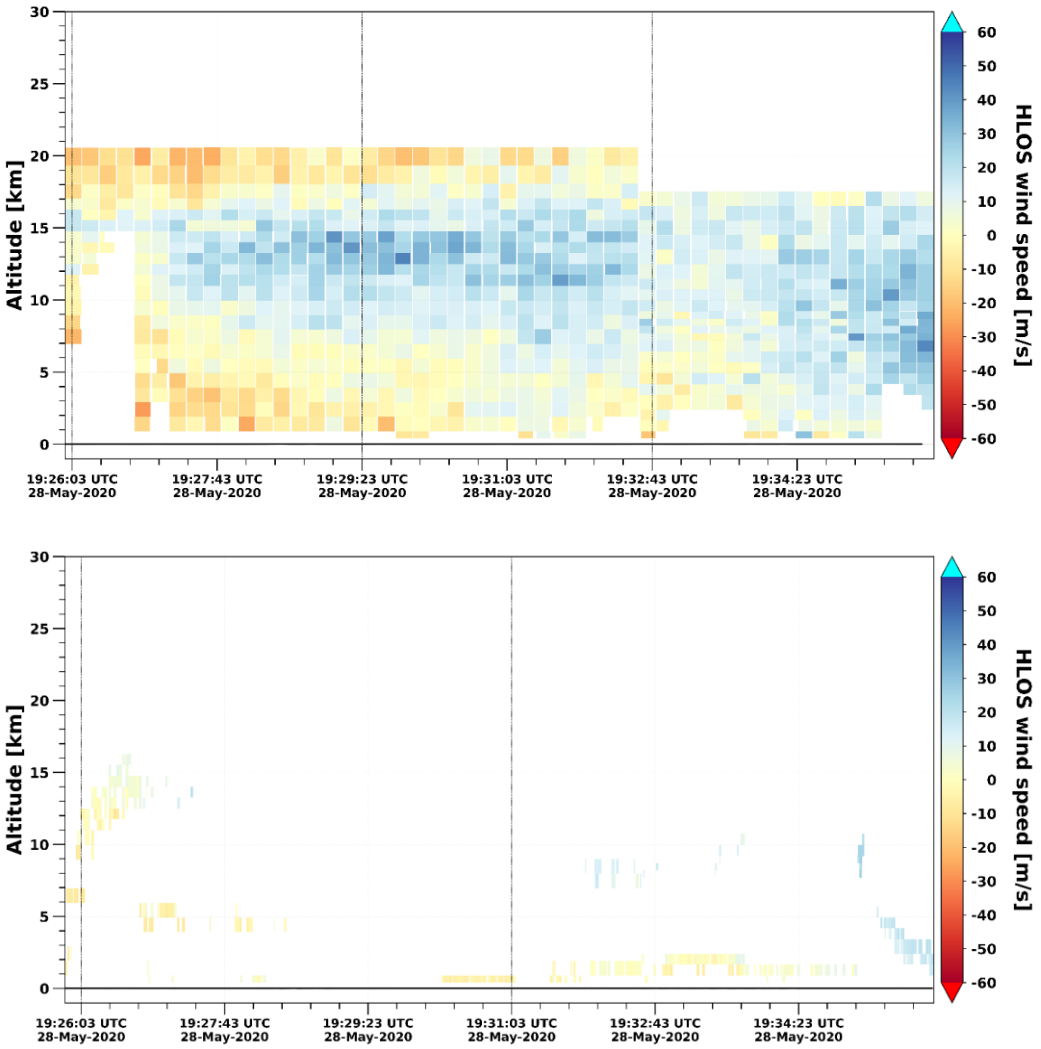

Figure 03: Aeolus Orbit (a), Rayleigh (b), and Mie (c) profiles at 355 nm on May 28th, 2020 on the ASKOS domain.

3.2. AEL-FM and AEL-PRO.

In the framework of the L2A+ project, the AEL-FM and AEL-PRO (Presentation of Dave Donovan) products for September 2021 period of the ESA-ASKOS/JATAC campaign will be produced within the DISC activities and will be delivered for the needs of the L2A+ study (personal communication with Dave Donovan). The AEL-FM (the Aeolus Feature Mask) detects "features" and classifies them as clouds or aerosols (associating strong features with clouds and weak features with aerosols). Accordingly, AEL-PRO retrieves profiles at 355nm of (1) backscatter coefficient, (2) extinction coefficient, and (3) lidar ratio. Through utilizing the (1) lidar ratio, (2) the scattering ratio, (3) the temperature, and (4) AEL-FM, AEL-PRO delivers a basic classification (water cloud, ice cloud or aerosol), along Aeolus orbit track.

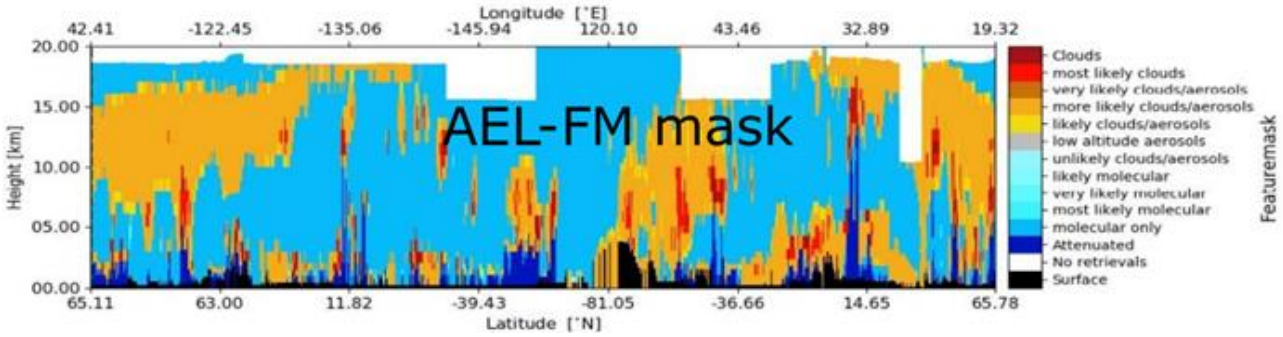

Figure 04: Example curtain profile of the AEL-FM mask.

4. L2A+ Accessible Datasets of Interest.

This DI01 Section provides a survey of (a) satellite-based and (b) ground-based accessible datasets – towards EO of airborne dust – to be used for the framework of the developments and validation of L2A+ (WP3000/4000) and the evaluation of the model simulations, including the comparisons for the impact assessment of aerosol assimilation in NWP (WP5000). More specifically, this task includes the consolidation of the ESA-ASKOS/JATAC dataset for L2A+ needs, including observations on the (a) provision of pure-dust profiles from ground-based lidar measurements, (b) water-vapour profiles, (c) wind profiles, (d) radiosondes (i.e., launched at Sal Island), (e) airborne dropsonde datasets, and (f) radiation measurements (i.e., Tenerife) to be used for evaluation of the NWP runs and impact studies (WP4000/5000).

4.1. Satellite-based EO of Dust.

Aerosol data from space have been acquired by several platforms through the last three decades, advancing our knowledge about suspended particles' spatiotemporal patterns at a global scale substantially. The majority of these observations relies on the implementation of passive remote sensing techniques applied on historical sensors such as AVHRR and modern spectro-radiometers such as SeaWIFS or MODIS and their continuation VIIRS, thus ensuring reliable long-term records which are of high importance for climate studies. Passive instruments provide spectral information about aerosol optical depth (AOD), at wavelengths spanning from UV to NIR, representative for the whole atmospheric column. Most of these observations are performed from single-view instruments flying onboard polar orbit satellites. In contrast, for dust particles' characterization, it is necessary the consideration of additional optical properties related to aerosols' size and nature. Apart from single view satellite sensors, optical properties can also be acquired from multi-view instruments, such as MISR (Multi-angle Imaging SpectroRadiometer) and ATSR (Along Track Scanning Radiometers), providing angular measurements, which can be utilized for the identification of non-spherical dust particles.

Dust AOD can be obtained from spaceborne UV-VIS-NIR aerosol observations, considering all the related assumptions on size and origin parameters. Nevertheless, it can be obtained directly by exploiting vibrational resonance peaks of silicates in the thermal infrared (Ackerman et al., 1997) (e.g., Infrared Atmospheric Sounding Interferometer - IASI). Most of the passive instruments are placed on Low Earth Orbiting (LEO) satellites thus providing aerosol observations at low sampling frequency due to sensors and orbital geometries. This observational gap has been complemented by radiometers on geostationary satellites (Meteosat Second Generation/Spanning Enhanced Visible Infrared Imager - MSG/SEVIRI, Geostationary Operational Environmental Satellite - GOES, Himawari, Geostationary Ocean Color Imager - GOCI; e.g., Luffarelli and Govaerts, 2019). Based on

these observations at thermal wavelengths, it has been achieved the monitoring and tracking of dust plumes at fine temporal resolution.

A major drawback of spaceborne passive columnar retrievals is their inability to describe dust layers' vertical structure that is critical for assessing the associated impacts on radiation and several atmospheric processes. CALIOP (Cloud-Aerosol Lidar with Orthogonal Polarization), onboard the Cloud-Aerosol Lidar and Infrared Pathfinder Satellite Observation (CALIPSO) satellite, provides vertically resolved aerosol information since June 2006 (Winker et al., 2010). CALIOP measures aerosol backscatter profiles at 532 and 1064 nm, including parallel and perpendicular components at 532 nm, at high horizontal and vertical resolution. At the next step of data processing, it is derived the linear particle depolarization ratio at 532 nm, an excellent indicator of dust presence attributed to the non-spherical shape of mineral particles, enabling dust detection by CALIOP at high accuracy (Burton et al., 2013). Similar vertical profiles, but at 1064 nm, are available over the period Feb 2015 – Oct 2017 from the Cloud-Aerosol Transport System (CATS; Yorks et al., 2014) installed at the International Space Station (ISS). Since August 2018, the ADM-AEOLUS satellite, operated by the European Space Agency (ESA), is carrying the first UV Doppler lidar in space (Flamant et al., 2008). ALADIN is a High Spectral Resolution Lidar (HSRL) with no depolarization capabilities.

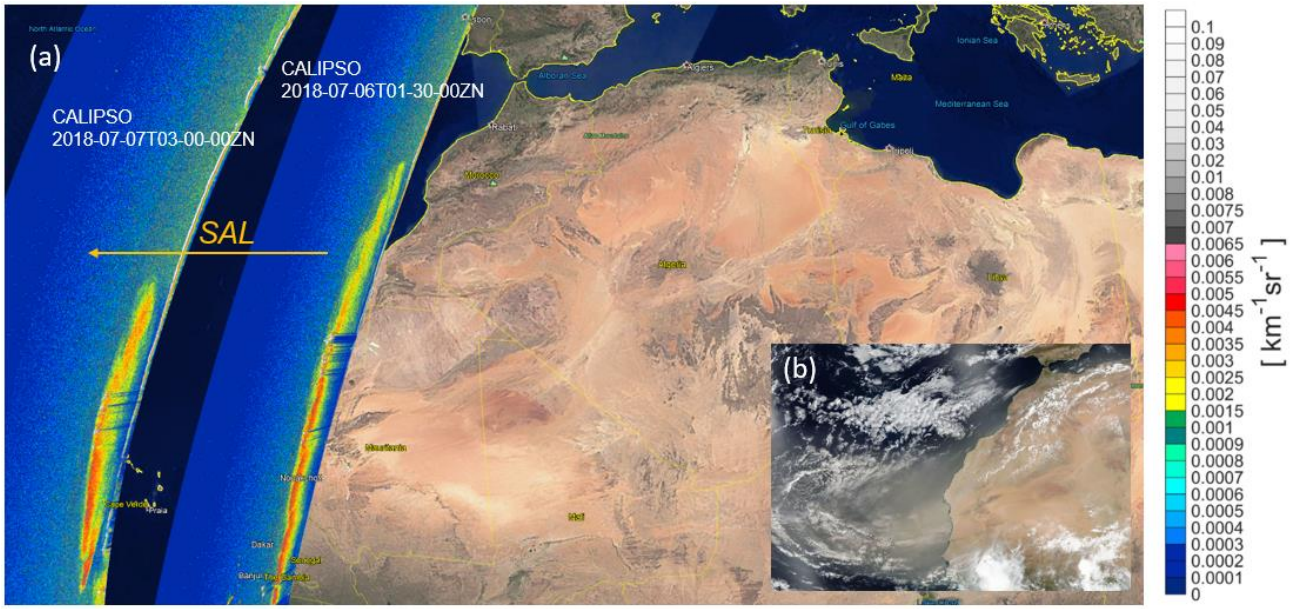

Figure 05. Example of a Saharan dust transport event along the Atlantic Ocean, as captured by (a) CALIPSO CALIOP on 20180706 and 20180707 and (b) Aqua and Terra MODIS on 20180706.

The following ESA-L2A+ DI01 sub-sections provide an overview of satellite-based Earth Observation datasets to be implemented in the framework of the developments and validation activities of L2A+ (WP3000/4000) and the evaluation of the model simulations, including the comparisons for the impact assessment of aerosol assimilation in NWP and L2A+ impact studies (WP5000).

4.1.1. CALIPSO and the LIVAS pure-dust product.

4.1.1.1. CALIPSO and CALIOP.

The Cloud-Aerosol Lidar and Infrared Pathfinder Satellite Observation (CALIPSO) mission (Winker et al., 2010) is a joint satellite project, developed, operating and maintained in close and ongoing collaboration between the National Aeronautics and Space Administration (NASA), the United States space agency, and the Centre National D'Études Spatiales (CNES), the French space agency. The satellite CALIPSO was launched on April 28th, 2006, to be integrated in the Afternoon-Train (A-Train) constellation of sun-synchronous polar-orbit satellites (Stephens et al., 2018), hosting a suite of three Earth-observing instruments, in a near-nadir-looking configuration: a single channel 645 wide field-of-view camera (WFC), a three channel (8.65, 10.6, 12.05 μm) Imaging Infrared Radiometer (IIR; Garnier et al., 2017), and the principal payload, the Cloud-Aerosol Lidar with Orthogonal Polarization (CALIOP) lidar (Hunt et al., 2009). The primal instrument, CALIOP, is a dual-wavelength polarization-sensitive elastic backscatter Nd:YAG lidar, that transmits linear polarized light pulses at 532 and 1064 nm, and accordingly, makes separate range-resolved measurements of the backscattered signals by atmospheric features, and specifically, of the parallel and perpendicular components of the backscattered photons at 532 nm with respect to the polarization plane of CALIOP emitted beam, and the total backscatter intensity at 1064 nm (Winker et al., 2009).

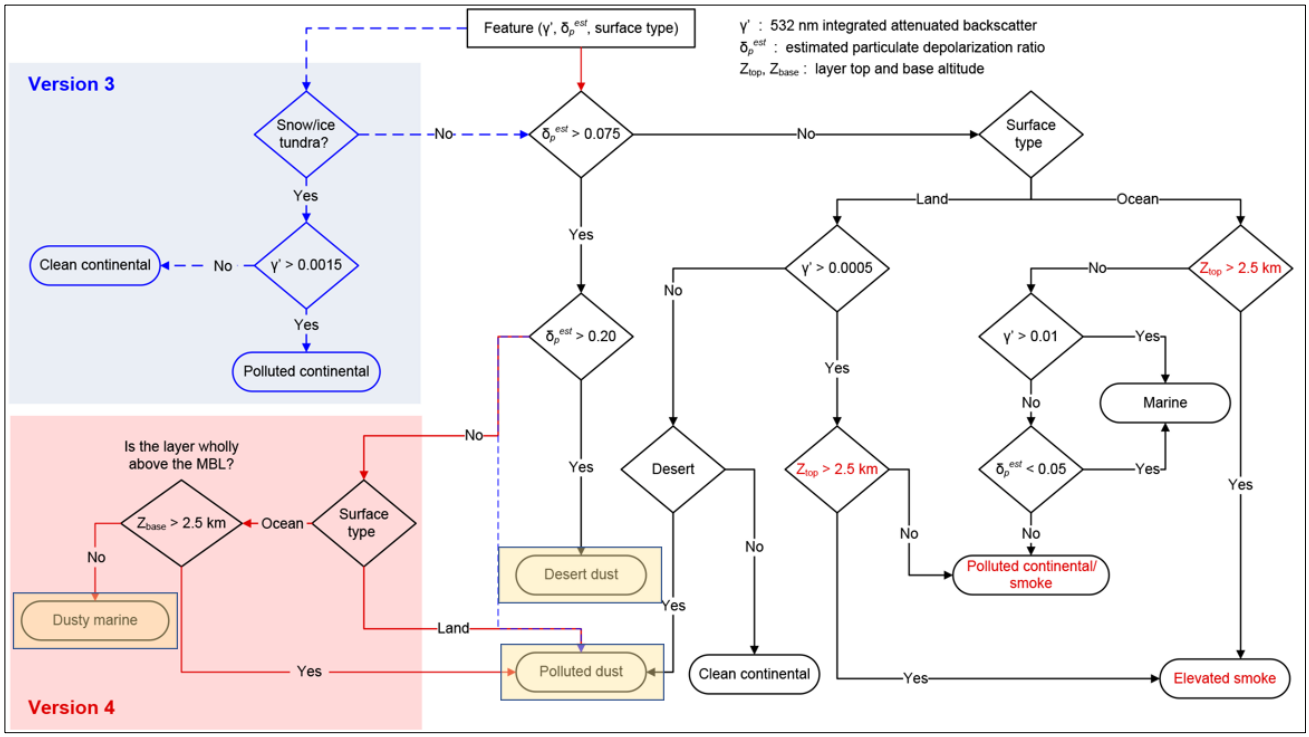

Figure 06: Flowchart of the CALIPSO aerosol subtype selection scheme for tropospheric aerosols (source: Kim et al., 2018). The shaded regions are used in the L2A+ project, towards the extraction of the "Pure-Dust" and the "non-Dust" atmospheric aerosol components (Section "Pure-Dust").

CALIOP measurements and products are provided in different levels of processing. The received measurements of attenuated backscatter from molecules and particles are provided in 1/3 km horizontal and 30 m vertical resolution and reported in CALIOP Level 1 data products. Subsequently, CALIOP Level 1 measurements are processed to CALIOP Level 2 products, following a sophisticated chain of algorithms (Winker et al., 2009) that perform a sequence of functions, including the

fundamental for the retrievals daytime and nighttime calibration of the three receiver channels (Powell et al., 2009; Kar et al., 2018; Vaughan et al., 2019), layer detection (Vaughan et al., 2009) and cloud-aerosol discrimination (Liu et al., 2009; Liu et al., 2019; Zeng et al., 2019). In addition, in the process to retrieve particulate extinction profiles (Young and Vaughan, 2009), an intermediate aerosol classification and Lidar Ratio (LR) selection algorithm for feature detection classifies atmospheric features between "clear-air", "tropospheric aerosol", "stratospheric aerosol", "cloud", "surface", "subsurface", "totally attenuated", and aerosol and cloud features of "low/no confidence". The algorithm modules further classify atmospheric features categorized as "tropospheric aerosol" between "marine", "dust", "polluted continental/smoke", "clean continental", "polluted dust", "elevated smoke" and "dusty marine" (Omar et al., 2009; Kim et al., 2018), and in the case of "stratospheric aerosol" between "PSC aerosol", "volcanic ash", and "sulfate/other" (Kar et al., 2019) – (Fig 06).

CALIOP Level 2 profiles of aerosol (APro) and cloud (CPro) provide continuous, vertically resolved measurements of optical and geometrical properties of atmospheric features, detected in the columns along the CALIPSO orbit path on a global scale since June 2006, at uniform 5 km horizontal and 60 m vertical resolution over a nominal altitude range from −0.5 to 20.2 km, and 180 m from 20.2 to 30 km height a.m.s.l. In the framework of L2A+ project we use CALIPSO Version 4.2 (V4.2) Level 2 profiles of altitude-resolved aerosol backscatter coefficient and particulate depolarization ratio at 532 nm, profile descriptors (e.g., longitude, latitude, time), the provided quality-assurance flags (e.g. CAD score), and the assigned atmospheric classification products, between September 1st and September 2021, to establish the L2A+ optical products (355 nm - w/wo cross-channel – linear/circular emitting configurations). Fig.07 provides the Feature Type and the Aerosol Subtype classifications for the CALIPSO orbit "2020-09-25T03-28-13ZN".

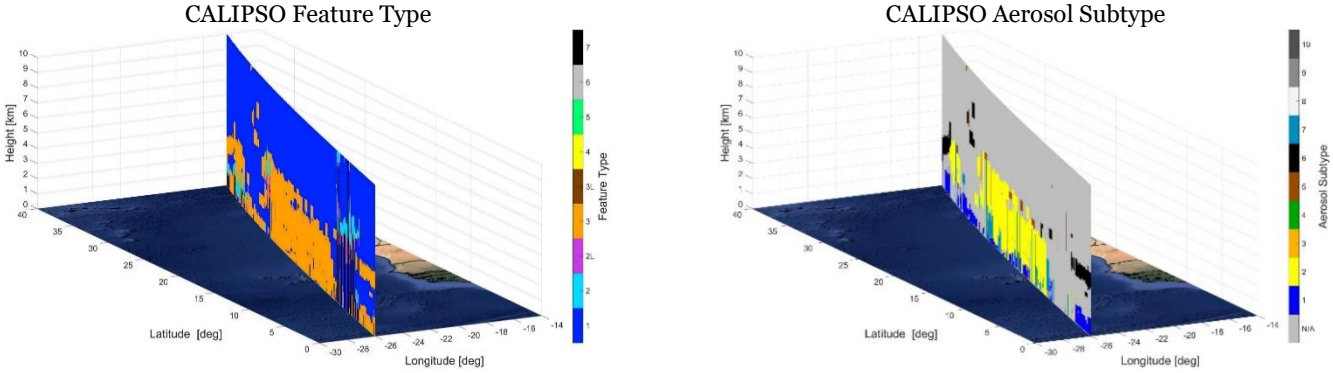

Figure 07: Feature Type (left) and Aerosol Subtype (right) classification of detected atmospheric layers for the CALIPSO orbit "2020-09-25T03-28-13ZN".

4.1.1.2. Quality Assurance procedures.

Quality screening procedures used to generate the quality-assured CALIPSO-based Lever 2 and Level 3 pure-marine aerosol product follow the quality control procedures used to generate the official CALIPSO Level 3 aerosol product (Tackett et al., 2018) and subsequent developments (Campbell et al., 2012; Amiridis et al., 2013; Toth et al., 2013; Marinou et al., 2017). The QA approach is conservative, weighting the removal of a significant number of erroneous features and retrievals, against preserving the dataset, to avoid inconsistencies, weighting effects and unrealistic shape of profiles. In this concept, the most aggressive quality control check is considered the cloud-free condition, applied in an entire profile-removal approach when cloud features are detected at CALIPSO Profile level at 5 km or greater horizontal resolution, resulting in minimizing detection, classification, retrieval errors, and avoiding attenuation and weighting effects (Tackett et al., 2018).

Accordingly, the sequence of conservative quality assurance filters iterates through all CALIPOS Level 2 cloud-free profiles, with aerosol features either accepted or excluded as inputs to the generation algorithm of the fine and coarse pure dust product.

In this process of quality screening controls, backscatter coefficient of atmospheric features classified a "clear-air" are assumed equal to 0.0 km-1sr-1, with the exception of "clear-air" samples adjacent to aerosol layers with surface base below 250 m a.g.l., which are considered as "not-detected" and ignored. Similarly, regarding aerosol layers that as a result of low Signal-to-Noise Ratio (SNR) are detected at 80 km horizontal averaging resolution, and are not in contact with other quality-assured (QA) aerosol layers, are considered noise artifacts and rejected. In terms of clouds misclassified as aerosol, and vice versa, aerosol features of CAD score in the range [-100, -20] are accepted, rejecting layers of CAD score outside this range due to the high probability of feature erroneous classification. In addition, aerosol layers above 4 km a.m.s.l., adjacent to ice clouds of Top Temperature below 0 ^{o}C are also rejected as cirrus fringes misclassified as aerosols. The series of QA procedures includes in addition rejection of the backscatter coefficient at 532 nm in cases of low quality in the retrieval of the corresponding extinction coefficient at 532 nm profiles. L2 aerosol features of extinction QC flags not equal to 0 (Lidar Ratio unchanged), 1 (Lidar Ratio measured), 16 (layer is opaque and the Lidar Ratio value unchanged), or 18 (layer is opaque and the Lidar Ratio value is reduced) are rejected, while in terms of random and systematic errors, aerosols feature of extinction uncertainty less of equal to 99.99 km-1 are also rejected. Finally, the sequence of backscatter coefficient at 532 nm QA controls accounts for large signal anomalies in cases of surface-attached aerosol layers, reporting either significant negative (less than -0.2 km-1) or large positive (higher than 2.0 km-1) extinction coefficient at 532 nm values, within 60 m a.g.l., features that are removed.

Table 01: Quality Assurance procedures applied to CALIPSO-CALIOP L2 APro and CPro optical products in the framework of the L2A+ project.

	Quality Assurance procedures
1	Screen out all cloud features.
2	Aerosol extinction coefficient for "clear air" assigned equal 0.0 km^{-1}.
3	Screen out atmospheric features of CAD score outside the range [-100, -20].
4	Screen out atmospheric features of Extinction QC flag ≠ 0, 1, 16 and 18.
5	Screen out atmospheric features of aerosol extinction uncertainty ≤ 99.9 km^{-1}.
6	Screen out misclassified cirrus fringes.
7	Screen out isolated aerosol features of horizontal resolution 80 km.
8	Features of large negative extinction coefficient values ≤ -0.2 km^{-1}, detected ≤ 60 m a.g.l., are removed.
9	Features of large positive extinction coefficient values ≥ 2.0 km^{-1}, detected ≤ 60 m a.g.l., are removed.
10	Screen out assigned "clear-air" atmospheric features below aerosol layers of base ≤ 240 m a.g.l.
11	"Clear-Sky" Mode

Overall, the quality filtering methods and control procedures are applied to counteract and reduce the impact of noise and clouds misclassified as aerosols, systematic and random errors and artifacts, and retrieval issues, while at the same time affecting CALIPSO aerosol profiles by the smallest amount possible, and maintaining a high-quality extended dataset, suitable for study cases and longer-scale studies – provided in Table 01. The effect of the QA procedures is demonstrated in Fig.08, for the CALIPSO orbit "2020-09-25T03-28-13ZN" case.

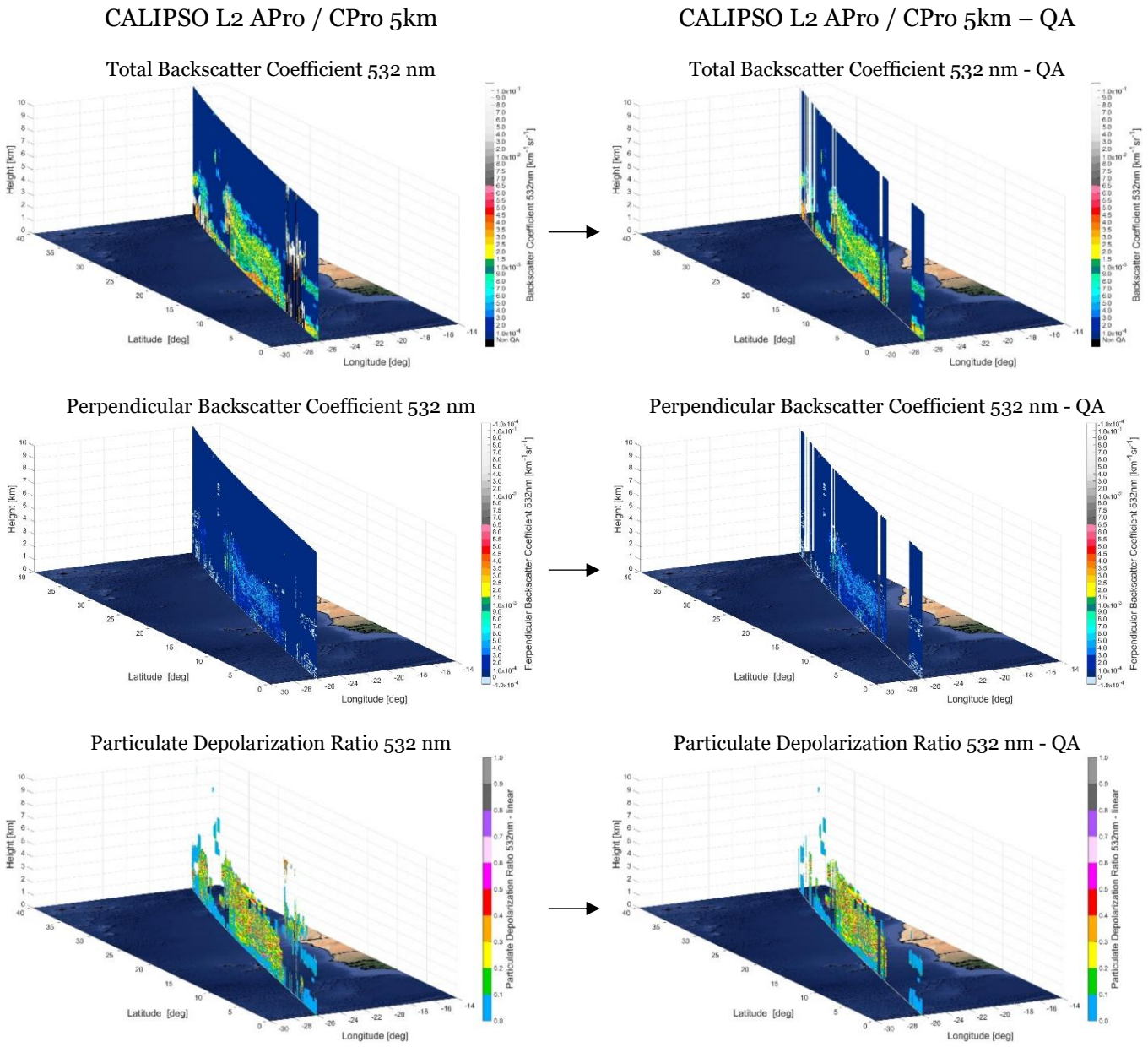

Figure 08: CALIOP L2 APro / CPro 5km raw (left column) and QA (right column) of total aerosol backscatter coefficient, perpendicular backscatter coefficient and particulate depolarization ratio at 532nm for the CALIPSO orbit "2020-09-25T03-28-13ZN".

4.1.1.1. The LIVAS Pure-Dust product.

The CALIPSO-based "Pure-Dust" and "non-Dust" optical products, corresponds to the QA atmospheric features classified as "Dust", "Dusty Marine", or "Polluted Dust" aerosol subtypes. The decoupling methodology of the "Pure-Dust" component follows the series of the well-established POLIPHON algorithms, and specifically the one-step POLIPHON (Tesche et al., 2009) for decoupling the pure-dust component from the total aerosol load. The retrieval schemes are straightforward and applicable to single-wavelength lidar observations, as long as linear-polarization height profiles are included (Mamouri and Ansmann, 2016). The proposed algorithm is applied to CALIPSO backscatter coefficient profiles at 532 nm to provide a three-dimensional global database of "Pure-Dust" and "non-Dust" aerosol observations.

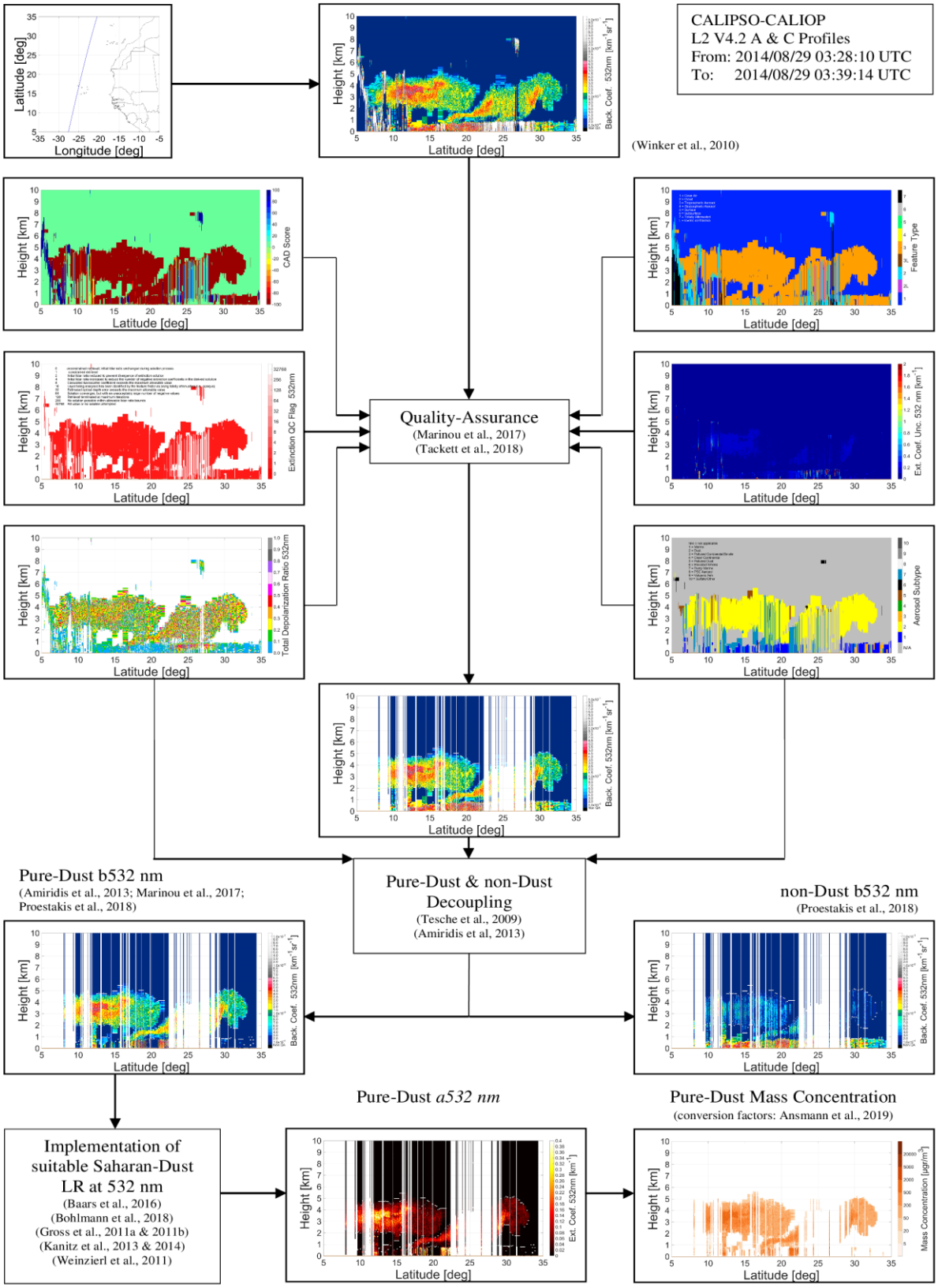

Figure 09. Flowchart of the methodology followed for the derivation of the CALIPSO-based pure-dust mass concentration.

The proposed algorithm (Fig. 09) decouples an external aerosol mixture of particles with different and distinct depolarizing properties, as proposed and developed in the framework of the European Aerosol Research Lidar Network (EARLINET; www.earlinet.org/; last visit: 03/01/2023; Pappalardo et al. 2014) and thoroughly discussed in Tesche et al., (2009). The approach is based on the distinct property of mineral airborne dust to decouple the polarization state of CALIOP linear polarized light. For dust, and the case of "δ_d", typical particle depolarization ratios of lofted dust-dominated aerosol layers, measured in the framework of field activities conducted in the proximity of the Saharan (Freudenthaler et al., 2009; Ansmann et al. 2011), Middle East (Mamouri et al., 2013; Filioglou et al., 2020), and Asian (Hofer et al., 2017) dust sources, show similar values in the range from 30% to 35%. These findings are in accordance with lidar measurements of particle depolarization ratio of airborne dust, studied during mid-range and long-range transport across Europe (Wiegner et al., 2011; Baars et al., 2016), North Atlantic Ocean (Gross et al., 2011; Gross et al., 2015; Tesche et al., 2011), and over the Pacific Ocean (Sakai et al., 2003). Therefore, the assumption that desert dust is characterized by particle depolarization ratio around 0.31 ± 0.4 at 532 nm is made, a characteristic (universal) property both close to sources of dust emission and after long-range transport. To date, the one-step POLIPHON technique has been applied towards a global pure-dust product, in the framework of the ESA - LIdar climatology of Vertical Aerosol Structure for space-based lidar simulation studies activity (LIVAS; Amiridis et al., 2015).

The “Pure-Dust” and “non-Dust” Products

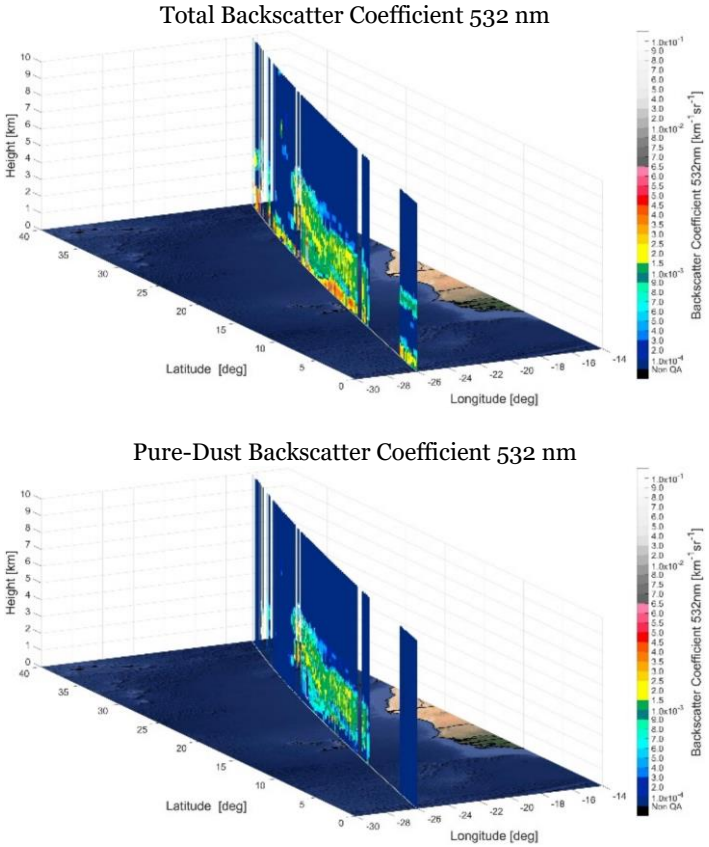

Figure 10: The CALIPSO total backscatter coefficient at 532 nm (upper panel), and the CALIPSO-based pure-dust product in terms backscatter coefficient at 532 nm (lower panel), for CALIPSO orbit “2020-09-25T03-28-13ZN”.

CALIOP need for a-priori information on aerosol subtype in order to retrieve extinction coefficient profiles from backscatter coefficient profiles. Therefore, considerations of a Lidar Ratio (LR) suitable for Saharan dust and for the domain of Western / Central Sahara Desert /North Atlantic Ocean is crucial for L2A+, for the Pure-Dust Optical Depth (DOD 532 nm) is the vertical integration of the pure-dust extinction coefficient at 532 nm. With respect to the pure-dust LR To improve the understanding of the optical, chemical and microphysical properties of Saharan dust, two large-scale field campaigns were conducted in the framework of the SAharan Mineral dUst ExperiMent (SAMUM) activity (Ansmann et al., 2011). The first stage of the campaign, SAMUM-1, conducted during May and June 2006 at Ouarzazate (Morocco), close to the dust source regions, with main science objective the characterization of pure and non-aged Saharan dust (Esselborn et al., 2009; Heintzenberg, 2009). The second stage of the campaign, SAMUM-2, fielded during January and February 2008 at the island of Santiago (Cape-Verde) in the North Atlantic Ocean, in the proximity of the Sahara Desert, to study and characterize possible changes in the optical, chemical and microphysical properties of aged dust, after a transport time of a few days (Gross et al., 2011). A brief synopsis of SAMUM key findings on dust intensive properties with respect to dust extinction-to-backscatter ratio at 532 nm, measured with airborne HSRL and ground-based Raman and polarization lidar systems, include Saharan dust lidar ratio values of 56 ± 5 sr (Tesche et al., 2009) for SAMUM-1, and HSRL 63 ± 6 sr (Gross et al., 2011a; 2011b), ground-based Raman 53–54 ± 10 sr (Tesche et al., 2011) for SAMUM-2.

Overall, these lidar ratio values of fresh and aged Saharan dust are in good agreement to lidar ratios measured after long-range transport over the North Atlantic Ocean (Weinzierl et al., 2016) and Europe (Marinou et al., 2017). During the last years several shipborne continuous multi-wavelength Raman and polarization lidar observations have been conducted, aboard the research vessels Polarstern and Meteor, on meridional expeditions across the Atlantic Ocean from north to south (Kanitz et al., 2013; Bolhmann et al., 2018), and zonal cruises along the main transport route of Saharan dust from western and central Africa to the Caribbean (Kanitz et al., 2014; Rittmeister et al., 2017), and vice versa, to optically characterize the Saharan Air Layer (SAL) over the Atlantic Ocean. Extinction-to-backscatter ratio measurements in the center of lofted air masses originated from the Saharan desert, reported pure dust lidar ratio values of 53 ± 2 sr (Bolhmann et al., 2018), 50–60 sr (Kanitz et al., 2013), and 55 ± 5 sr (Kanitz et al., 2014), values in good agreement with SAMUM observations. In good agreement with the shipborne and SAMUM-campaign observations are in addition the respective findings of advanced lidar measurements, conducted in the broader Caribbean region in Barbados regime and the respective performed in the framework of the SALTRACE activity (Weinzierl et al., 2016), where mean Saharan dust lidar ratios of 50–60 sr (Haaring et al., 2017) and 56 ± 7 sr (Gross et al., 2015) at 532 nm, are reported.

Table 02: Pure-Dust LR at 532 nm for the L2A+ domain.

Region	Recommended dust Lidar Ratio at 532 nm [sr]	Indicative references of dust Lidar Ratio at 532 nm [sr]
Western / Central Sahara Desert North Atlantic Ocean	56 ± 8	Tesche et al., 2009; Gross et al., 2011a; Gross et al., 2011b; Tesche et al., 2011; Kanitz et al., 2013; Kanitz et al., 2014; Gross et al., 2015; Weinzierl et al., 2016; Haaring et al., 2017; Rittmeister et al., 2017; Bolhmann et al., 2018

(a) Total Backscatter Coefficient 532 nm (JJA 2006-2020).

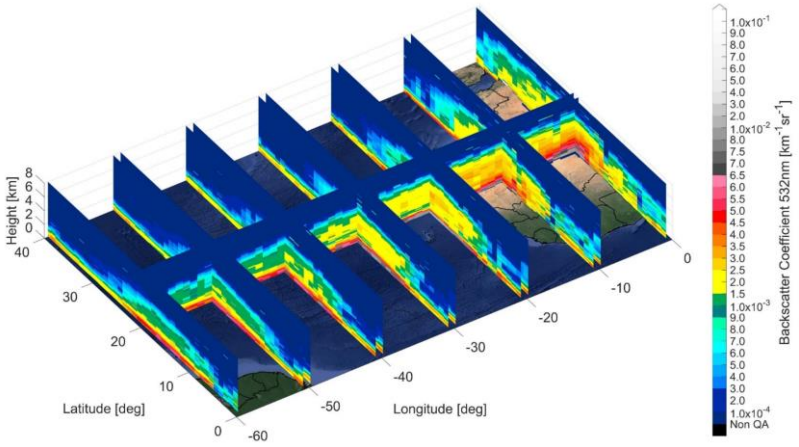

(b) Pure-Dust Backscatter Coefficient 532 nm (JJA 2006-2020).

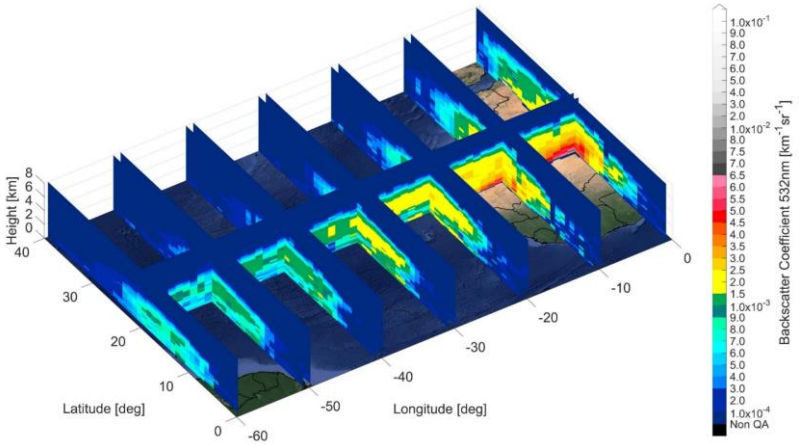

(c) Pure-Dust Extinction Coefficient 532 nm (JJA 2006-2020).

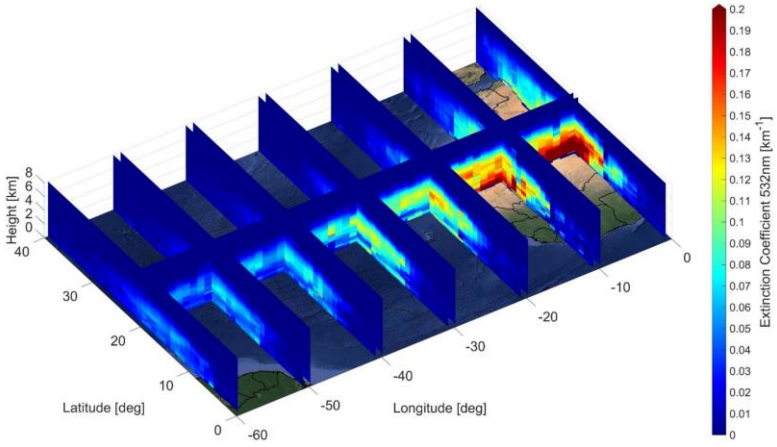

Figure 11: The (a) Total Backscatter Coefficient 532 nm, (b) Pure-Dust Backscatter Coefficient 532 nm, and (c) Pure-Dust Extinction Coefficient 532 nm (JJA 2006-2020).

4.1.2. MODIS and MIDAS.

4.1.2.1. MODIS.

The MODerate resolution Imaging Spectroradiometer (MODIS) is a passive sensor measuring the top of atmosphere (TOA) reflectances in order to retrieve Aerosol Optical Depth (AOD), among other aerosol optical properties, at various wavelengths spanning from the visible to the near-infrared spectrum range. MODIS, mounted on the NASA's twin polar satellites of Terra and Aqua, has acquired high-quality aerosol data since 2000 and 2002, respectively, while, thanks to its wide swath (~2330 km), provides near-global observations almost on a daily basis. The derivation of AOD is achieved through the implementation of two retrieval algorithms based on the Dark Target (DT) approach, valid over oceans (Remer et al., 2002, 2005, 2008) and vegetated continental areas (Levy et al., 2007a, b, 2010) but relying on different assumptions and bands, and the Deep Blue (DB) approach (Hsu et al., 2004; Sayer et al., 2013), providing retrievals over all cloud-free and snow-free land surfaces, including arid and semi-arid surfaces. For the purpose of MIDAS fine-spatial resolution pure-dust product the Collection 6.1 (C061) MODIS-Aqua Level 2 (L2) retrievals over the period 2003–2020, which are reported at 5 min swath granules (Levy et al., 2013) and are accessible from the Atmosphere Archive and Distribution System (LAADS) Distributed Active Archive Center (DAAC) (https://ladsweb.modaps.eosdis.nasa.gov/). For each MODIS L2 retrieval a quality assurance (QA) flag is assigned - 1 (marginal), 2 (good), and 3 (very good). MODIS AOD retrievals are acquired based on different algorithms according to the underlying surface type, based on the normalized difference vegetation index (NDVI) and the highest accuracy criterion (Sayer et al., 2014). With respect to MIDAS, two quality filtering criteria are applied to the raw MODIS AODs. AODs associated with cloud fraction (CF) higher than 0.8, and those with no adjacent retrievals, are masked out (Anderson et al., 2005; Hyer et al., 2011), accounting for potential cloud contamination on AODs while the second one discards suspicious retrievals from the data set.

4.1.2.2. MIDAS.

MIDAS fine-spatial resolution DOD at 550 nm is retrieved based on MODIS L2 retrievals, provided at a fine spatial resolution, via the synergy with the MERRA-2 products. More specifically, the MERRA-2 dust fraction (MDF) to total AOD550 nm (Eq.01) is multiplied with the MODIS AOD550 nm in order to calculate DOD550 nm at swath level (Eq.02). Towards MIDAS, MODIS and MERRA-2 datasets are temporally and spatially collocated. Then, the MDF is used to calculate the DOD at 550 nm from the MODIS AOD at 550 nm.

$$MDF(z) = \frac{AOD_{Dust,Merra2}}{AOD_{Total,Merra2}} \quad \text{(Eq.01)}$$

$$DOD_{MODIS} = AOD_{MODIS} * MDF \quad \text{(Eq.02)}$$

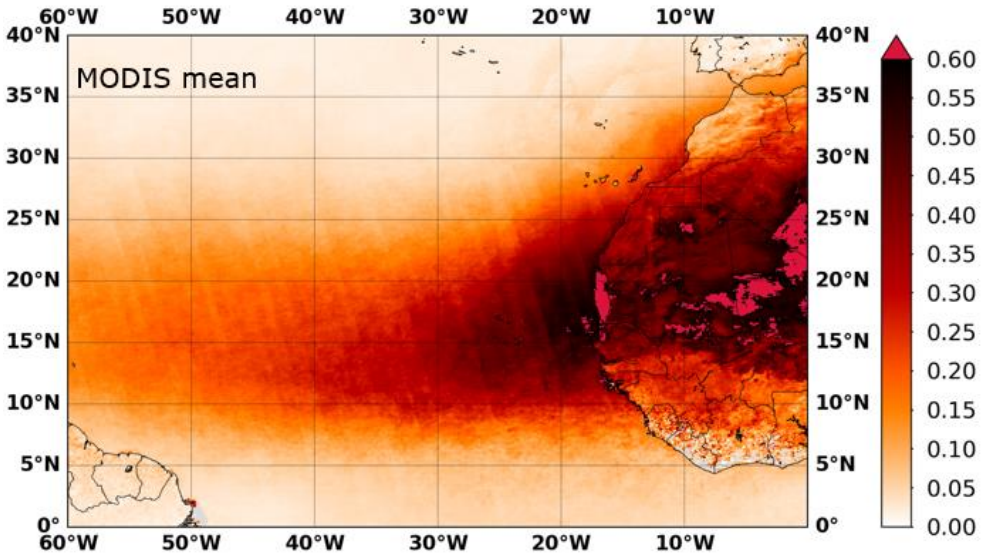

Figure 12: The MIDAS DOD 550 nm based on MODIS-Aqua (Level 2, Collection 6.1), JJA for 2003 – 2019 dust climatology of Saharan Dust outflow (Gkikas et al., 2020).

4.1.3. Metop IASI pure-dust.

The method for the retrieval of dust characteristics from IASI (Infrared Atmospheric Sounding Interferometer) observations was originally developed for application to AIRS (Pierangelo et al., 2004, 2005), and accordingly modified as described in detail in Peyridieu et al., 2010, 2013 and in Capelle et al., 2014. It is a three-step algorithm based on a "Look-Up-Table" (LUT) approach. LUTs are computed for a large selection of atmospheric situations from the climatological database "Thermodynamic Initial Guess Retrieval" (TIGR) (Chédin et al., 1985; Chevallier et al., 1998).

Developed by CNES in collaboration with EUMETSAT, the IASI instrument, onboard the ESA-EUMETSAT MetOp-A polar platforms, is a Fourier Transform Spectrometer that measures Earth-emitted infrared radiation. Launched in October 2006 and operational since July 2007, it provides 8461 spectral channels, between 15.5 μm (645 cm-1) and 3.63 μm (2755 cm-1) with a spectral resolution of 0.50 cm−1, and a regular spectral sampling interval of 0.25 cm−1. MetOp-A crosses the Equator at 9:30 p.m., Local Time (LT), on its ascending node. IASI provides a near global coverage twice a day at a spatial resolution of 12 km at nadir.

In the framework of L2A+, the output pure-dust products developed by IMAR, LMD, MAPIR, and ULB are used, in L3 (1x1 grids), and for the domain and period of interest, for the IASI instruments developed by CNES (French Space Agency) on board of ESA-EUMETSAT Metop-A satellite.

IMAR

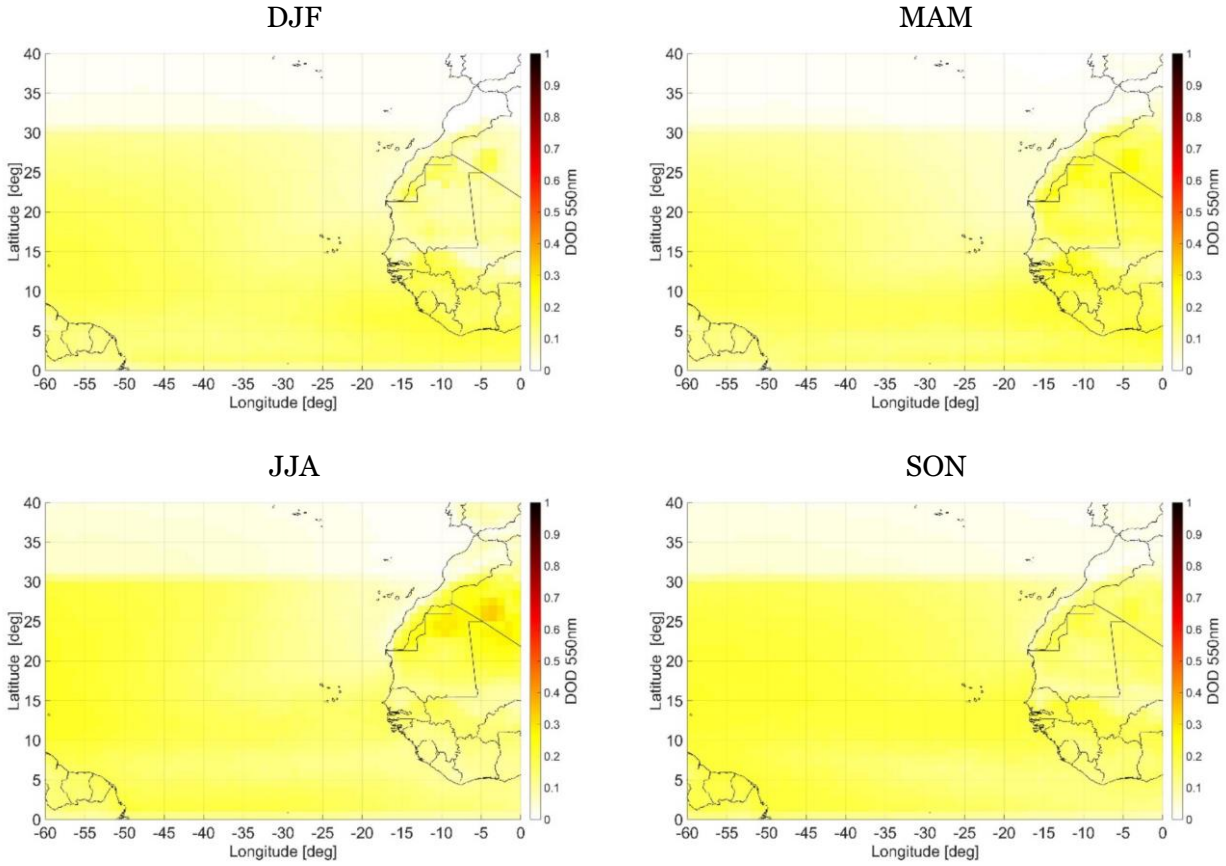

Figure 13: Metop-A IASI DOD at 550 nm based on IMAR algorithm.

LMD

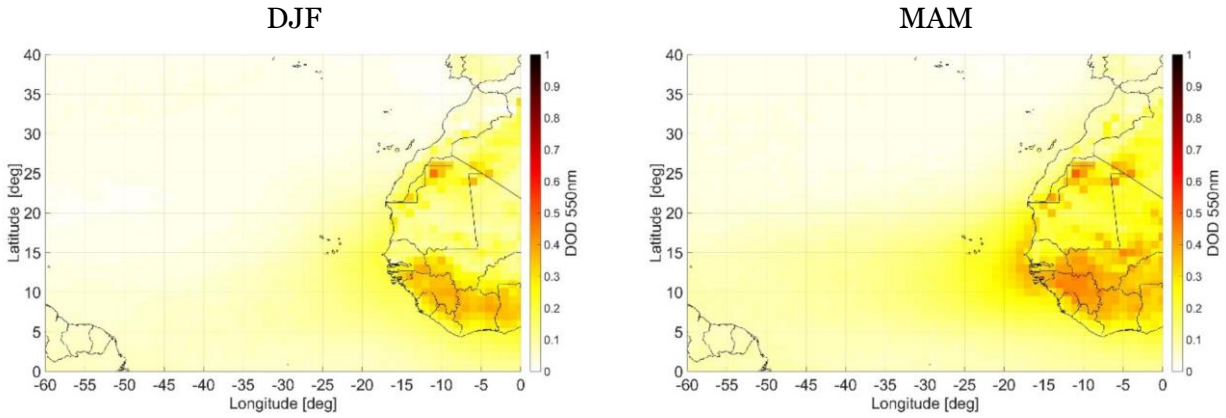

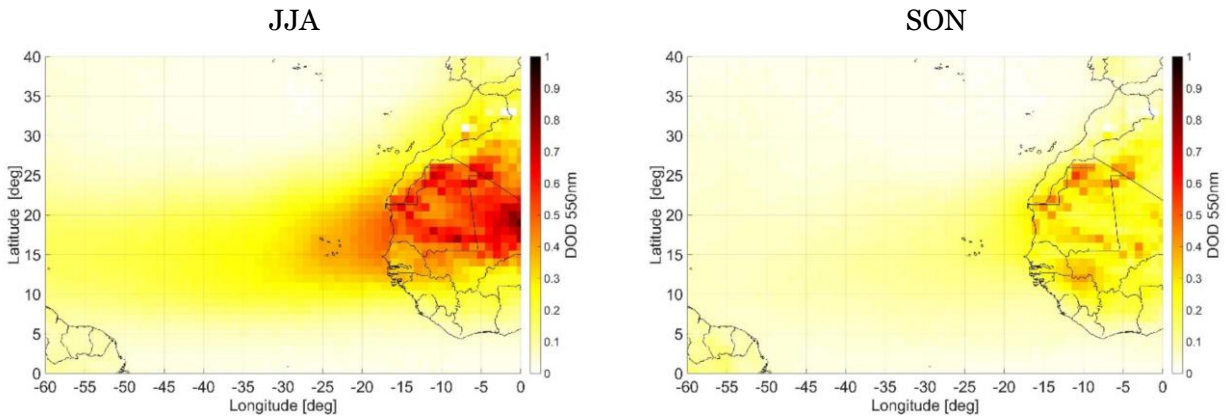

Figure 14: Metop-A IASI DOD at 550 nm based on LMD algorithm.

MAPIR

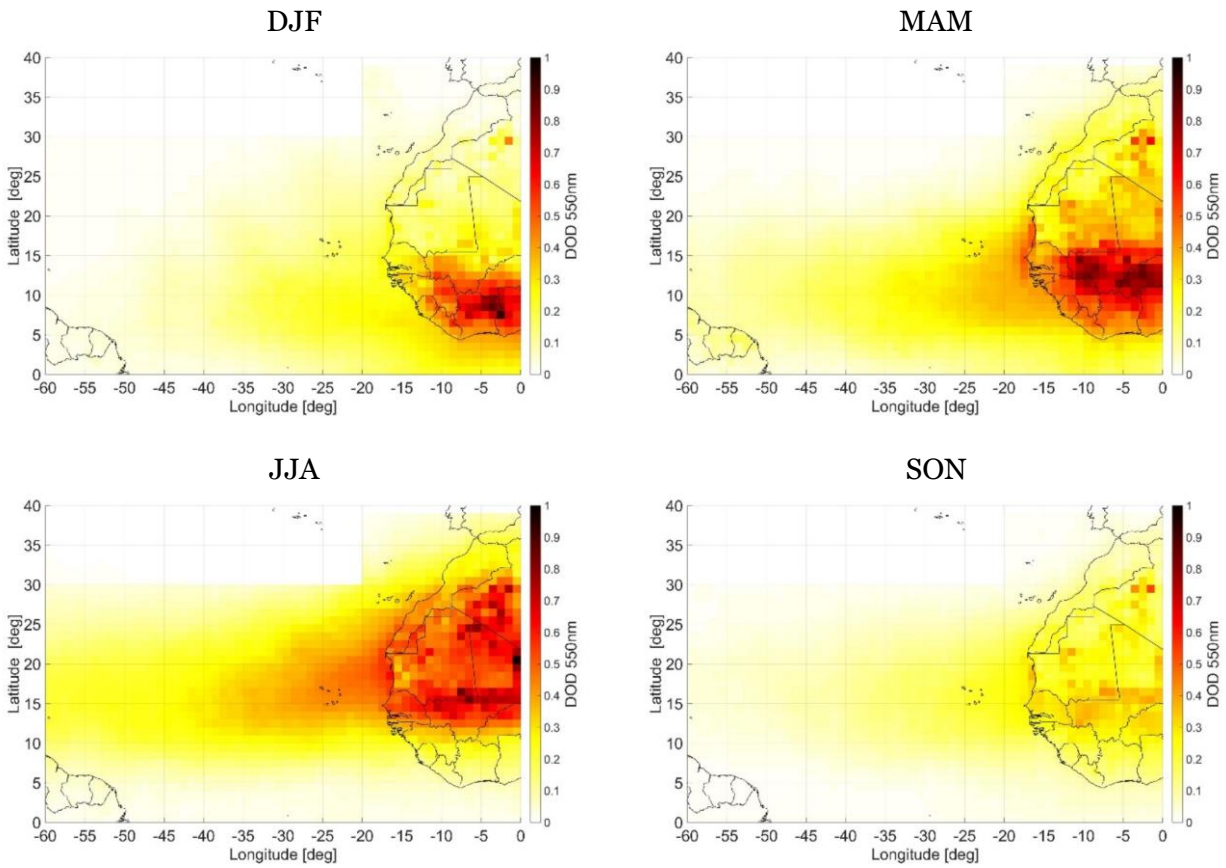

Figure 15: Metop-A IASI DOD at 550 nm based on MAPIR algorithm.

ULB

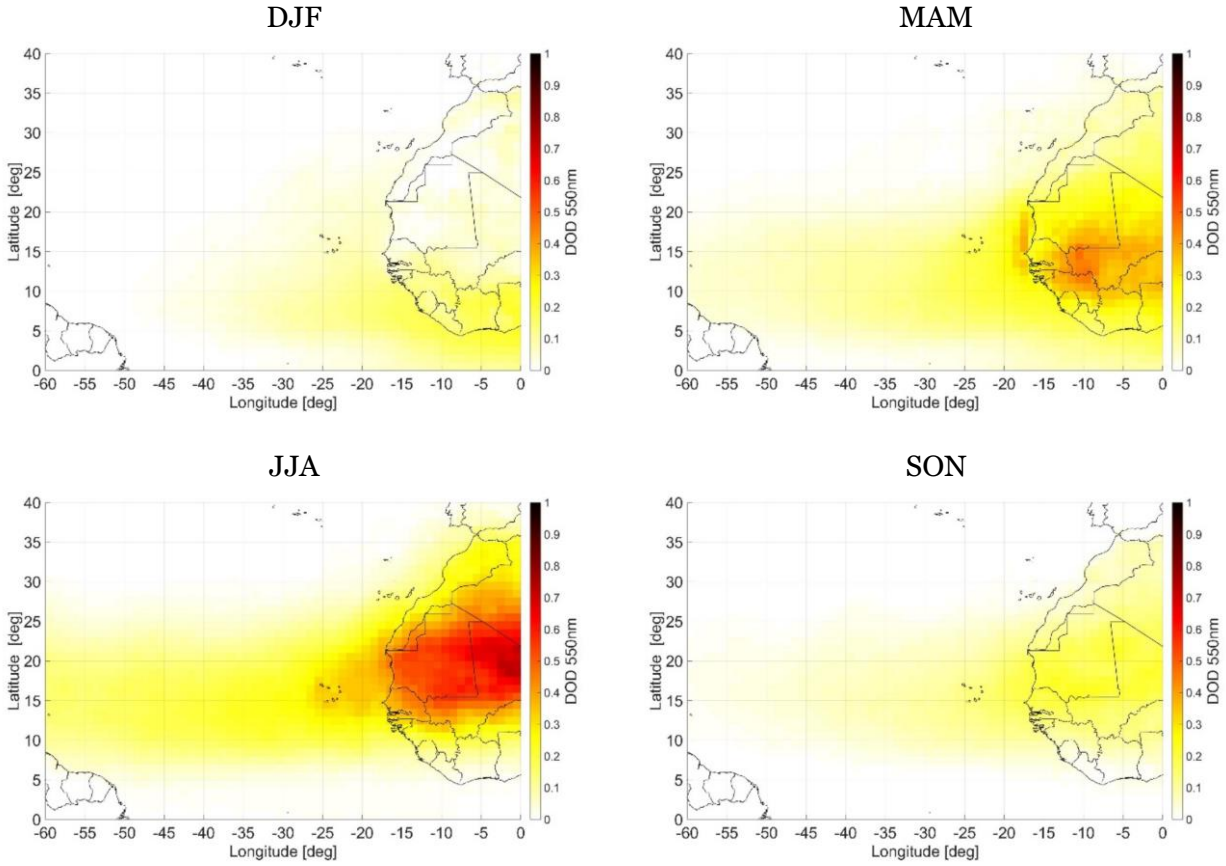

Figure 16: Metop-A IASI DOD at 550 nm based on ULB algorithm.

4.1.4. Sentinel 3A/B.

The main objective of the Sentinel-3 mission is to measure sea surface topography, sea and land surface temperature, and ocean and land surface colour with high accuracy and reliability to support ocean forecasting systems, environmental monitoring and climate monitoring. The Sentinel-3 Mission Guide provides a high-level description of the mission objectives, satellite description and ground segment. It also covers an introduction to heritage missions, thematic areas and services, orbit characteristics and coverage, instrument payloads and data products. The Sentinel-3 mission is jointly operated by ESA and EUMETSAT to deliver operational ocean and land observation services. The SYNergy (OLCI&SLSTR) Level-2 AOD product will provide one measurement data file with Aerosol Optical Depth (AOD) values and associated parameters on a 4.5 Km resolution grid, plus a number of annotation data files including information in support of the measurement data files, on a global scale. The measurement data file includes:

1. AOD at 440, 550, 670, 985, 1600 and 2250 nm,
2. Error estimates (1 s.d.) in AOD at 440, 550, 670, 985, 1600 and 2250 nm,
3. SSA at 440, 550, 670, 985, 1600 and 2250 nm,
4. Fine-mode aerosol optical depth at 550nm,
5. Aerosol Angstrom parameter between 550 and 865nm,
6. Dust aerosol optical depth at 550nm,
7. Aerosol absorption optical depth at 550nm.

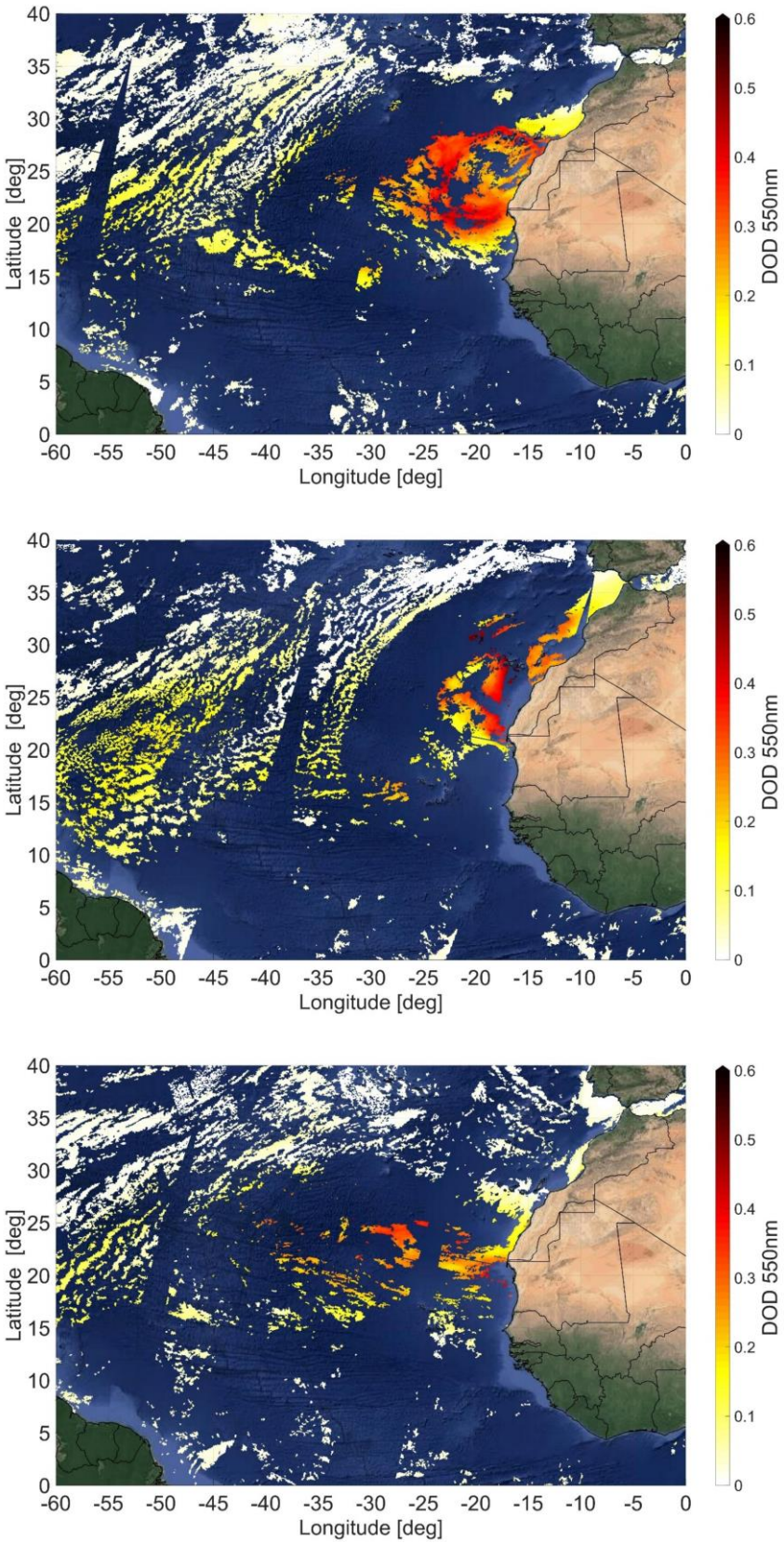

Figure 17: Sentinel 3A - OLCI&SLSTR DOD at 550nm for a dust event between for 27/28/29 of August 2020.

4.1.5. MSG.

For the cloud screening of the Aeolus L2A and AEL-PRO profiles, the Cloud Mask product (CLM), derived directly from the scene analysis of the MSG-SEVIRI (Meteosat Second Generation - Spinning Enhanced Visible and InfraRed Imager) imagery, will be processed. In CLM, it is merely provided a categorisation of the clear and cloudy pixels rather than a detailed information of clouds' macrophysical properties (i.e., cloud coverage), phase (i.e., ice, water, mixed) or types (i.e., low, middle, high). MSG, placed above the intersection of the Equator and the Greenwich Meridian, at a distance of ~36000km, samples a disk of the Earth including Europe, Africa and the Atlantic Ocean. SEVIRI, the main payload on MSG, completes a full Earth scan every 15 minutes providing observations at 12 channels, spanning from visible to infrared wavelengths, and at 3 (11 channels) or 1km (one channel) spatial resolution (nadir view). Therefore, thanks to the MSG-SEVIRI observational geometry and its high sampling frequency, it can be achieved an exact spatial and an almost coincident temporal collocation with Aeolus overpasses. Finally, the MSG-SEVIRI native files are freely accessible via the EUMETSAT Data Store.

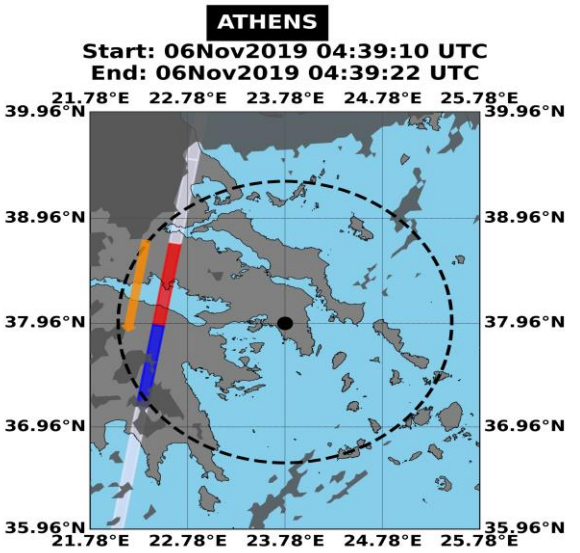

Figure 18: The white stripe indicates the ALADIN's measurements track and the colored rectangles correspond to the BRCs falling within a circle (dashed black line) of 120 km radius centered at the station coordinates (black dot), whereas the orange arrow shows the Aeolus flight directions (descending orbit). MSG-SEVIRI: Spatial coverage of the cloud mask product (CLM) in dark grey colors at the nearest time of Aeolus overpass. The starting and ending time (in UTC) of ALADIN observations are given in the plot's title.

4.2. Ground-based Observations of Interest.

Passive and active remote sensing techniques are applied on photometers and lidars operating at the ground. Through automatic measurements of the direct solar spectral irradiance, photometers can provide AOD at several wavelengths as well as size-related parameters (Ängström exponent, AE) whereas lunar (night-time) aerosol observations have been realized recently (Barreto et al., 2019). For the "derivation" of DOD, numerous studies have been relied either on the parallel processing of AOD and size parameters (Basart et al., 2009) or the utilization of coarse mode AOD, estimated through inversion algorithms (O'Neill et al., 2003), ignoring the presence of sea-salt particles or using advanced products obtained by more sophisticated algorithms like the Generalized Retrieval of Aerosol and Surface Properties (GRASP) (Dubovik et al., 2014). The three main networks

obtaining photometric observations are: (i) the Aerosol Robotic NETwork (AERONET, Holben et al., 1998), (ii) the Skynet (Takamura and Nakajima, 2004), and (iii) the GAW Precision Filter Radiometer (GAW-PFR) (Kazadzis et al., 2018a). Over oceanic regions, in the framework of the Maritime Aerosol Network (MAN; Smirnov et al., 2009), ship-borne sunphotometric measurements are obtained by the Microtops instrument following the same calibration and data processing standards and procedures applied in CIMEL (AERONET) sunphotometers.

Better and more accurate identification and characterization of dust layers, as well as the depiction of their vertical structure, has been achieved by taking advantage of the unique capabilities of the lidar technique (Mona et al., 2012). Automatic and elastic backscatter lidars (e.g., Welton et al., 2001) and more advanced multi-wavelength Raman and HSRL lidars have provided vertical profiles of the particle depolarization ratio allowing the discrimination of dust from non-dust species and the consequent derivation of the pure-dust backscatter coefficient profile (Ansmann et al., 2012) and, in case of Raman/HSRL lidar systems, the dust extinction coefficient profile (Tesche et al., 2009) and DOD by the integration of the dust extinction profile. The depolarization capability is nowadays available also for ceilometers (elastic backscatter lidars with very low Signal to Noise Ratio designed for cloud height determination) operating at 24/7 mode. Due to their low cost, a large number of ceilometers is distributed worldwide, and in Europe they have been integrated into the operational network of E-PROFILE of the European Meteorological Services Network (EUMETNET, www.eumetnet.eu/e-profile/).

Several aerosol lidar networks (Figure 19) are providing coordinated standardized observations at regional level: (i) the European Aerosol Research Lidar Network/Aerosol, Clouds, and Trace gases Research InfraStructure (ACTRIS/EARLINET) (Pappalardo et al., 2014), (ii) the Asian Dust Network (AD-Net, Shimizu et al., 2017), (iii) the Latin America Lidar Network (LALINET a.k.a ALINE, Antuña-Marrero et al., 2017), and (iv) the Micropulse Lidar Network (MPL-Net, Welton et al., 2001). Harmonization and coordination among these regional networks are fostered by the GAW Aerosol LIdar Observation Network (GALION) promoted by the WMO (GAW 2007; WMO 2007). Further GALION cooperating networks are the National Oceanic and Atmospheric Administration (NOAA) Cooperative Science Center for Earth System Sciences and Remote Sensing Technologies (CESSRST a.k.a. CREST) Lidar network, and the Network for the Detection of Atmospheric Composition Change (NDACC).

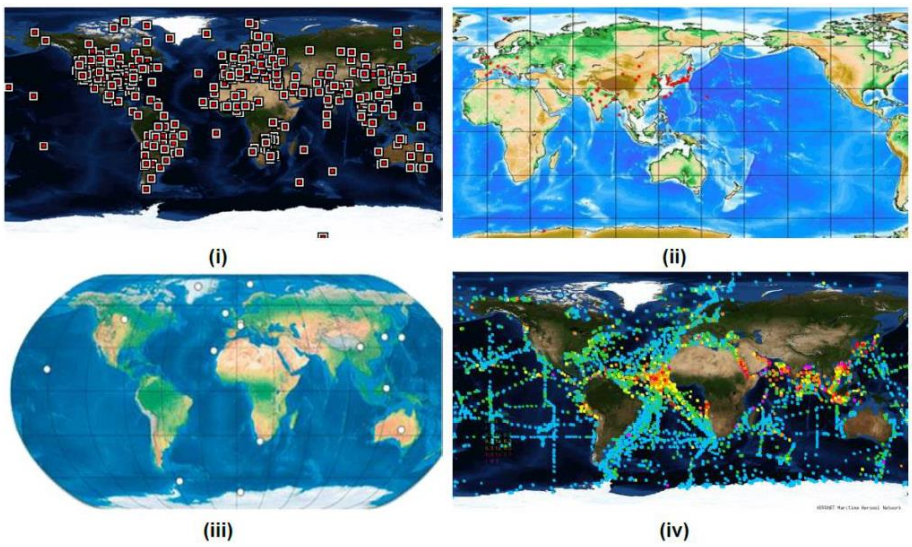

Figure 19: (i) AERONET, (ii) SKYNET, (iii) GAW-PFR and (iv) MAN.

4.2.1. The ESA-ASKOS Campaign.

4.2.1.1. ASKOS Observational activities.

At OSCM, an aerosol and cloud remote sensing facility of the Aerosol, Clouds, and Trace Gases Research Infrastructure (ACTRIS) was set up to operate in September 2021. The set-up instrumentation included a multiwavelength Raman-polarization lidar (Polly^{XT}), an AERONET sun-photometer, a Scanning Doppler wind lidar (HALO), a microwave radiometer and a cloud radar belonging to ESA fiducial reference network (FRM4Radar). Next to these aerosol, cloud, and wind remote sensing facilities, ESA's novel ground reference lidar system eVe, a combined linear/circular polarization lidar system with Raman capabilities, was deployed.

Figure 20: The ACTRIS ground-based instruments installed at the OSCM premises for the ASKOS experiment.

Table 03: List of the deployed instruments for the ASKOS experiment, PIs, and Affiliations.

Instrument	*PI*		
	Name	*Affiliation*	*Email*
eVe lidar	V. Amiridis	National Observatory of Athens	vamoir@noa.gr
PollyXT lidar	H. Baars	Leibniz Institute for Tropospheric Research	baars@tropos.de
Wind lidar	J. Bühl	Leibniz Institute for Tropospheric Research	johannes.buehl@tropos.de
Sun-photometer	H. Baars	Leibniz Institute for Tropospheric Research	baars@tropos.de
Microwave Radiometer	H. Baars	Leibniz Institute for Tropospheric Research	baars@tropos.de
Cloud Radar	D. Nicolae	National Institute of R&D for Optoelectronics	nnicol@inoe.ro
In-situ sensors	G. Mocnik	University of Nova Gorica	grisa.mocnik@ung.si

During this intensive period in September 2021, very different aerosol conditions were observed above and around Mindelo. Usually, the marine boundary layer up to an altitude of about 1 km was topped with a layer of Saharan dust reaching up to 6 km altitude. The amount and height of the Saharan dust aerosol varied during the 3-weeks campaign, providing a wide variety of aerosol conditions. Finally, volcanic aerosol from the Cumbre Vieja volcano eruption on the island of La Palma, Canary Islands, was observed on the island in the local boundary layer and partly above.

4.2.1.2. ESA-eVe.

The eVe lidar operated by NOA is the ESA's ground reference system for the Aeolus L2A products validation since it is specifically designed and manufactured by Raymetrics S.A. to provide the Aeolus mission with ground reference measurements of the aerosols and clouds optical properties.

eVe is a combined linear/circular polarization lidar system with Raman capabilities that operates at 355 nm. The lidar is designed to be a mobile and flexible system and it is implemented in a dual-laser/dual-telescope configuration that allows the lidar to simultaneously reproduce the operation of the deployed lidar onboard Aeolus (ALADIN) operating with circularly polarized emission at 355 nm as well as the operation of a traditional linear polarization lidar system. The system has also scanning-capabilities since the lidar head can point at multiple azimuths and off-zenith angles for a lidar measurement. As such, the lidar can reproduce the operation and the pointing geometry of any lidar (spaceborne or ground-based) that emit linearly or circularly polarized light. A detailed description of the lidar system can be found in Paschou et al. (2021). The L1 eVe lidar products are the range-corrected lidar signals and the attenuated backscatter signals from both linear and circular emission, and the volume linear and circular depolarization ratios. The L2 eVe lidar products are the vertical profiles of the particle backscatter and extinction coefficients retrieved using the linear and the circular emission, the lidar ratio, and the linear and circular depolarization ratios at 355 nm. Additionally, to the L2 products, eVe is able to directly retrieve the Aeolus-like backscatter coefficient and Aeolus-like lidar ratio (Paschou et al., 2021) which are the ground-based lidar products harmonized with the Aeolus L2A products that will be used in the Aeolus L2A validation.

The eVe dataset of the ASKOS experiment on September 2021 includes testing and routine lidar measurements at multiple pointing angles (vertical and off-zenith) that were performed during daytime and nighttime, and targeted measurements during the nearest Aeolus overpass from OSCM. Therefore, eight (04) collocated eVe-Aeolus measurements were collected on September, 2021. Additionally targeted eVe measurements were also performed during the overflights of experimental aircrafts carrying in-situ and remote sensing instrumentation implemented by UNG (Advantic WT-10), DLR (Falcon 20), LATMOS (Safire) under the JATAC operations.

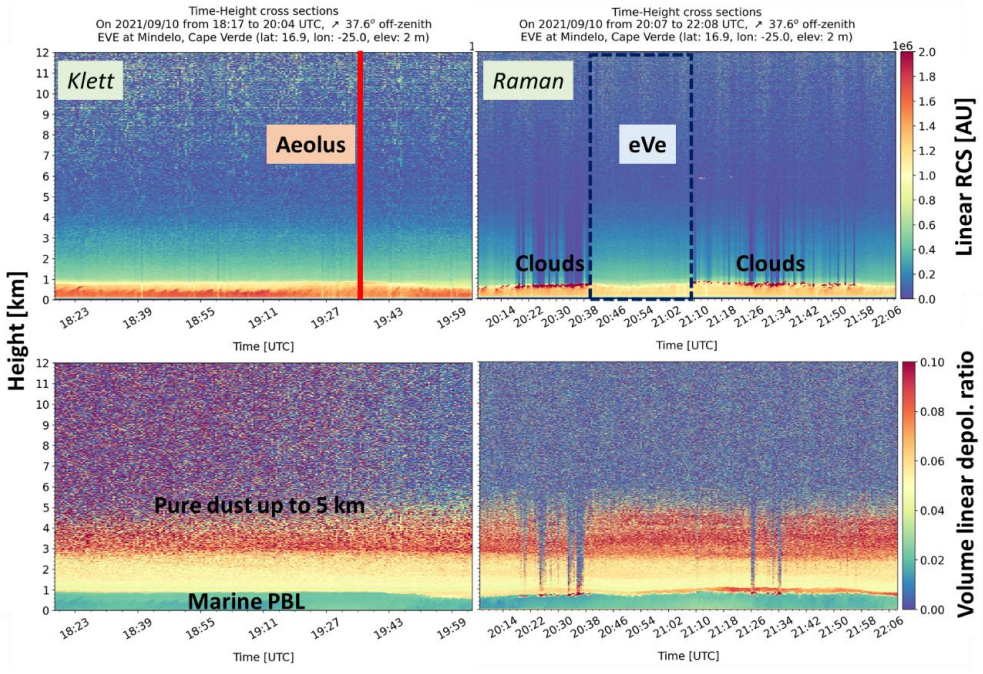

Figure 21: Time-height cross sections of the L1 products of the range-corrected signal and the volume linear depolarization ratio from eVe measurements on 10 September 2021.

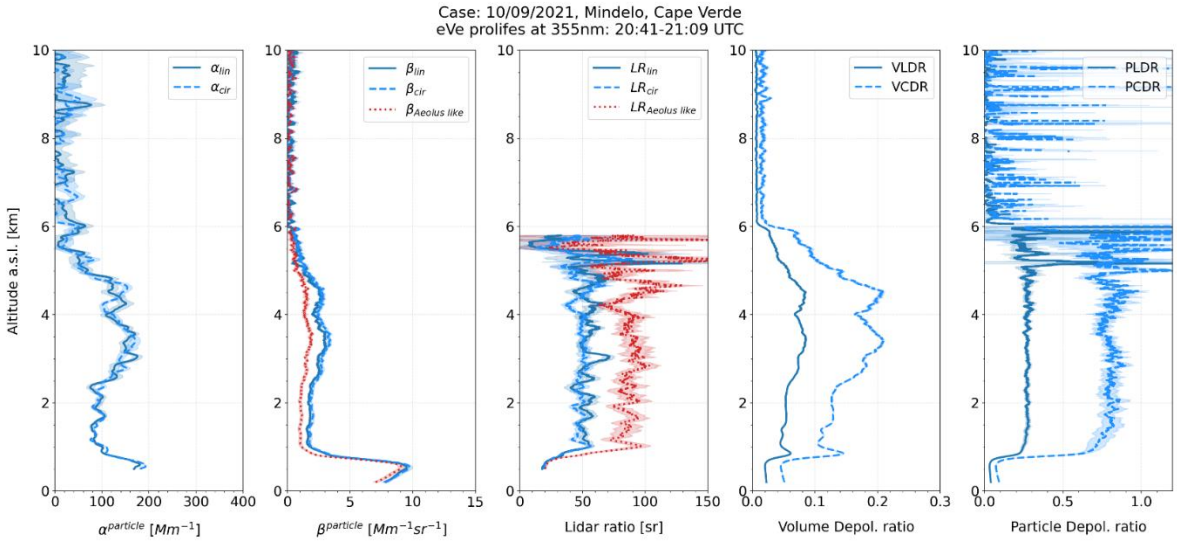

Figure 22: The L2 eVe products from the collocated measurement with Aeolus during the nearest Aeolus overpass on Friday 10 September 2021.

4.2.1.3. PollyXT.

The Polly^{XT}, provided by the TROPOS Institute, is an automated multiwavelength Raman polarization and water vapor lidar capable of measuring the aerosol loads in the boundary layer and the free troposphere (Fig.23). The lidar operated with 3 elastic backscatter channels (355, 532, 1064 nm), 3 Raman extinction channels (387, 607, 1058 nm), 3 depolarization channels (355, 532, 1064 nm) and one water–vapor sensitive channel (407 nm). The near-range receiver with 4 channels (elastic and Raman at 355 nm, elastic and Raman at 532 nm) provided a full overlap above 100 m allowing the detection of particles in low altitudes. The L1 measured parameters of the lidar are the range-corrected lidar signals at all operating wavelengths as well as the attenuated backscatter signals. The L2 PollyXT lidar products are the profiles of the particle backscatter and extinction coefficients at 355, 532, 1064 nm, the lidar ratio at 355 and 532 nm, the volume and particle linear depolarization ratios at 355 and 532 nm, the angstrom exponent (355/532 nm, 532/1064 nm), and the water vapor mixing ratio.

The PollyXT along with the rest instrumentation provided by TROPOS (microwave radiometer, wind lidar, sun-photometer) operated on automated-mode 24/7 starting from July 2021. The lidar is housed inside the OSCM, thus it can be operated under various climatic conditions. The full description of the original lidar system can be found in Engelmann et al. (2016). An overview of the suspended aerosols that were measured by the PollyXT lidar over the operations site (OSCM) during the intense phase of ASKOS experiment (September 2021) is provided below (Fig.24).

Figure 23: The PollyXT lidar during the ASKOS operations at the OSCM.

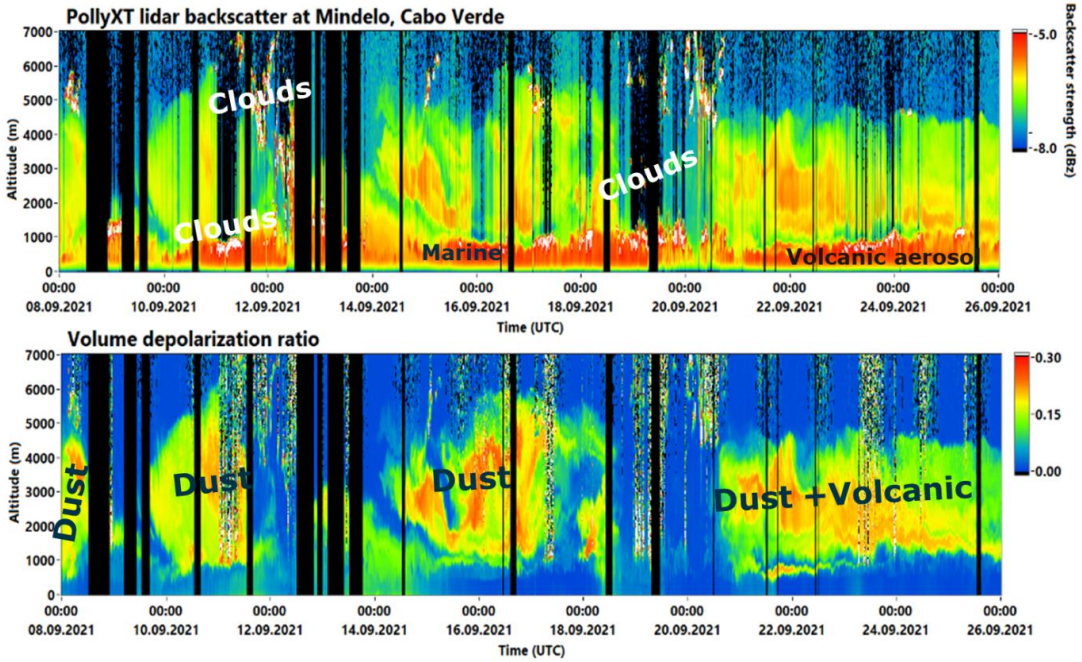

Figure 24: Overview of the lidar backscatter (top) and the volume depolarization ratio (bottom) at 532 nm retrieved from the PollyXT lidar during the ASKOS operations.

4.2.1.4. HALO wind lidar.

The Streamline-XR Doppler lidar of HALO Photonics company emits infrared light at a wavelength of 1.5μm. The lidar was provided by the TROPOS Institute. It has a maximum vertical resolution of 18m and it is sensitive to backscatter coefficient and velocity of the observed aerosol particles. Usually, the system is operated in vertical-stare mode, measuring the vertical component of the wind. Every 10min, the lidar performs a conical scan for retrieving the 3D wind vector. In this way, the distribution of wind speed and direction can be derived within the turbulent mixing layer and at cloud bases. The measured parameters of the lidar are the wind components, the wind speed and direction, the attenuated backscatter coefficient at 1.5 μm, the Doppler velocity, and the dissipation velocity.

Figure 25: The HALO Streamline-XR Doppler wind lidar on the rooftop of the OSCM, Cape Verde.

4.2.1.5. Sun-photometer.

The CE318 from CIMEL is a multiband photometer recognized as the worldwide reference for aerosol observing networks. The latest version, the CE318-T Sun Sky Lunar photometer, is now the only version supported by AERONET for new entering photometers. Taking advantage of the latest technologies, it features additional communications means and easier user-friendly operation. The improved tracking and detection chain increases measurement precision and makes it the only commercially available photometer to perform moon measurements and provide AODs also at nighttime. In addition to nighttime lunar measurements, the CE318-T version features a control unit with enhanced functionalities and ergonomics and a robot control as well as additional communication means. The instrument was provided by the TROPOS Institute and the measured parameters are the aerosol optical depth (AOD) at 8 wavelengths, the angstrom exponent for 6 wavelength ratios, the volume size distribution, the refractive index, the single scattering albedo, the absorption AOD, the extinction AOD, the asymmetry factor, and the phase function.

Figure 26: The CE318 photometer from CIMEL on the rooftop of the OSCM, Cape Verde.

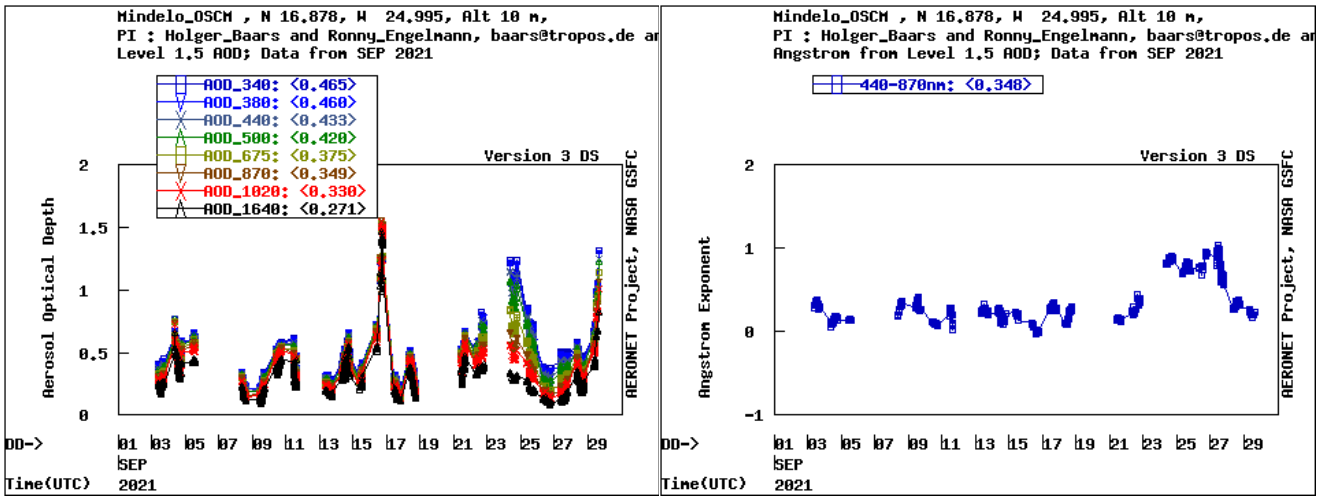

Figure 27: The L1.5 AERONET retrievals of AOD (left) and Angstrom exponent (right) from the CIMEL photometer during September 2021 (intense operations phase of ASKOS).

4.2.1.6. Microwave Radiometer.

The microwave radiometer manufactured by RPG and was provided by the TROPOS Institute, detects the atmospheric radiation temperatures in two frequencies ranges, 22-31 GHz (7 channels in the absorption band of water vapor) and 51-58 GHz (7 channels in the absorption band of oxygen). The 7 channels of the first band (22-31 GHz; water vapor) provide highly accurate information on atmospheric humidity and cloud liquid water content, whereas, the 7 channels of the second HATPRO band (51-58 GHz; oxygen) provide information on the vertical profile of temperature within the lower and middle troposphere due to the homogeneous mixing of oxygen. The receivers of each frequency band are designed as filter-banks in order to acquire each frequency channel in parallel. The measured parameters are the vertical profiles of the atmospheric air temperature and the absolute humidity, the liquid water path (LWP), and the integrated water vapor content.

Figure 28: The RPG microwave radiometer installed on the rooftop of the OSCM, Cape Verde.

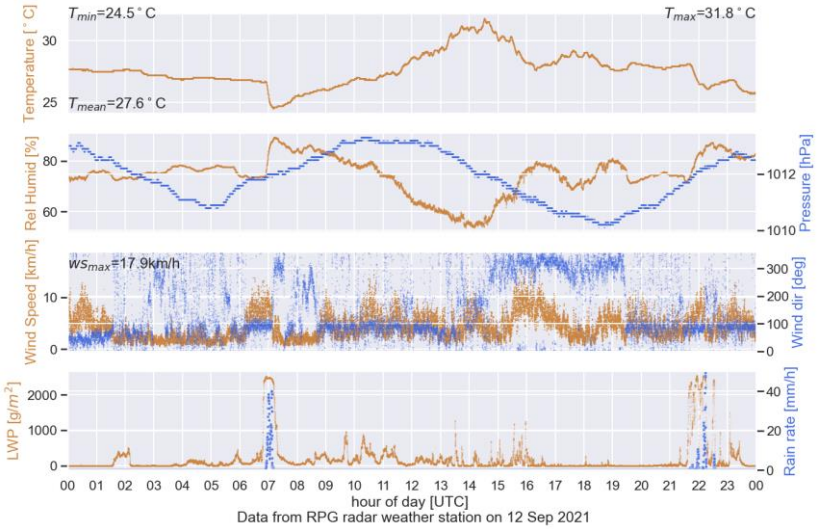

Figure 29: The temperature, relative humidity, wind speed, liquid water path parameters retrieved by the RPG microwave radiometer during a heavy rain event on 12 September 2021.

4.2.1.7. W-band Doppler Cloud Radar.

The RPG-FMCW-94 cloud radar, developed by RPG and provided by the INOE Institute operates at 3.2 mm wavelength which allows for reaching high sensitivity with small sizes of the instrument. The W-band Doppler cloud radar utilizes frequency modulated continuous wave (FMCW) signals and therefore has high range resolution down to 1 m. Doppler and polarimetric (optional) capabilities of the radar make a good basis for a classification of particles and a quantitative characterization of hydrometeors. The radar provides range profiles of parameters that contain information about scatterers in the atmosphere such as cloud particles, raindrops, snowflakes and insects. More specifically the measured parameters of the radar are the radar reflectivity, the doppler velocity, the spectrum width, the linear depolarization ratio for Hydrometeors and Non-Hydrometeorological targets, as well as the target classification (Fig. 30). The cloud radar arrived at Mindelo, Cape Verde on 7 September and it was installed in the rooftop of the OSCM by the INOE and NOA. The 24/7 operation of the cloud radar started on 10 September 2021.

Figure 30: The installation of the 94 GHz FMCW Doppler Cloud Radar on the rooftop of the OSCM, Cape Verde.

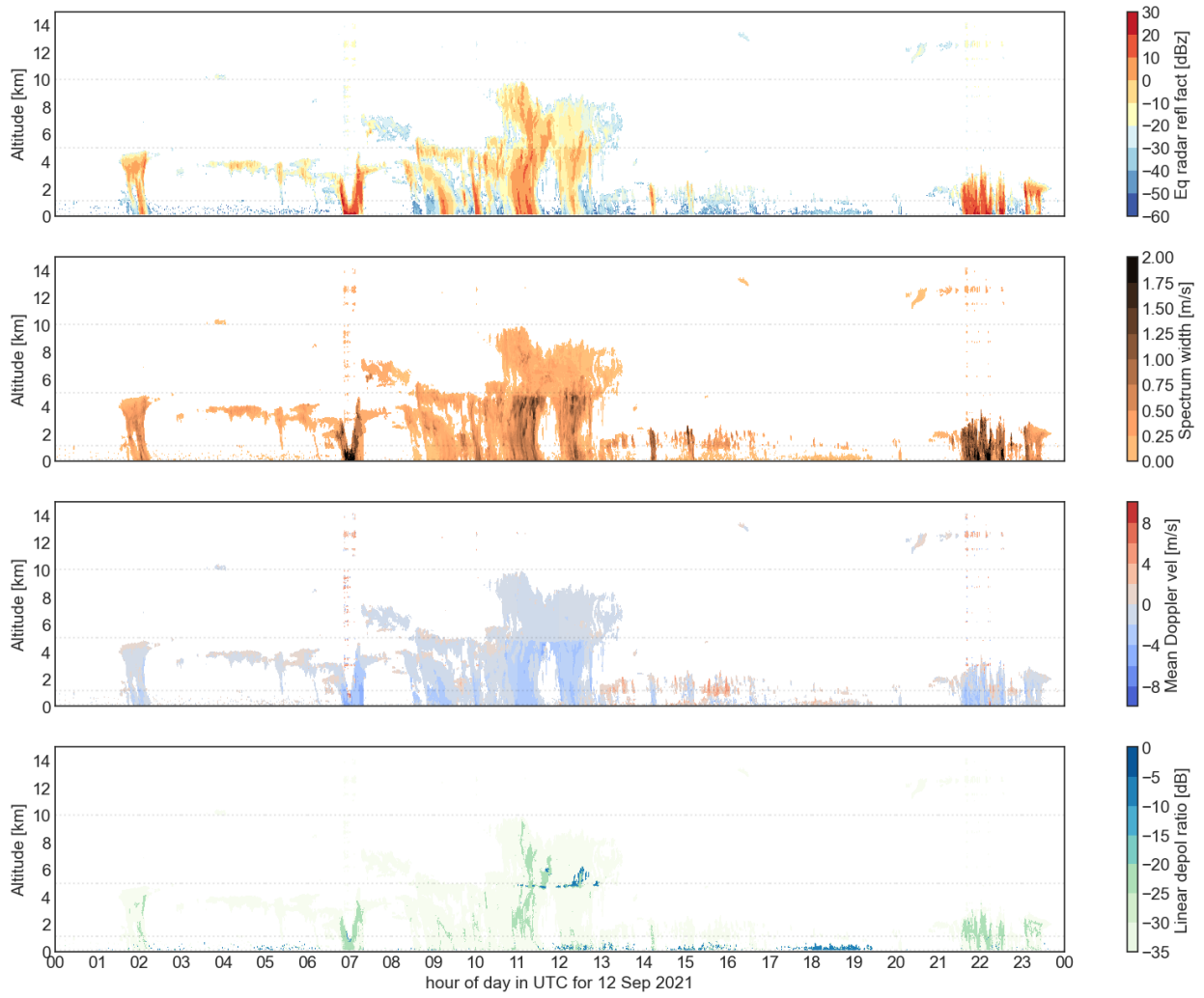

Figure 31: From top to bottom, the radar reflectivity, the spectrum width, the doppler velocity and the linear depolarization ratio during a heavy rain event on 12 September 2021.

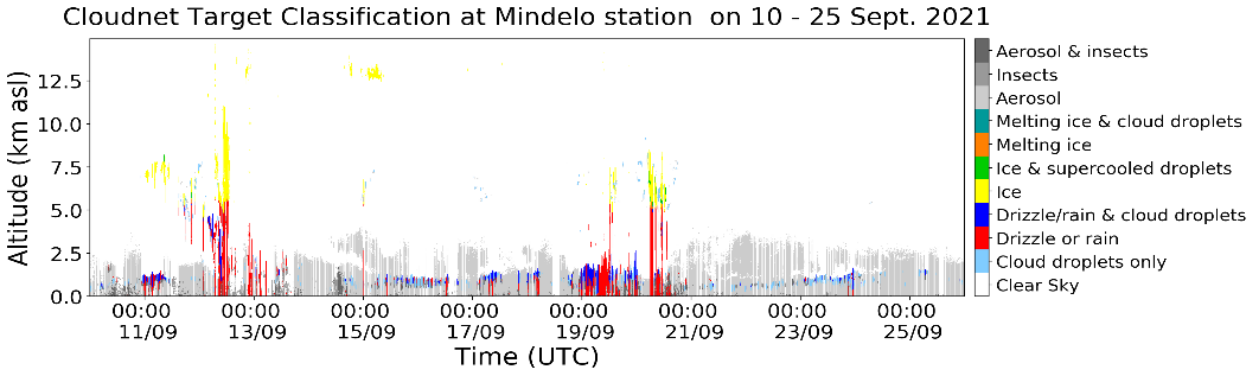

Figure 32: Target classification of clouds from the cloud radar operation during the ASKOS experiment.

4.3. Models

4.3.1. CAMS.

The Copernicus Atmosphere Monitoring Service (CAMS) reanalysis, produced by the European Centre for Medium-Range Weather Forecasts (ECMWF), consists of three-dimensional time-consistent atmospheric composition fields, including aerosols and chemical species (Inness et al., 2019). The CAMS aerosol model component of the IFS is a hybrid bulk–bin scheme with 12 prognostic tracers, consisting of three bins for sea salt depending on size (0.03–0.5, 0.5–5 and 5–20 μm), three bins for dust (0.030–0.55, 0.55–0.9 and 0.9–20 μm), hydrophilic and hydrophobic organic matter (OM), and black carbon (BC), plus sulfate aerosol and a gas-phase sulfur dioxide (SO2) precursor, treated as externally mixed. In this content, CAMS reanalysis datasets provide long-term series (2003 to present) of AODs, aerosol typing and dust deposition fields based on modelled emissions, transport and assimilated satellite observations, that will be utilised in L2A+.

(a) Dust

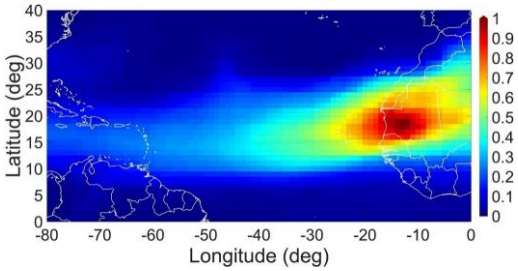

(b) Sea Salt

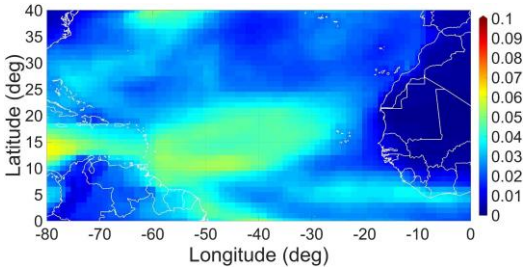

(c) Black Carbon

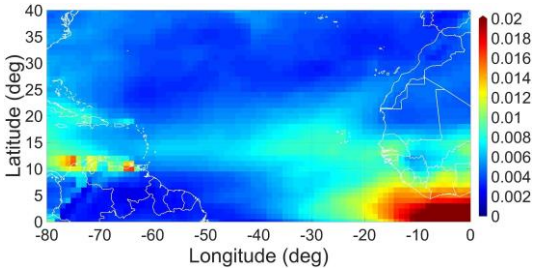

(d) Organic Matter

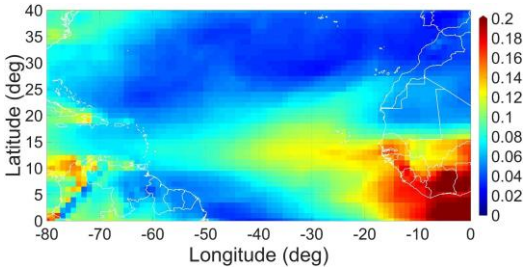

(e) Sulphate Aerosol

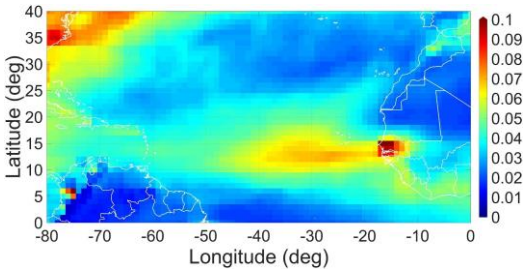

Figure 33: CAMS-based approach to qualitatively address the complementary aerosol-subtypes to dust for 06-2020. CAMS (a) Dust, (b) Sea Salt, (c) Black Carbon, (d) Organic Matter, and (d) Sulfate Aerosol.

4.3.2. Assimilation.

The enhanced L2A+ product will be evaluated through a series of NWP assimilation experiments. These experiments will compare the results of the WRF-L (modified version of WRF-CHEM) regional model when either L2A or L2A+ are assimilated. Preliminary investigations will pave the road to the way of the assimilation experiments will be conducted.

Developments on the Local Analysis and Prediction System (LAPS by the National Oceanic and Atmospheric Administration (NOAA) has ended, reducing the usability of any AEOLUS-aerosol assimilation system developed in this framework. To tackle this, the Data Assimilation Research Testbed (DART), an open-source toolkit developed at NCAR will be implemented. DART is under active development and includes the necessary tools to facilitate the use of new novel datasets and integrate with new models.

The assimilation experiments will utilize the Ensemble Kalman Filter (EnKF) algorithm, as implemented in DART. This technique relies on the implementation of several, independent, simulations to estimate the forecast error and therefore on how to correct it with measurements. Figure 34 presents a visual explanation of the way on how the proposed algorithm operates. EnKF has been successfully used in other satellite assimilation experiments.

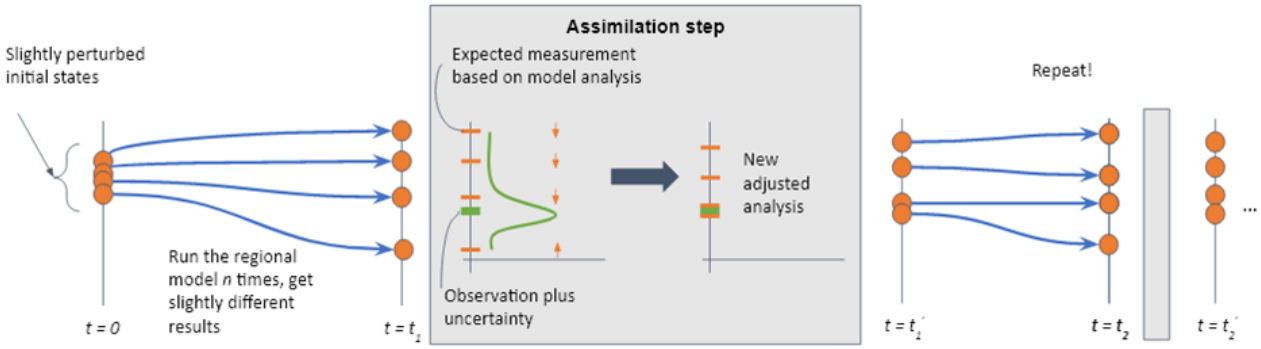

Figure 34: Visual representation of the Ensemble Kalman Filter algorithm.

The assimilation methodology requires multiple independent simulations rendering the EnKF algorithm computationally intensive. For the needs of the project computing resources would be allocated in the National High-Performance Computing (HPC) infrastructure (GRNET, https://hpc.grnet.gr/en/, last visit 31/01/2023). The preliminary tests of the performance of the code show that the configuration of 12x12 km² is computationally challenging. To accommodate this, we decided to reduce the spatial resolution of our runs from 12×12 km² to 24×24 km². The new resolution dramatically reduces computational requirements while it remains sufficient for the

model to capture typical mesoscale meteorological effects. The reduction in required resources also helps to safeguard the project in case any issues arise when accessing HPC systems, where access is awarded through a competitive process. Test runs for the model setup on ARIS, the national HPC infrastructure of Greece, operated by GRNET are performed. Initial results show that experiments with 24×24 km² spatial resolution can be completed during one production project on the HPC.

5. ESA-L2A+ Relevant Projects.

Task 1.3: A survey of current and ongoing initiatives and projects related to the investigated topic will be performed. L2A+ will work in close collaboration with the groups participating in ESA ASKOS, eVe, NEWTON, and DOMOS studies, whereas more activities will be integrated during the course of the project.

5.1. ESA-ASKOS

From July to September 2021, the European Space Agency (ESA) and the National Aeronautics and Space Administration (NASA) organized the Joint Aeolus Tropical Atlantic Campaign (JATAC) in the tropical islands of Cabo Verde with the main aim of providing quality-assured reference measurements for the validation of the products the ongoing ESA's satellite mission of Aeolus and the preparation of the forthcoming EarthCARE mission. ASKOS is the ground-based component of JATAC that was held in Mindelo on the island of Sao Vicente in Cabo Verde where high quality of ground-based wind, aerosol and cloud observations were collected using advanced instrumentation aiming to provide reference values for the Aeolus calibration and validation (Cal/Val) efforts. The ASKOS campaign has been implemented in two phases, the first phase was implemented during the July and September 2021 operations of the JATAC campaign while the second phase was implemented a year later in June and September 2022.

Figure 35: ASKOS team on 2021/09/11. From right to left: Dr. Nikos Siomos (NOA), Matevz Lenarcic (UNG; CAVA-AW/JATAC), Dr. Eleni Marinou (NOA), Peristera Paschou (NOA), Dr. Grisa Mocnik (UNG; CAVA-AW/JATAC), Elizandro Rodrigues (OSCM), Eder Silva (OSCM), Razvan Pirloaga (INOE), Dr. Ronny Engelmann (TROPOS), Dr. Annett Skupin (TROPOS).

The site of operations during ASKOS was the Ocean Science Center of Mindelo (OSCM) on the island of Sao Vicente in Cabo Verde (Figure 36). The OSCM is a joint facility of the GEOMAR Helmholtz Centre for Ocean Research Kiel, Germany, and the Instituto do Mar (IMar) in Mindelo, Cabo Verde. OSCM has been operating in Mindelo since 2017, providing a multifunctional basis for long-term ocean observation and field research in the tropical Northeast Atlantic region.

The islands of Cabo Verde are located in an ideal position in the Tropics for studying the impact of Aeolus observations on circulation patterns, atmospheric dynamics, as well as impacts on precipitation and desert dust. The generally high aerosol loadings in this region are a prerequisite to provide good quality backscatter signals for the lidar. During boreal summer, the midlevel African easterly jet (AEJ) is located near Cabo Verde and allows for the formation of synoptic-scale African easterly waves (AEWs) through baroclinic-barotropic instability. AEW disturbances typically reach their maximum intensity close to the coast of West Africa.

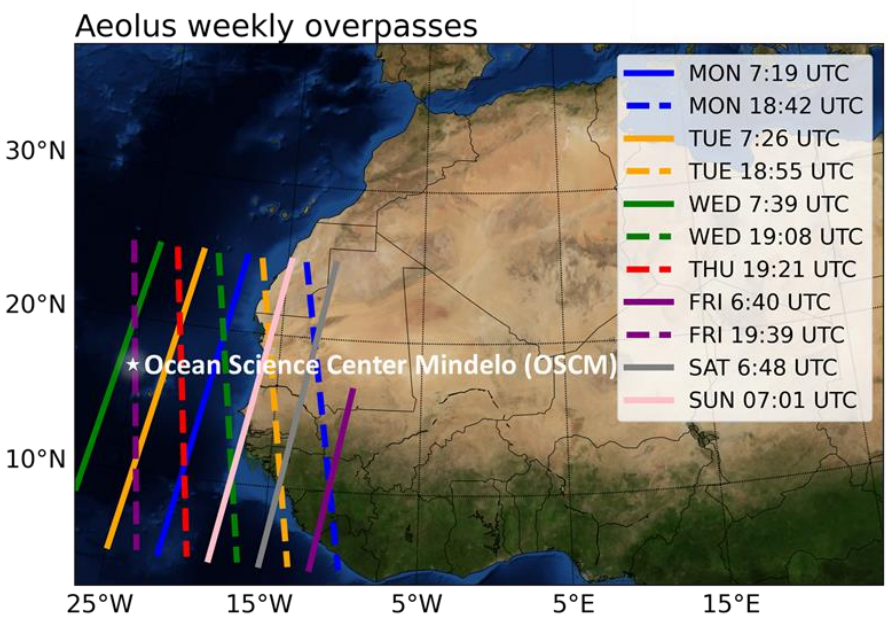

Figure 36: Location of the operations site, the Ocean Science Center Mindelo and the nearest Aeolus orbits from the site.

The Cabo Verde environment is ideal for aerosol studies and desert dust specifically. Situated downwind of the Sahara Desert, Cabo Verde receives a large influx of dust, particularly in summer during the peak of the dust season (Figure 37). Mindelo is located at the north part of Sao Vicente Island. The surrounding topography includes a series of mountains in Sao Vicente not exceeding 500-600 m east and south of Mindelo and higher mountains (~1400 m) at the neighboring island of Santo Antao at about 25 km north of Mindelo.

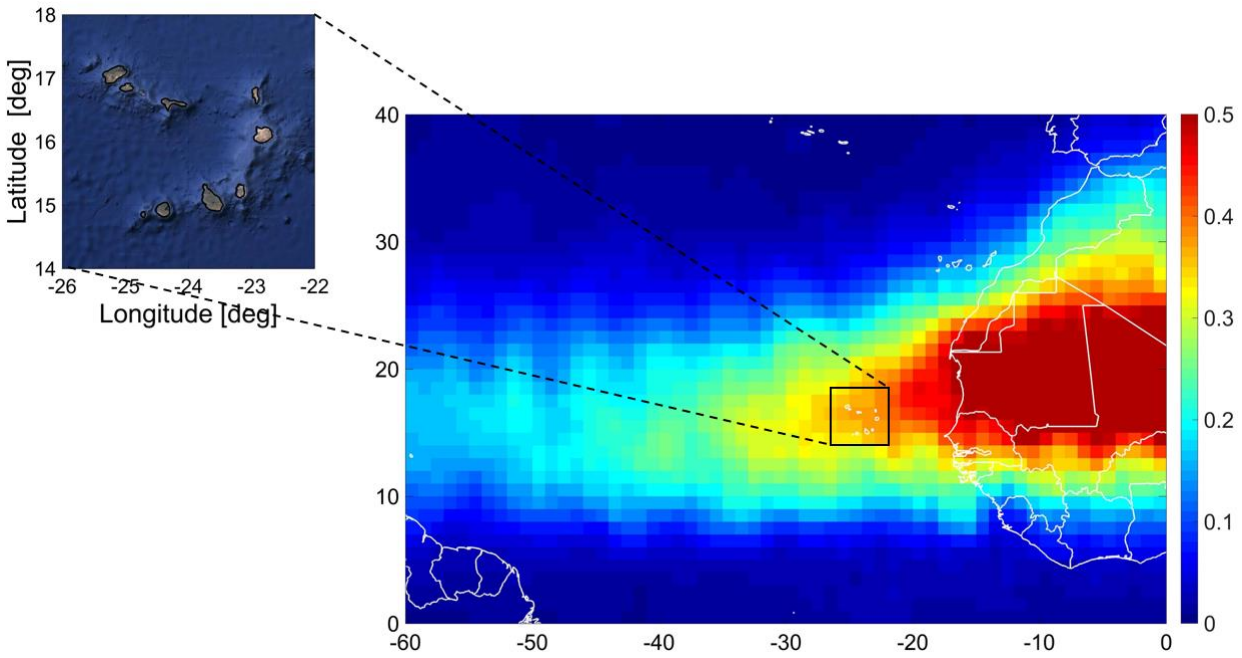

Figure 37: Dust Optical Depth (DOD) over Cabo Verde in 10°x10° grid resolution for the period 2007-2015 acquired from CALIOP (CALIPSO).

The main objective of JATAC was to provide quality-assured reference measurements for the validation of the products of the ESA-Aeolus satellite mission. ASKOS has been held in Mindelo on the island of Sao Vicente in Cape Verde deploying advanced active and passive remote sensing instrumentation such as a series of different lidars (eVe lidar, PollyXT lidar, HALO wind lidar), a microwave radiometer, a cloud radar, and a sunphotometer for ground-based observations of wind, aerosol and clouds, as well as in-situ instrumentation onboard a light aircraft for in-situ observations of the aerosol properties. As such, the ASKOS dataset contains measurements of the aerosol optical and physical properties, wind lidar data, cloud radar data, and water vapour, temperature and humidity profiles. In the context of the AVATART and CADDIWA operations, radiosondes over the Sal Island have been launched along with airborne dropsondes in the RoI, which will be used as input for the assessment of potential NWP improvements (WP5000). Moreover, the ASKOS campaign was supported by NOA's operational modelling simulations for meteorological and atmospheric composition forecasting on a daily basis with the Weather Research and Forecasting (WRF), the WRF-Chem, and the FLEXPART-WRF. More specifically, the forecasts of the meteorological fields and the aerosols and clouds include the dust AOD, the dust and sea salt concentrations, the 3-hours accumulated precipitation, the cloud fraction, the wind speed at 10 m, the vertical profiles of the dust and sea salt concentrations and the atmospheric (pressure, temperature, relative humidity) parameters, the FLEXPART 5-days backward airmass trajectories and calculations of the observed aerosols at 0-7 km, and the dust mass and sea salt concentrations cross section over the Aeolus overpasses.

5.2. ESA-EVE

The eVe lidar operated by NOA is the ESA's ground reference system for the Aeolus L2A products validation since it is specifically designed and manufactured by Raymetrics S.A. to provide the Aeolus mission with ground reference measurements of the aerosols and clouds optical properties.

eVe is a combined linear/circular polarization lidar system with Raman capabilities that operates at 355 nm. The lidar is designed to be a mobile and flexible system and it is implemented in a dual-laser/dual-telescope configuration that can point at multiple azimuths and off-zenith angles allowing eVe to simultaneously reproduce the operation of the deployed lidar onboard Aeolus (ALADIN) which operates with circularly polarized emission at 355 nm as well as the operation of a traditional linear polarization lidar system. As such, the lidar can reproduce the operation and the pointing geometry of any lidar (spaceborne or ground-based) that emits linearly or circularly polarized light. A detailed description of the lidar system can be found in Paschou et al., (2022). The L1 eVe lidar products are the range-corrected lidar signals and the volume linear and circular depolarization ratios. The L2 eVe lidar products are the vertical profiles of the particle backscatter and extinction coefficients and lidar ratio retrieved using the linear and the circular emission, and the linear and circular depolarization ratios at 355 nm. Additionally, to the L2 products, eVe is able to directly retrieve the Aeolus-like backscatter coefficient and Aeolus-like lidar ratio (Paschou et al., 2022) which are the ground-based lidar products harmonized with the Aeolus L2A products that will be used in the Aeolus L2A validation. An example plot of the available eVe products is provided in Figure 38.

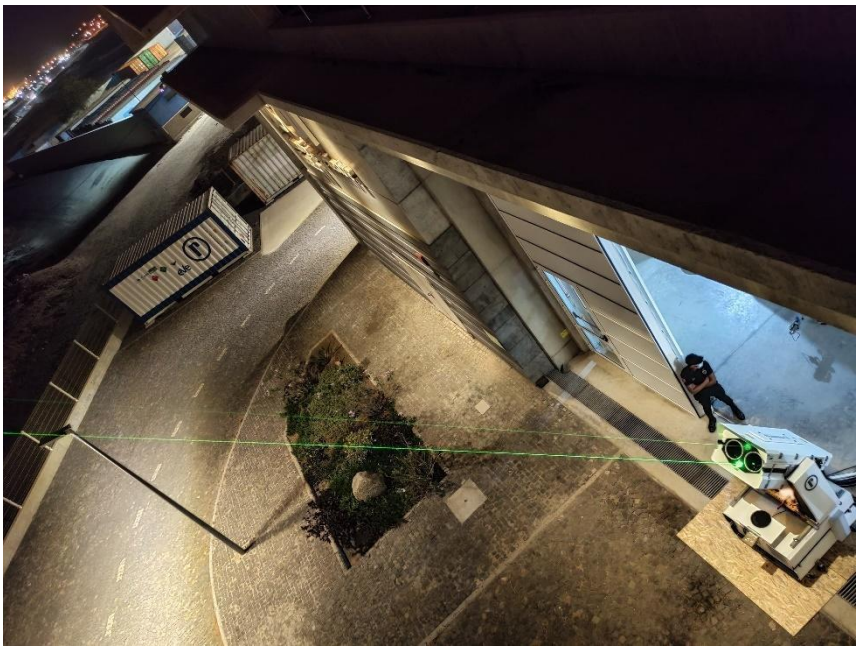

Figure 38: Operation of the eVe lidar during the ASKOS campaign

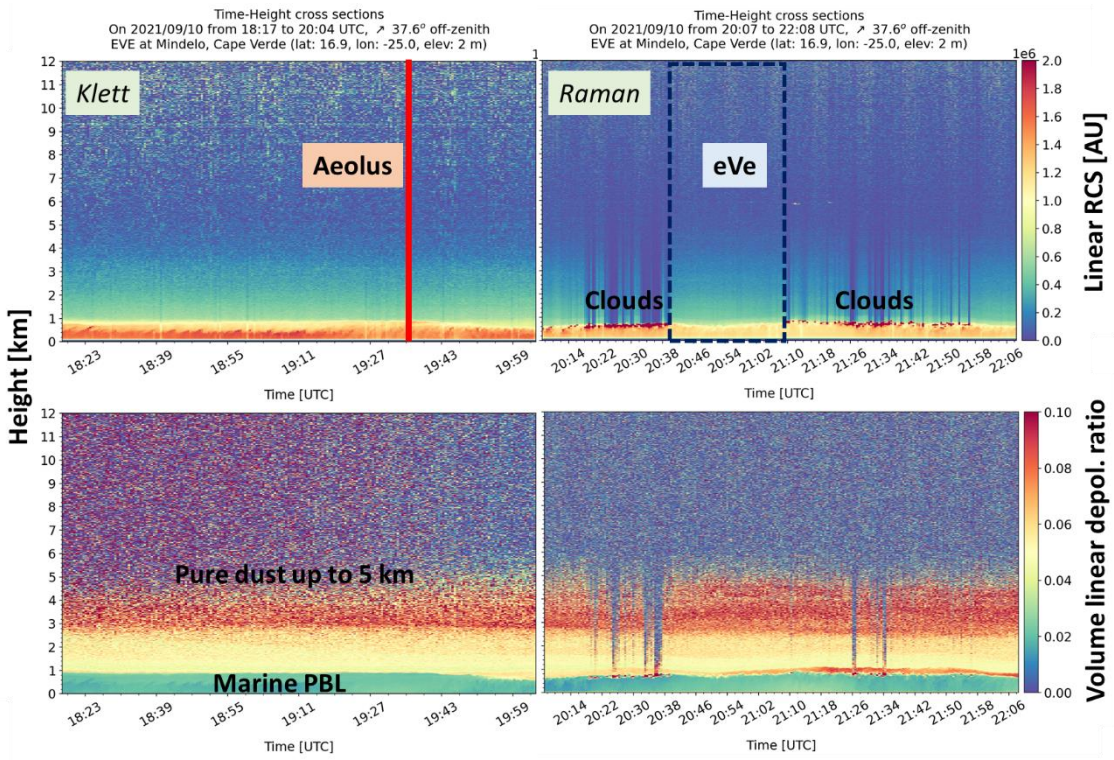

Figure 39: Time-height cross sections of the L1 products of the range-corrected signal and the volume linear depolarization ratio from eVe measurements on 10 September 2021.

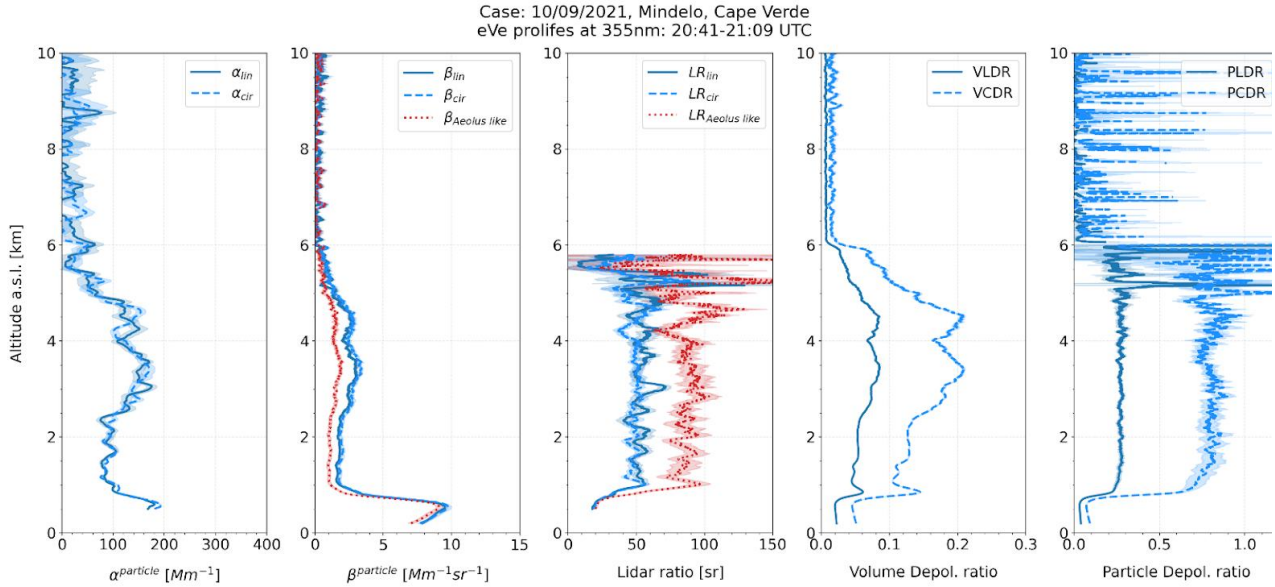

Figure 40: The L2 eVe products from the collocated measurement with Aeolus during the nearest Aeolus overpass on Friday 10 September 2021.

The eVe dataset of the ASKOS experiment (July/September 2021 & June/September 2022) includes testing and routine lidar measurements at multiple pointing angles (vertical and off-zenith) that were performed during daytime and nighttime, and targeted measurements during the nearest Aeolus overpass from site on Friday evenings where the eVe lidar had the same pointing geometry with Aeolus in order to reproduce the Aeolus measurements from ground. Fourteen collocated eVe-Aeolus measurements were collected (8 in 2021 and 6 in 2022) for the Aeolus L2A Cal/Val. Additionally, targeted eVe measurements were also performed during the overflights from the experimental aircrafts carrying in-situ and remote sensing instrumentation implemented by UNG (Advantic WT-10), DLR (Falcon 20), LATMOS (Safire Falcon 20) and NASA (DC-8) under the CAVA-AW, CADDIWA, AVATART, and CPEX-CV operations, respectively. Finally, the eVe dataset contains lidar measurements while implementing the dual-FOV technique for evaluating the multiple scattering effects on lidar signals under cloudy and dusty conditions.

5.3. ESA-NEWTON

The ESA-NEWTON project aimed to demonstrate the potential improvement of short-term dust forecasts when the numerical simulations are initialized from meteorological fields in which Aeolus observations are assimilated. To realize the overarching objectives of NEWTON, regional dust simulations were initialized with IFS numerical outputs provided by the ECWMF, for specific regions of the planet (i.e., West Sahara-Tropical Atlantic Ocean and Eastern Mediterranean). In a nutshell, the NEWTON project aimed to (1) assess the potential improvements on short-term regional dust forecasts attributed to the assimilation of Aeolus profiles, (2) investigate the modifications of dust emission and transport mechanisms by contrasting numerical simulations initialized with and without Aeolus observations, and (3) highlight the benefits and the necessity of Aeolus data on dust research, paving the way for future operational satellite missions. The NEWTON approach was based on a synergy of numerical simulations and sophisticated observations, considered in the framework of the NEWTON project.

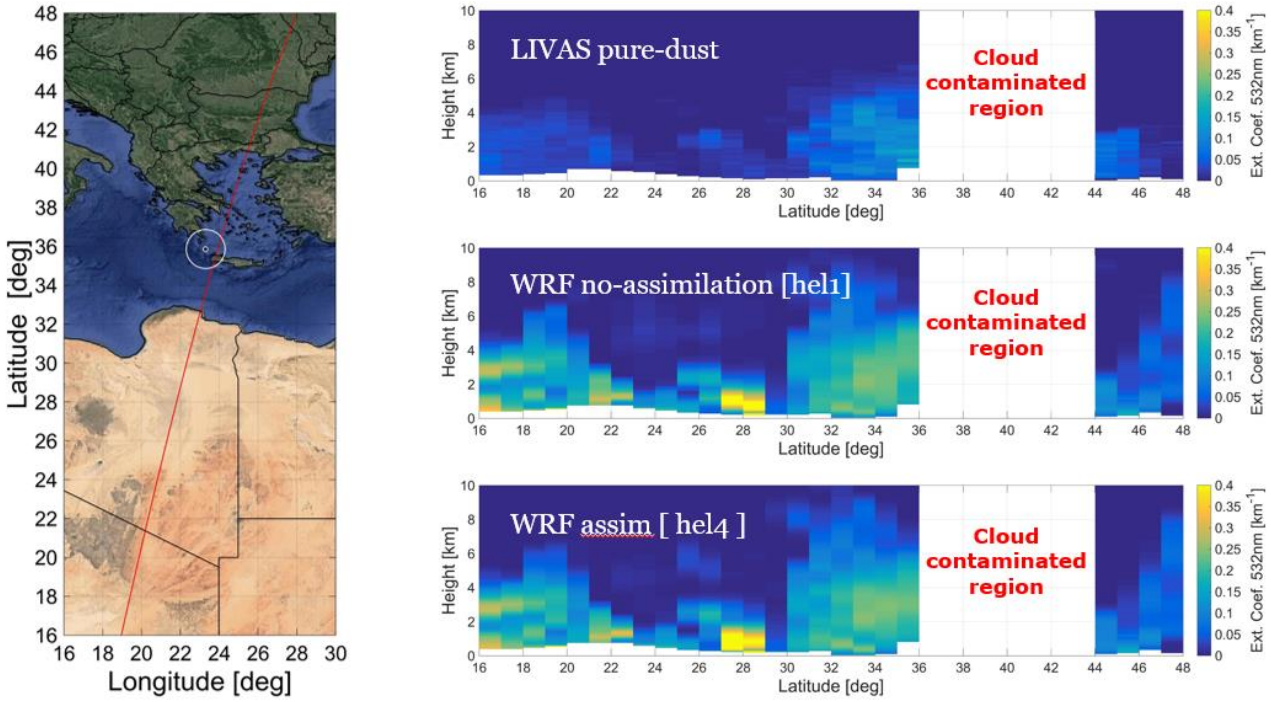

Figure 41: (left): CALIPSO overpass. (right): CALIPSO Extinction Coefficient 532 nm, WRF L2A no-assimilation, and WRF L2A assimilation.

5.4. ESA-LIVAS

In the framework of L2A+, and towards the four-dimensional evaluation of the enhanced L2A product (WP3000), the evaluation of the assimilation experiments (WP4000) and the impact studies (WP5000), the pure-dust product of the LIVAS database will be utilized. LIVAS consists a four-dimensional global database of aerosol and cloud optical properties on a uniform 10x10 grid resolution, developed in the framework of the European Space Agency (ESA) project "LIdar climatology of Vertical Aerosol Structure for space-based lidar simulation studies", (Amiridis et al., 2015). The database is established based on multiyear CALIPSO (Cloud-Aerosol Lidar and Infrared Pathfinder Satellite Observations; Winker et al., 2007; Winker et al., 2009) CALIOP (Cloud Aerosol Lidar with Orthogonal Polarization) Level 2 (L2) Version 4 (V4.20) aerosol and cloud profiles extending between 06/2006 and 12/2020. In addition, LIVAS includes a pure-dust atmospheric product, developed based on the one-step POLIPHON technique (POlarization-LIdar PHOtometer Networking; Tesche et al., 2009), established in the framework of EARLINET (European Aerosol Research Lidar Network (Pappalardo et al., 2014, http://www.earlinet.org/; last access: 10/01/2023). More specifically, the one-step POLIPHON method is applied to CALIPSO atmospheric layers classified as "dust", "polluted dust", and "dusty marine" (Kim et al., 2018), eventually enabling to decouple the "pure-dust" component from the total aerosol load, in terms of CALIPSO backscatter coefficient at 532nm, extinction coefficient at 532nm, and Mass Concentration (Amiridis et al., 2013).

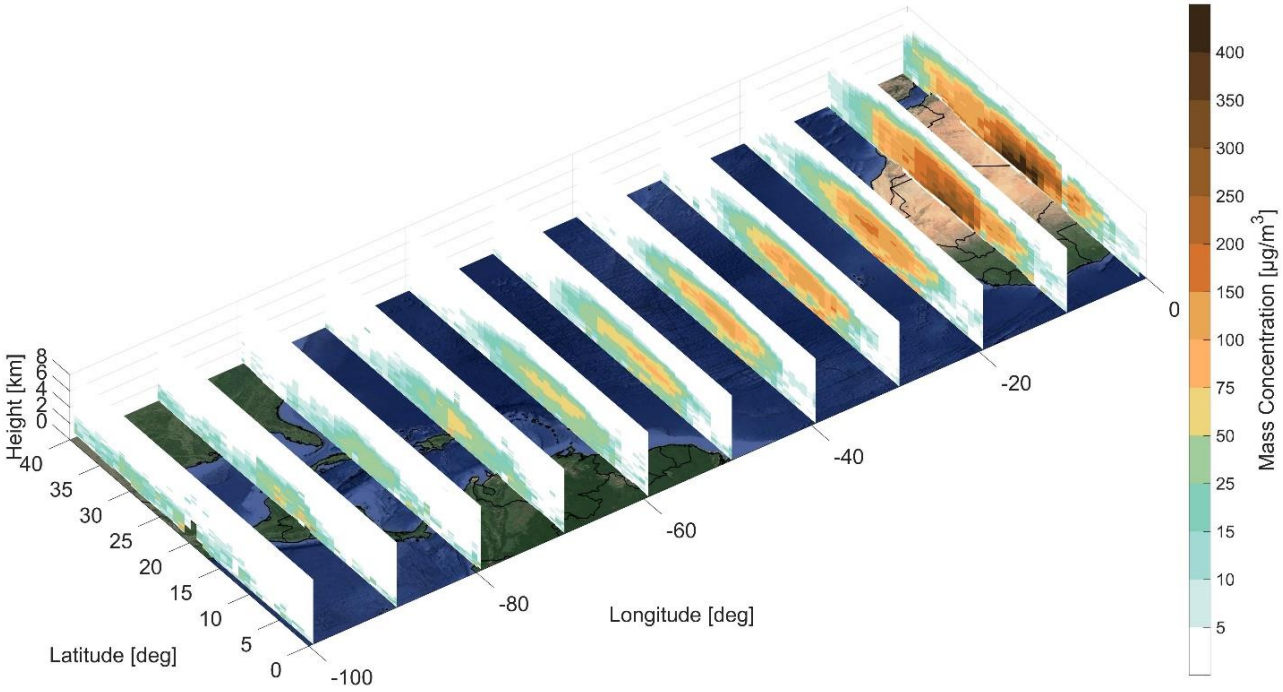

Figure 42: LIVAS Pure-Dust Mass Concentration climatology for JJA 2006-2020.

The pure-dust optical depth (DOD) is obtained through the vertical integration of the corresponding pure-dust extinction coefficient at 532nm profiles (Marinou et al., 2017; Proestakis et al., 2018). In the framework of the study, the mean pure-dust extinction coefficient at 532nm profiles and the corresponding DODs at 532nm LIVAS products, pre-processed on a uniform 1°x1° grid for L2A+ RoI.

(b) LIVAS Aerosol Optical Depth at 532nm.

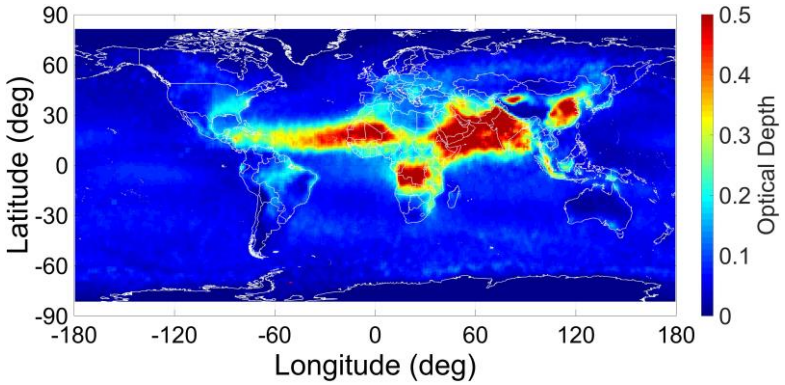

(b) LIVAS Pure-Dust Optical Depth at 532nm.

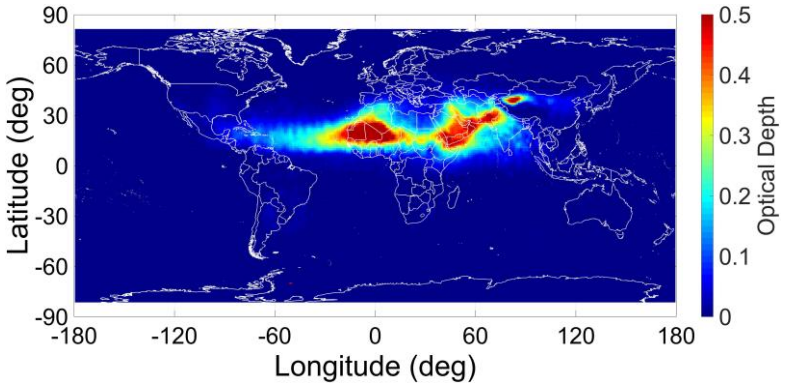

Figure 43: LIVAS (a) AOD and (b) DOD at 532nm climatology for JJA 2006-2020.

5.5. ESA-DOMOS

The ESA "4D-Atlantic Dust-Ocean Modelling & Observing Study" (DOMOS) kicked off in September 2021, with an overarching objective to advance our fundamental understanding on the complex atmospheric dust-ocean interactions and processes governing the Atlantic Ocean, in the context of climate change, through an innovative approach of integrated use of modelling, EO-based products and in-situ datasets.

DOMOS has established and validated against in-situ observations and existing datasets of dust deposition, a novel EO-based product of dust deposition fluxes. The project has developed through exploitation of (1) the CALIPSO-based ESA-LIVAS pure-dust database, (2) the MODIS-MIDAS and Metop-IASI MAPIR/IMARS/LMD/ULB atmospheric pure-dust products, and (3) ERA5 U/V wind components, a product of pure-dust deposition fluxes across for the broader Atlantic Ocean and for the year 2007-2020. Moreover, DOMOS has provided a validation of the dust deposition field from the CAMS reanalysis and has performed assimilation tests of IASI and Aeolus aerosol products with the goal of providing a better description of the dust aerosol transport over the Tropical Atlantic.

The DOMOS products contribute to an improved representation of the physical and chemical characteristics of dust deposition over the ocean which is crucial to interpret the observed climatic change responses and to better describe the future ones. This includes a better understanding and quantification of the deposition of soluble iron from natural and anthropogenic dust and of its contribution relative to biomass burning and anthropogenic aerosols which has been achieved through the use of a climate model (EC-Earth3-Iron).

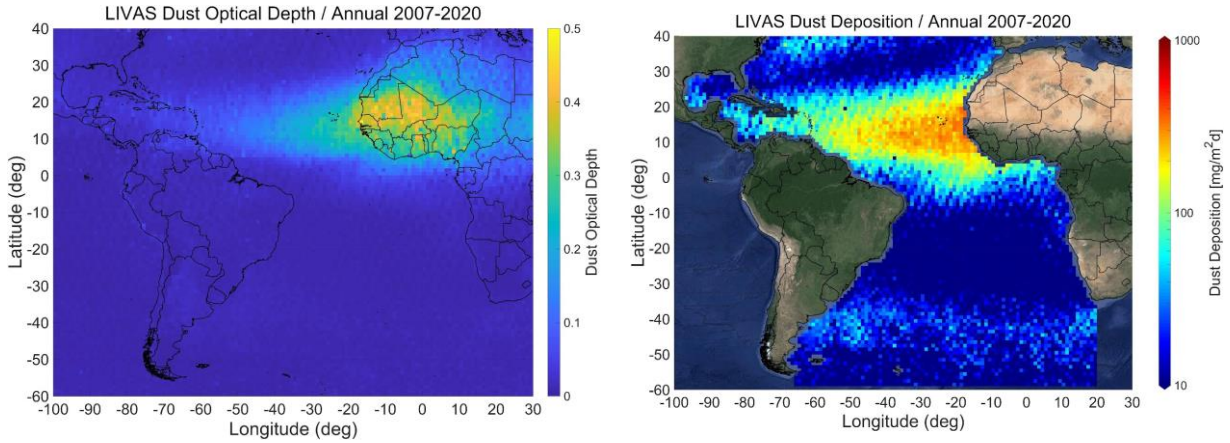

Figure 44: LIVAS DOD at 532nm (left) and DOMOS Dust Deposition Rate (right), for the broader Atlantic Ocean and for the period 01/2007-12/2020.

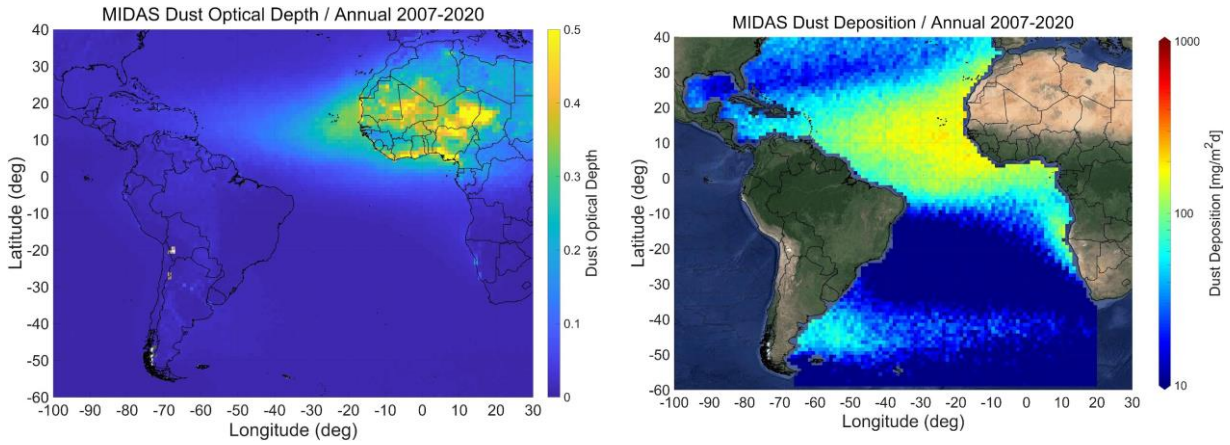

Figure 45: MIDAS DOD at 550nm (left) and DOMOS Dust Deposition Rate (right), for the broader Atlantic Ocean and for the period 01/2007-12/2020.

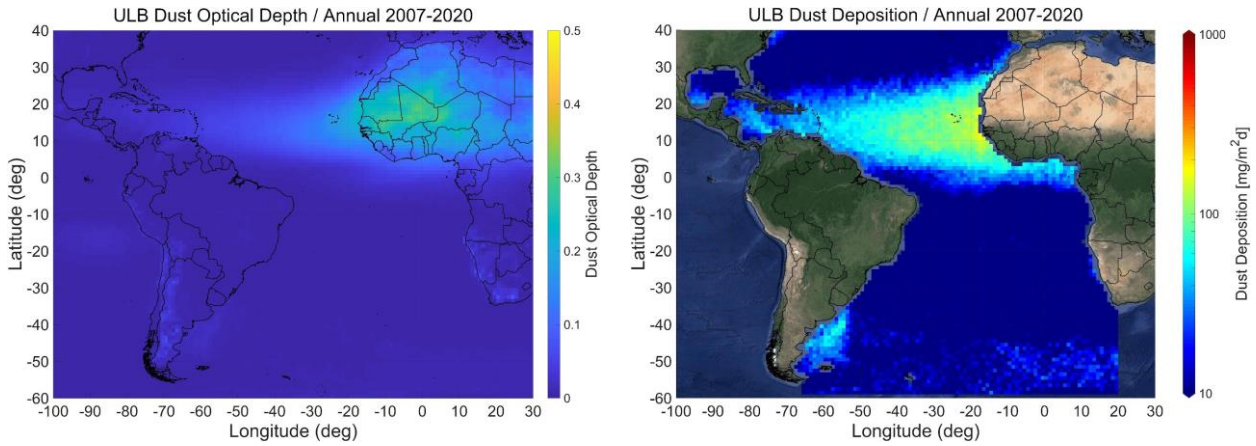

Figure 46: ULB DOD at 550nm (left) and DOMOS Dust Deposition Rate (right), for the broader Atlantic Ocean and for the period 01/2007-12/2020.

6. Approach.

A schematic workflow of the L2A+ project is illustrated in Figure 46. Each block corresponds to the main components of the workflow starting with the "Development of the L2A+ aerosol product" (WP3000), continuing with the "Assimilation of L2A/L2A+ and application of WRF-L experiments" (WP4000), and finally addressing the identified "Impact Studies" (PW5000).

As a first step - the "Development of the L2A+ aerosol product" (WP3000) block - the development approach of the refined Aeolus aerosol optical product (L2A+) is illustrated, based on AEL-FM/AEL-PRO algorithms, geostationary AOD products, CAMS, and new AOD retrievals from the Aeolus itself. The product will be thoroughly compared with L2A and validated against quality-assured measurements from the ESA-ASKOS/JATAC experiment in Cabo Verde.

As a second step - the "Assimilation of L2A/L2A+ and application of WRF-L" block - the examination of the impact of L2A and L2A+ on aerosol assimilation and dust transport models is illustrated. Constraining aerosol loads through Aeolus assimilation is expected to improve dust emission fluxes over the Sahara Desert and transport simulations of the full particle size range (from fine to giant dust particles).

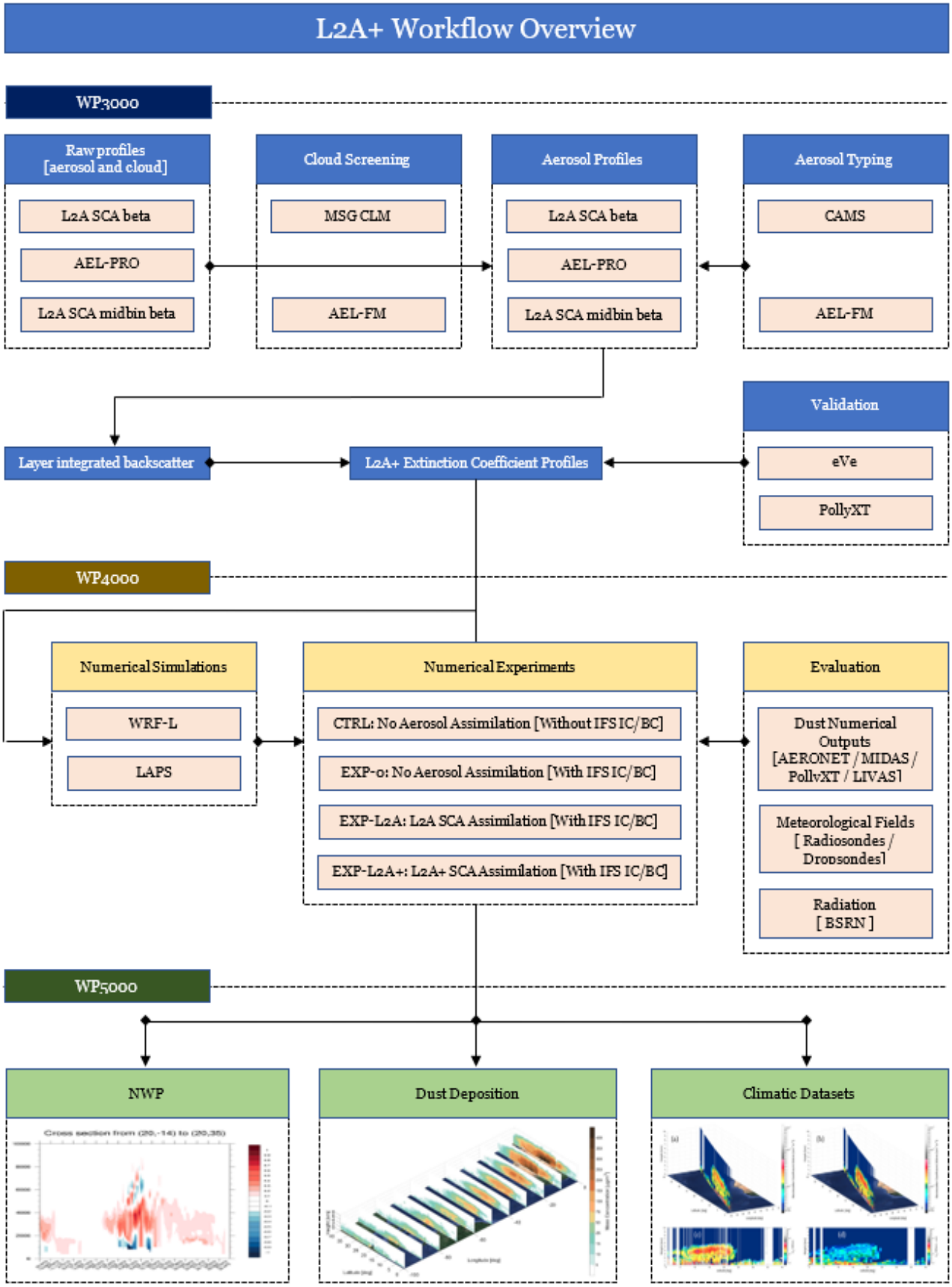

Figure 47: L2A+ Workflow Overview.

As a third step - the "Impact Studies" block – provides information on the three identified studies of (a) to assess the impact of Aeolus on NWP, utilising L2A+ aerosol assimilation in an online coupled regional model driven by Aeolus wind-assimilated meteorological fields, (2) to highlight the benefit of the Aeolus joint aerosol and wind assimilation for simulating dust deposition fields, and compare with CAMS reanalysis to assess the impact of L2A+ for ocean biogeochemistry studies (i.e., ESA-DOMOS study), and to compare the monthly averaged L2A+ product with the CALIPSO L3 product, to assess the climatological value of L2A+ for aerosol database of the ESA-LIVAS long-term climate dataset.

All the data that will be produced will be available through the L2A+ website (DI07) to authorized users upon request. In order to facilitate their exploitation, the data produced in L2A+ will be delivered in netcdf format containing variables (along with their global/local attributes). Depending on their source (i.e., models or observations) they will be available at different spatial and temporal resolutions.

7. L2A+ RoI.

The L2A+ study focuses over the extended tropical domain that includes the Sahara Desert and expands over the Atlantic, from the Cape Verde islands to the Caribbean Sea. The region has been selected for the following reasons:

1) L2A suffers the most for strongly depolarizing targets such as desert dust. The Atlantic is affected from frequent long-range transport of Saharan dust (Saharan Air Layer - SAL), a strongly depolarizing target that highly affects Aeolus retrievals due to the missing cross-channel.
2) The positive Aeolus impact is largest for winds in the Tropics, throughout the troposphere and lower stratosphere (Rennie et al., 2021). Furthermore, the aerosol stratification over the Atlantic is more pronounced than other regions of the world, making it easier to use feature masks from AER-FM/AER-PRO, and combine Aeolus with other sensors and models.
3) The case studies selected for L2A+ are supported by high-quality measurements performed in the framework of the ASKOS/JATAC Tropical campaign in Cape Verde (including CPEX in Puerto Rico).
4) The ESA-DOMOS study on the impact of dust deposition on ocean productivity is implemented in parallel with L2A+ over the same region of interest (the Atlantic).
5) The ESA-NEWTON study on the impact of wind assimilation on desert dust models and the trans-Atlantic dust transport.

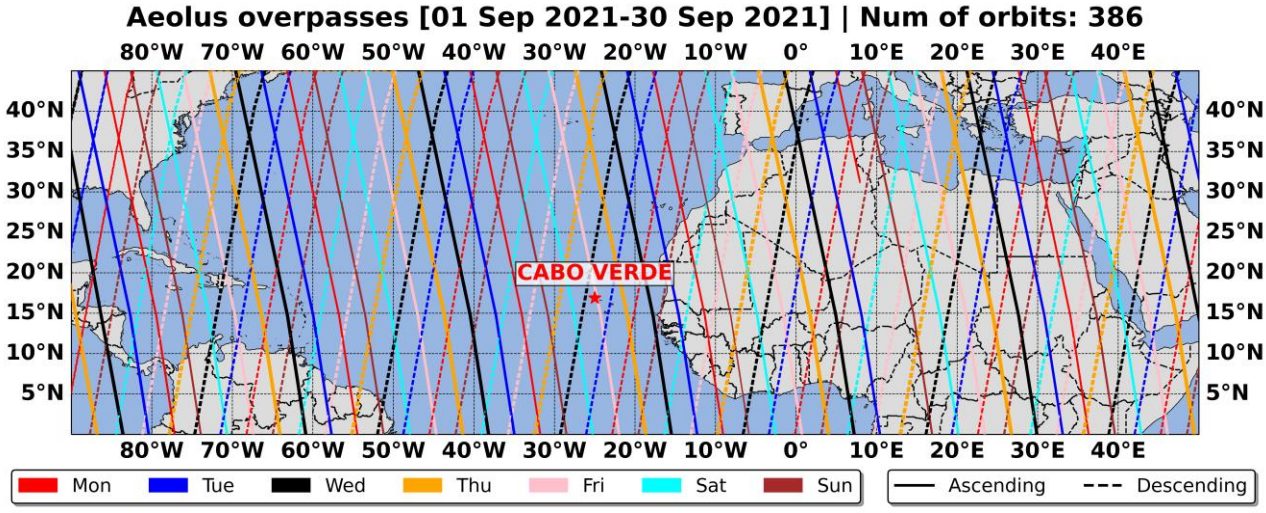

Figure 48: L2A+ Region of Interest (RoI).

8. Risk Analysis.

A consolidated risk analysis plan has been prepared pointing out which risks (technical or scientific constraints) can deviate the timely accomplishment of the project, how these can affect the scheduled activities and which solutions must be adopted in advance. The risk mitigation plan will be monitored throughout the project period by the PI (Dr. Vassilis Amiridis) who will be in continuous contact with the Agency reporting the progress and the modifications of the initial implementation plan that may be needed. In Table 04 are listed a short description of the potential risks, the levels of probability and impact as well as the mitigation approaches.

Table 04: Identified Risks, Probability, Impact and Contingency Plan.

Risk no.	Risk Description	Probability	Impact	Contigency Plan
1.	AEL-FM Cloud Screening failure.	Medium.	Low.	Implementation of MSC CF.
2.	AEL-FM Aerosol Subtype and CAMS failure.	Medium.	Low.	Implementation of CALIPSO climatological aerosol subtype.
3.	L2A+ significant errors.	Low.	Low.	Implementation of CALIPSO-based Aeolus like optical properties.
4.	Inability to access to HPC resources for assimilation experiments.	Low.	High.	Investigate alternative ways to access computational resources (e.g., renting hardware). Use a smaller amount of ensemble members to reduce computational resource needs.

Acronyms and Abbreviations

ACTRIS	Aerosol, Clouds, and Trace Gases Research Infrastructure.
AERONET	AErosol RObotic NETwork.
AOD	Aerosol Optical Dept.
A/C Pro	Aerosol/Cloud Profile.
ATSR	Along Track Scanning Radiometers.
BC	Black Carbon.
CAD Score	Cloud Aerosol Discrimination Score.
CAMS	Copernicus Atmosphere Monitoring Service.
CATS	Cloud-Aerosol Transport System.
CCI	Climate Change Initiative.
CF	cloud fraction.
CALIOP	Cloud-Aerosol Lidar with Orthogonal Polarization.
CALIPSO	Cloud-Aerosol Lidar and Infrared Pathfinder Satellite Observation.
CESSRST	Cooperative Science Center for Earth System Sciences
CLM	Cloud Mask product
CNES	Centre National D'Études Spatiales
DAAD	Distributed Active Archive Center
DART	Data Assimilation Research Testbed.
DOD	Dust Optical Depth.
DOMOS	Dust-Ocean Modelling & Observing Study.
DI	Deliverable Item.
DB	Deep Blue
DT	Dark Target
DWL	Doppler Wind Lidar
EARLINET	European Aerosol Research Lidar Network
ECMWF	European Centre for Medium-Range Weather Forecasts.
EnKF	Ensemble Kalman Filter.
EO	Earth Observation
ESA	European Space Agency
EUMETSAT	European Organisation for the Exploitation of Meteorological Satellites
GALION	GAW Aerosol LIdar Observation Network
GAW-PFR	GAW Precision Filter Radiometer.
GRASP	Generalized Retrieval of Aerosol and Surface Properties.
GOES	Geostationary Operational Environmental Satellite.
HALO	Scanning Doppler wind lidar.
HLOS	Horizontal Line-of-Sight
HPC	High Performance Computing.
HSRL	High Spectral Resolution Lidar
IASI	Infrared Atmospheric Sounding Interferometer
IIR	Imaging Infrared Radiometer.
IMar	Instituto do Mar.
ISS	International Space Station
JATAC	Joint Aeolus Tropical Atlantic Campaign
L1/2/3	Level 1/2/3
L2A+	Enhanced Aeolus L2A for depolarizing targets and impact on aerosol research and NWP.
LAADS	Atmosphere Archive and Distribution System
LALINET	Latin America Lidar Network
LAPS	Local Analysis and Prediction System

LEO	Low Earth Orbiting.
LIVAS	LIdar climatology of Vertical Aerosol Structure for space-based lidar simulation studies
LWP	liquid water path.
LR	Lidar Ratio
LT	Local Time.
LUT	Look-Up-Table
MC	Mass Concentration
MERRA-2	Modern-Era Retrospective analysis for Research and Applications, version 2
MISR	Multi-angle Imaging SpectroRadiometer.
MODIS	MODerate resolution Imaging Spectroradiometer
MPL-Net	Micropulse Lidar Network.
MSG/SEVIRI	Meteosat Second Generation/Spanning Enhanced Visible Infrared Imager.
NASA	National Aeronautics and Space Administration
NDACC	Network for the Detection of Atmospheric Composition Change.
NDVI	normalized difference vegetation index
NOA	National Observatory of Athens
NOAA	National Oceanic and Atmospheric Administration
NWP	Numerical Weather Prediction.
OM	Organic Matter.
OSCM	Ocean Science Centre Mindelo
PBL/MBL	Planetary / Marine Boundary Layer
POLIPHON	POlarization-LIdar PHOtometer Networking
Polly^{XT}	Raman-polarization lidar
QA	Quality-Assurance
RBD	Requirements Baseline Document.
SAL	Saharan Air Layer
SALTRACE	Saharan Aerosol Long-range Transport and Aerosol-Cloud-Interaction Experiment
SAMUM 1/2	SAharan Mineral dUst ExperiMent 1/2
SNR	Signal-to-Noise Ratio
SO2	sulfur dioxide.
SYNergy	OLCI&SLSTR.
TIGR	Thermodynamic Initial Guess Retrieval.
TOA	Top Of Atmosphere.
TROPOS	Leibniz Institute for Tropospheric Research
V##	Version
WFC	wide field-of-view camera
WRF	Weather Research and Forecasting.
WP	Work Package.

List of Figures

List of Tables

References

Ackerman, S. A., 1997: Remote sensing aerosols using satellite infrared observations. J. Geophys. Res., 102, 17069–17079.

Amiridis, V., Wandinger, U., Marinou, E., Giannakaki, E., Tsekeri, A., Basart, S., Kazadzis, S., Gkikas, A., Taylor, M., Baldasano, J., and Ansmann, A.: Optimizing CALIPSO Saharan dust retrievals, Atmos. Chem. Phys., 13, 12089–12106, https://doi.org/10.5194/acp-13-12089-2013, 2013.

Amiridis, V., Marinou, E., Tsekeri, A., Wandinger, U., Schwarz, A., Giannakaki, E., Mamouri, R., Kokkalis, P., Binietoglou, I., Solomos, S., Herekakis, T., Kazadzis, S., Gerasopoulos, E., Proestakis, E., Kottas, M., Balis, D., Papayannis, A., Kontoes, C., Kourtidis, K., Papagiannopoulos, N., Mona, L., Pappalardo, G., Le Rille, O., and Ansmann, A.: LIVAS: a 3-D multi-wavelength aerosol/cloud database based on CALIPSO and EARLINET, Atmos. Chem. Phys., 15, 7127–7153, https://doi.org/10.5194/acp-15-7127-2015, 2015.

Anderson, T. L., Wu, Y., Chu, D. A., Schmid, B., Redemann, J., and Dubovik, O.: Testing the MODIS satellite retrieval of aerosol fine-mode fraction, J. Geophys. Res., 110, D18204, https://doi.org/10.1029/2005JD005978, 2005.

Ansmann, A., Wandinger, U., Le Rille, O., Lajas, D. and Straume, A. G.: Particle backscatter and extinction profiling with the spaceborne high-spectral-resolution Doppler lidar ALADIN: methodology and simulations, Appl. Optics, 46(26), 6606–6622, doi:10.1364/AO.46.006606, 2007.

Ansmann, A., Petzold, A., Kandler, K., Tegen, I., Wendisch, M., Müller, D., Weinzierl, B., Müller, T., and Heintzenberg, J.: Saharan Mineral Dust Experiments SAMUM–1 and SAMUM–2: what have we learned?, 63, 403–429, https://doi.org/10.1111/j.1600-0889.2011.00555.x, 2011.

Ansmann, A., Seifert, P., Tesche, M., and Wandinger, U., 2012: Profiling of fine and coarse particle mass: case studies of Saharan dust and Eyjafjallajökull/Grimsvötn volcanic plumes, Atmos. Chem. Phys., 12, 9399–9415, doi:10.5194/acp-12-9399-2012.

Antuña-Marrero, J.C., and Coauthors, 2017: LALINET: The First Latin American–Born Regional Atmospheric Observational Network. Bull. Amer. Meteor. Soc., 98(6) 1255-1275, https://doi.org/10.1175/BAMS-D-15-00228.1.

Baars, H., Kanitz, T., Engelmann, R., Althausen, D., Heese, B., Komppula, M., Preissler, J., Tesche, M., Ansmann, A., Wandinger, U., Lim, J.-H., Ahn, J. Y., Stachlewska, I. S., Amiridis, V., Marinou, E., Seifert, P., Hofer, J., Skupin, A., Schneider, F., Bohlmann, S., Foth, A., Bley, S., Pfuller, A., Giannakaki, E., Lihavainen, H., Viisanen, Y., Hooda, R. K., Pereira, S. N., Bortoli, D., Wagner, F., Mattis, I., Janicka, L., Markowicz, K. M., Achtert, P., Artaxo, P., Pauliquevis, T., Souza, R. A. F., Sharma, V. P., van Zyl, P. G., Beukes, J. P., Sun, J., Rohwer, E. G., Deng, R., Mamouri, R.-E., and Zamorano, F.: An overview of the first decade of Polly(NET): an emerging network of automated Raman-polarization lidars for continuous aerosol profiling, Atmos. Chem. Phys., 16, 5111–5137, https://doi.org/10.5194/acp-16-5111-2016, 2016.

Baars, H., Radenz, M., Floutsi, A. A., Engelmann, R., Althausen, D., Heese, B., Ansmann, A., Flament, T., Dabas, A., Trapon, D., Reitebuch, O., Bley, S., and Wandinger, U.: Californian Wildfire Smoke Over Europe: A First Example of the Aerosol Observing Capabilities of Aeolus Compared to Ground-Based Lidar, Geophysical Research Letters, 48, e2020GL092194, https://doi.org/10.1029/2020GL092194, 2021.

Barreto, Á., and Coauthors, 2019: Evaluation of night-time aerosols measurements and lunar irradiance models in the frame of the first multi-instrument nocturnal intercomparison campaign. Atmos. Environ., 202, 190-211.

Basart, S., Pérez, C., Cuevas, E., Baldasano, J. M., and Gobbi, G. P., 2009: Aerosol characterization in Northern Africa, Northeastern Atlantic, Mediterranean Basin and Middle East from direct-sun AERONET observations. Atmos. Chem. Phys., 9, 8265-8282, https://doi.org/10.5194/acp-9-8265-2009.

Bohlmann, S., Baars, H., Radenz, M., Engelmann, R. and Macke, A.: Ship-borne aerosol profiling with lidar over the Atlantic Ocean: from pure marine conditions to complex dust-smoke mixtures, Atmos. Chem. Phys., 18(13), 9661–9679, doi:10.5194/acp-18-9661-2018, 2018.

Burton, S. P., Hair, J. W., Kahnert, M., Ferrare, R. A., Hostetler, C. A., Cook, A. L., Harper, D. B., Berkoff, T. A., Seaman, S. T., Collins, J. E., Fenn, M. A. and Rogers, R. R.: Observations of the spectral dependence of linear particle depolarization ratio of aerosols using NASA Langley airborne High Spectral Resolution Lidar, Atmos. Chem. Phys., 15(23), 13453–13473, doi:10.5194/acp-15-13453-2015, 2015.

Campbell, J. R., Tackett, J. L., Reid, J. S., Zhang, J., Curtis, C. A., Hyer, E. J., Sessions, W. R., Westphal, D. L., Prospero, J. M., Welton, E. J., Omar, A. H., Vaughan, M. A., and Winker, D. M.: Evaluating nighttime CALIOP 0.532 μm aerosol optical depth and extinction coefficient retrievals, 5, 2143–2160, https://doi.org/10.5194/amt-5-2143-2012, 2012.

Capelle V., Chédin A., Siméon M., Tsamalis C., Pierangelo C., Pondrom M., Armante R., Crevoisier C., Crépeau L. and Scott. N.A., Evaluation of IASI derived dust aerosols characteristics over the tropical belt. Atmos. Chem. Phys. , 14, 9343-9362 doi:10.5194/acp-14-9343-2014 (2014).

Chédin, A., Scott, N. A., Wahiche, C., a nd Moulinier, P.: The improved initialisation inversion method: A high resolution physical method for temperature retrievals from satellites of the TIROS-N series, J. Clim. Appl. Meteorol., 24, 128–143, 1985.

Chevallier, F., Chéruy, F., Scott, N. A., and Chédin, A.: A neural network approach for a fast and accurate computation of a longwav e radiative budget, J. Appl. Meteorol., 37, 1385–1397, 1998.

Dabas, A.: Observing the atmospheric wind from space, C. R. Geosci., 342(4–5), 370–379, doi:10.1016/j.crte.2009.09.014, 2010.

Dubovik, O., and Coauthors, 2014: GRASP: a versatile algorithm for characterizing the atmosphere, in: SPIE 2014, doi:10.1117/2.1201408.005558.

Ehlers, F., et al.: https://doi.org/10.5194/amt-15-185-2022, 2022.

Antuña-Marrero, J.C., and Coauthors, 2017: LALINET: The First Latin American–Born Regional Atmospheric Observational Network. Bull. Amer. Meteor. Soc., 98(6) 1255-1275, https://doi.org/10.1175/BAMS-D-15-00228.1.

Esselborn, M., Wirth, M., Fix, A., Weinzierl, B., Rasp, K., Tesche, M. and Petzold, A.: Spatial distribution and optical properties of Saharan dust observed by airborne high spectral resolution lidar during SAMUM 2006, Tellus Ser. B-Chem. Phys. Meteorol., 61(1), 131–143, doi:10.1111/j.1600-0889.2008.00394.x, 2009.

Filioglou, M., Giannakaki, E., Backman, J., Kesti, J., Hirsikko, A., Engelmann, R., O'Connor, E., Leskinen, J. T. T., Shang, X., Korhonen, H., Lihavainen, H., Romakkaniemi, S., and Komppula, M.: Optical and geometrical aerosol particle properties over the United Arab Emirates, 1–26, https://doi.org/10.5194/acp-2020-133, 2020.

Flamant, P., Cuesta, J., Denneulin, M.-L., Dabas, A. and Huber, D.: ADM-Aeolus retrieval algorithms for aerosol and cloud products, Tellus Ser. A-Dyn. Meteorol. Oceanol., 60(2), 273–286, doi:10.1111/j.1600-0870.2007.00287.x, 2008.

Flament, T., et al.: https://doi.org/10.5194/amt-14-7851-2021, 2021.

Freudenthaler, V., Esselborn, M., Wiegner, M., Heese, B., Tesche, M., Ansmann, A., Mueller, D., Althausen, D., Wirth, M., Fix, A., Ehret, G., Knippertz, P., Toledano, C., Gasteiger, J., Garhammer, M., and Seefeldner, A.: Depolarization ratio profiling at several wavelengths in pure Saharan dust during SAMUM 2006, Tellus Ser. B-Chem. Phys. Meteorol., 61, 165–179, https://doi.org/10.1111/j.1600-0889.2008.00396.x, 2009.

Garnier, A., Scott, N. A., Pelon, J., Armante, R., Crépeau, L., Six, B., and Pascal, N.: Long-term assessment of the CALIPSO Imaging Infrared Radiometer (IIR) calibration and stability through

simulated and observed comparisons with MODIS/Aqua and SEVIRI/Meteosat, 10, 1403–1424, https://doi.org/10.5194/amt-10-1403-2017, 2017.

Gkikas, A., Proestakis, E., Amiridis, V., Kazadzis, S., Di Tomaso, E., Tsekeri, A., Marinou, E., Hatzianastassiou, N., and Pérez García-Pando, C.: ModIs Dust AeroSol (MIDAS): a global fine-resolution dust optical depth data set, Atmos. Meas. Tech., 14, 309–334, https://doi.org/10.5194/amt-14-309-2021, 2021.

Groß, S., Tesche, M., Freudenthaler, V., Toledano, C., Wiegner, M., Ansmann, A., Althausen, D. and Seefeldner, M.: Characterization of Saharan dust, marine aerosols and mixtures of biomass-burning aerosols and dust by means of multi-wavelength depolarization and Raman lidar measurements during SAMUM 2, Tellus B: Chemical and Physical Meteorology, 63(4), 706–724, doi:10.1111/j.1600-0889.2011.00556.x, 2011a.

Gross, S., Wiegner, M., Freudenthaler, V. and Toledano, C.: Lidar ratio of Saharan dust over Cape Verde Islands: Assessment and error calculation, J. Geophys. Res.-Atmos., 116, D15203, doi:10.1029/2010JD015435, 2011b.

Gross, S., Freudenthaler, V., Wiegner, M., Gasteiger, J., Geiss, A. and Schnell, F.: Dual-wavelength linear depolarization ratio of volcanic aerosols: Lidar measurements of the Eyjafjallajokull plume over Maisach, Germany, Atmos. Environ., 48, 85–96, doi:10.1016/j.atmosenv.2011.06.017, 2012.

Gross, S., Freudenthaler, V., Schepanski, K., Toledano, C., Schaefler, A., Ansmann, A. and Weinzierl, B.: Optical properties of long-range transported Saharan dust over Barbados as measured by dual-wavelength depolarization Raman lidar measurements, Atmos. Chem. Phys., 15(19), 11067–11080, doi:10.5194/acp-15-11067-2015, 2015.

Haarig, M., Ansmann, A., Gasteiger, J., Kandler, K., Althausen, D., Baars, H., Radenz, M., and Farrell, D. A.: Dry versus wet marine particle optical properties: RH dependence of depolarization ratio, backscatter, and extinction from multiwavelength lidar measurements during SALTRACE, Atmos. Chem. Phys., 17, 14199–14217, https://doi.org/10.5194/acp-17-14199-2017, 2017.

Hofer, J., Althausen, D., Abdullaev, S. F., Makhmudov, A. N., Nazarov, B. I., Schettler, G., Engelmann, R., Baars, H., Fomba, K. W., Mueller, K., Heinold, B., Kandler, K., and Ansmann, A.: Long-term profiling of mineral dust and pollution aerosol with multiwavelength polarization Raman lidar at the Central Asian site of Dushanbe, Tajikistan: case studies, Atmos. Chem. Phys., 17, 14559–14577, https://doi.org/10.5194/acp-17-14559-2017, 2017.

Holben, B.N., and Coauthors,1998: AERONET-A federated instrument network and data archive for aerosol characterization. Remote Sens. Environ., 66, 1–16.

Hsu, N. C., Tsay, S. C., King, M. D., and Herman, J. R.: Aerosol Properties Over Bright-Reflecting Source Regions, IEEE T. Geosci. Remote, 42, 557–569, https://doi.org/10.1109/TGRS.2004.824067, 2004.

Hunt, W. H., Winker, D. M., Vaughan, M. A., Powell, K. A., Lucker, P. L., and Weimer, C.: CALIPSO Lidar Description and Performance Assessment, J. Atmos. Oceanic Technol., 26, 1214–1228, https://doi.org/10.1175/2009JTECHA1223.1, 2009.

Hyer, E. J., Reid, J. S., and Zhang, J.: An over-land aerosol optical depth data set for data assimilation by filtering, correction, and aggregation of MODIS Collection 5 optical depth retrievals, Atmos. Meas. Tech., 4, 379–408, https://doi.org/10.5194/amt-4-379-2011, 2011.

Imaki, M., Takegoshi, Y. and Kobayashi, T.: Ultraviolet high-spectral-resolution lidar with Fabry-Perot filter for accurate measurement of extinction and lidar ratio, Jpn. J. Appl. Phys. Part 1 - Regul. Pap. Brief Commun. Rev. Pap., 44(5A), 3063–3067, doi:10.1143/JJAP.44.3063, 2005.

Inness, A., Ades, M., Agustí-Panareda, A., Barré, J., Benedictow, A., Blechschmidt, A.-M., Dominguez, J. J., Engelen, R., Eskes, H., Flemming, J., Huijnen, V., Jones, L., Kipling, Z., Massart, S., Parrington, M., Peuch, V.-H., Razinger, M., Remy, S., Schulz, M., and Suttie, M.: The CAMS reanalysis of atmospheric composition, Atmospheric Chemistry and Physics, 19, 3515–3556, https://doi.org/10.5194/acp-19-3515-2019, 2019.

Kampouri, A., Amiridis, V., Solomos, S., Gialitaki, A., Marinou, E., Spyrou, C., Georgoulias, A. K., Akritidis, D., Papagiannopoulos, N., Mona, L., Scollo, S., Tsichla, M., Tsikoudi, I., Pytharoulis, I., Karacostas, T., and Zanis, P.: Investigation of Volcanic Emissions in the Mediterranean: "The Etna–Antikythera Connection," Atmosphere, 12, 40, https://doi.org/10.3390/atmos12010040, 2021.

Kanitz, T., Ansmann, A., Engelmann, R. and Althausen, D.: North-south cross sections of the vertical aerosol distribution over the Atlantic Ocean from multiwavelength Raman/polarization lidar during Polarstern cruises, Journal of Geophysical Research: Atmospheres, 118(6), 2643–2655, doi:10.1002/jgrd.50273, 2013.

Kanitz, T., Engelmann, R., Heinold, B., Baars, H., Skupin, A. and Ansmann, A.: Tracking the Saharan Air Layer with shipborne lidar across the tropical Atlantic, Geophysical Research Letters, 41(3), 1044–1050, doi:10.1002/2013GL058780, 2014.

Kar, J., Vaughan, M. A., Lee, K.-P., Tackett, J. L., Avery, M. A., Garnier, A., Getzewich, B. J., Hunt, W. H., Josset, D., Liu, Z., Lucker, P. L., Magill, B., Omar, A. H., Pelon, J., Rogers, R. R., Toth, T. D., Trepte, C. R., Vernier, J.-P., Winker, D. M., and Young, S. A.: CALIPSO lidar calibration at 532 nm: version 4 nighttime algorithm, 11, 1459–1479, https://doi.org/10.5194/amt-11-1459-2018, 2018.

Kar, J., Lee, K.-P., Vaughan, M. A., Tackett, J. L., Trepte, C. R., Winker, D. M., Lucker, P. L., and Getzewich, B. J.: CALIPSO level 3 stratospheric aerosol profile product: version 1.00 algorithm description and initial assessment, 12, 6173–6191, https://doi.org/10.5194/amt-12-6173-2019, 2019.

Holben, B.N., and Coauthors,1998: AERONET-A federated instrument network and data archive for aerosol characterization. Remote Sens. Environ., 66, 1–16.

Kim, M.-H., Omar, A. H., Tackett, J. L., Vaughan, M. A., Winker, D. M., Trepte, C. R., Hu, Y., Liu, Z., Poole, L. R., Pitts, M. C., Kar, J. and Magill, B. E.: The CALIPSO version 4 automated aerosol classification and lidar ratio selection algorithm, Atmospheric Measurement Techniques, 11(11), 6107–6135, doi:https://doi.org/10.5194/amt-11-6107-2018, 2018.

Levy, R. C., Remer, L. A., Mattoo, S., Vermote, E. F., and Kaufman, Y. J.: Second-generation operational algorithm: Retrieval of aerosol properties over land from inversion of Moderate Resolution Imaging Spectroradiometer spectral reflectance, J. Geophys. Res.-Atmos., 112, D13211, https://doi.org/10.1029/2006JD007811, 2007b.

Levy, R. C., Leptoukh, G. G., Kahn, R., Zubko, V., Gopalan, A., and Remer, L. A.: A critical look at deriving monthly aerosol optical depth from satellite data, IEEE T. Geosci. Remote, 47, 2942–2956, https://doi.org/10.1109/TGRS.2009.2013842, 2009.

Levy, R. C., Remer, L. A., Kleidman, R. G., Mattoo, S., Ichoku, C., Kahn, R., and Eck, T. F.: Global evaluation of the Collection 5 MODIS dark-target aerosol products over land, Atmos. Chem. Phys., 10, 10399–10420, https://doi.org/10.5194/acp-10-10399-2010, 2010.

Levy, R. C., Mattoo, S., Munchak, L. A., Remer, L. A., Sayer, A. M., Patadia, F., and Hsu, N. C.: The Collection 6 MODIS aerosol products over land and ocean, Atmos. Meas. Tech., 6, 2989–3034, https://doi.org/10.5194/amt-6-2989-2013, 2013.

Liu, Z., Vaughan, M., Winker, D., Kittaka, C., Getzewich, B., Kuehn, R., Omar, A., Powell, K., Trepte, C., and Hostetler, C.: The CALIPSO Lidar Cloud and Aerosol Discrimination: Version 2 Algorithm and Initial Assessment of Performance, J. Atmos. Ocean. Technol., 26, 1198–1213, https://doi.org/10.1175/2009JTECHA1229.1, 2009.

Liu, Z., Kar, J., Zeng, S., Tackett, J., Vaughan, M., Avery, M., Pelon, J., Getzewich, B., Lee, K.-P., Magill, B., Omar, A., Lucker, P., Trepte, C., and Winker, D.: Discriminating between clouds and aerosols in the CALIOP version 4.1 data products, 12, 703–734, https://doi.org/10.5194/amt-12-703-2019, 2019.

Lolli, S., Delaval, A., Loth, C., Garnier, A. and Flamant, P. H.: 0.355-micrometer direct detection wind lidar under testing during a field campaign in consideration of ESA's ADM-Aeolus mission, Atmos. Meas. Tech., 6(12), 3349–3358, doi:10.5194/amt-6-3349-2013, 2013.

Mamouri, R. E., Ansmann, A., Nisantzi, A., Kokkalis, P., Schwarz, A., and Hadjimitsis, D.: Low Arabian dust extinction-to-backscatter ratio, 40, 4762–4766, https://doi.org/10.1002/grl.50898, 2013.

Mamouri, R.-E. and Ansmann, A.: Potential of polarization lidar to provide profiles of CCN- and INP-relevant aerosol parameters, Atmospheric Chemistry and Physics, 16, 5905–5931, https://doi.org/10.5194/acp-16-5905-2016, 2016.

Marinou, E., Amiridis, V., Binietoglou, I., Tsikerdekis, A., Solomos, S., Proestakis, E., Konsta, D., Papagiannopoulos, N., Tsekeri, A., Vlastou, G., Zanis, P., Balis, D., Wandinger, U., and Ansmann,

A.: Three-dimensional evolution of Saharan dust transport towards Europe based on a 9-year EARLINET-optimized CALIPSO dataset, Atmospheric Chemistry and Physics, 17, 5893–5919, https://doi.org/10.5194/acp-17-5893-2017, 2017.

Marinou, E., Tesche, M., Nenes, A., Ansmann, A., Schrod, J., Mamali, D., Tsekeri, A., Pikridas, M., Baars, H., Engelmann, R., Voudouri, K.-A., Solomos, S., Sciare, J., Groß, S., Ewald, F., and Amiridis, V.: Retrieval of ice-nucleating particle concentrations from lidar observations and comparison with UAV in situ measurements, Atmospheric Chemistry and Physics, 19, 11315–11342, https://doi.org/10.5194/acp-19-11315-2019, 2019.

Mona, L., Liu, Z., Müller, D., Omar, A., Papayannis, A., Pappalardo, G., Sugimoto, N., Vaughan, M., 2012: Lidar measurements for desert dust characterization: an Overview. Adv. Meteorol., Article ID 356265, 36 pp, doi:10.1155/2012/356265.

Omar, A. H., Winker, D. M., Vaughan, M. A., Hu, Y., Trepte, C. R., Ferrare, R. A., Lee, K.-P., Hostetler, C. A., Kittaka, C., Rogers, R. R., Kuehn, R. E., and Liu, Z.: The CALIPSO Automated Aerosol Classification and Lidar Ratio Selection Algorithm, J. Atmos. Oceanic Technol., 26, 1994–2014, https://doi.org/10.1175/2009JTECHA1231.1, 2009.

O'Neill, N.T., Eck, T.F., Smirnov, A., Holben, B.N. and Thulasiraman, S., 2003: Spectral discrimination of coarse and fine mode optical depth. J. Geophys. Res., 108, D17, 4559, doi:10.1029/2002JD002975.

Pappalardo, G., Amodeo, A., Apituley, A., Comeron, A., Freudenthaler, V., Linne, H., Ansmann, A., Boesenberg, J., D'Amico, G., Mattis, I., Mona, L., Wandinger, U., Amiridis, V., Alados-Arboledas, L., Nicolae, D., and Wiegner, M.: EARLINET: towards an advanced sustainable European aerosol lidar network, Atmos. Meas. Tech., 7, 2389–2409, https://doi.org/10.5194/amt-7-2389-2014, 2014.

Paschou, P., Siomos, N., Tsekeri, A., Louridas, A., Georgoussis, G., Freudenthaler, V., Binietoglou, I., Tsaknakis, G., Tavernarakis, A., Evangelatos, C., von Bismarck, J., Kanitz, T., Meleti, C., Marinou, E., and Amiridis, V.: The eVe reference polarisation lidar system for Cal/Val of Aeolus L2A product, Atmos. Meas. Tech. Discuss. [preprint], https://doi.org/10.5194/amt-2021-268, in review, 2021.

Paschou, P., Siomos, N., Tsekeri, A., Louridas, A., Georgoussis, G., Freudenthaler, V., Binietoglou, I., Tsaknakis, G., Tavernarakis, A., Evangelatos, C., von Bismarck, J., Kanitz, T., Meleti, C., Marinou, E., and Amiridis, V.: The eVe reference polarisation lidar system for the calibration and validation of the Aeolus L2A product, Atmospheric Measurement Techniques, 15, 2299–2323, https://doi.org/10.5194/amt-15-2299-2022, 2022.

Peyridieu, S., Chédin, A., Tanré, D., Capelle, V., Pierangelo, C., Lamquin, N., and Armante, R.: Saharan dust infrared optical depth and altitude retrieved from AIRS: a focus over North Atlantic – comparison to MODIS and CALIPSO, Atmos. Chem. Phys., 10, 1953-1967, doi:10.5194/acp-10-1953-2010, 2010.

Peyridieu S., Chédin A., Capelle V., Tsamalis C., Pierangelo C., Armante R., Crevoisier C., Crépeau L., Siméon M., Ducos F., Scott N.A. : Characterization of dust aerosols in the infrared from IASI and comparison with PARASOL, MODIS, MISR, CALIOP, and AERONET observations., Atmos. Chem. Phys., 13, 6065-6082 doi:10.5194/acp-13-6065-2013, 2013.

Pierangelo, C., Chédin, A., Heilliette, S., Jac quinet-Husson, N., and Armante, R.: Dust altitude and infrared optical depth from AIRS, Atmos. Chem. Phys., 4, 1813-1822, doi:10.5194/acp-4-1813-2004, 2004.

Pierangelo, C., Mishchenko, M.,Balkanski, Y. and Chédin, A.: Retrieving the effective radius of Saharan dust coarse mode from AIRS, Geophys. Res. Lett., 32, L20813, doi:10.1029/2005GL023425, 2005.

Powell, K. A., Hostetler, C. A., Vaughan, M. A., Lee, K.-P., Trepte, C. R., Rogers, R. R., Winker, D. M., Liu, Z., Kuehn, R. E., Hunt, W. H., and Young, S. A.: CALIPSO Lidar Calibration Algorithms. Part I: Nighttime 532-nm Parallel Channel and 532-nm Perpendicular Channel, J. Atmos. Oceanic Technol., 26, 2015–2033, https://doi.org/10.1175/2009JTECHA1242.1, 2009.

Proestakis, E., Amiridis, V., Marinou, E., Georgoulias, A. K., Solomos, S., Kazadzis, S., Chimot, J., Che, H., Alexandri, G., Binietoglou, I., Daskalopoulou, V., Kourtidis, K. A., de Leeuw, G., and van der A, R. J.: Nine-year spatial and temporal evolution of desert dust aerosols over South and East

Asia as revealed by CALIOP, Atmospheric Chemistry and Physics, 18, 1337–1362, https://doi.org/10.5194/acp-18-1337-2018, 2018.

Reitebuch, O., Lemmerz, C., Lux, O., Marksteiner, U., Rahm, S., Weiler, F., Witschas, B., Meringer, M., Schmidt, K., Huber, D., Nikolaus, I., Geiss, A., Vaughan, M., Dabas, A., Flament, T., Stieglitz, H., Isaksen, L., Rennie, M., Kloe, J. de, Marseille, G.-J., Stoffelen, A., Wernham, D., Kanitz, T., Straume, A.-G., Fehr, T., Bismarck, J. von, Floberghagen, R., and Parrinello, T.: Initial Assessment of the Performance of the First Wind Lidar in Space on Aeolus, EPJ Web Conf., 237, 01010, https://doi.org/10.1051/epjconf/202023701010, 2020.

Remer, L. A., Tanre, D., Kaufman, Y. J., Ichoku, C., Mattoo, S., Levy, R., Chu, D. A., Holben, B., Dubovik, O., Smirnov, A., Martins, J. V., Li, R. R., and Ahmad, Z.: Validation of MODIS aerosol retrieval over ocean, Geophys. Res. Lett., 29, MOD3.1–MOD3.4, https://doi.org/10.1029/2001GL013204, 2002.

Remer, L. A., Kaufman, Y. J., Tanre, D., Mattoo, S., Chu, D. A., Martins, J. V., Li, R. R., Ichoku, C., Levy, R. C., Kleidman, R. G., Eck, T. F., Vermote, E., and Holben, B. N.: The MODIS aerosol algorithm, products, and validation, J. Atmos. Sci., 62, 947–973, https://doi.org/10.1175/JAS3385.1, 2005.

Remer, L. A., Kleidman, R. G., Levy, R. C., Kaufman, Y. J., Tanré, D., Mattoo, S., Martins, J. V., Ichoku, C., Koren, I., Yu, H. and Holben, B. N.: Global aerosol climatology from the MODIS satellite sensors, J. Geophys. Res.-Atmos., 113, D14S07, https://doi.org/10.1029/2007JD009661, 2008.

Rennie, M. P., Isaksen, L., Weiler, F., de Kloe, J., Kanitz, T., and Reitebuch, O.: The impact of Aeolus wind retrievals on ECMWF global weather forecasts, Quarterly Journal of the Royal Meteorological Society, 147, 3555–3586, https://doi.org/10.1002/qj.4142, 2021.

Sakai, T., Nagai, T., Nakazato, M., Mano, Y., and Matsumura, T.: Ice clouds and Asian dust studied with lidar measurements of particle extinction-to-backscatter ratio, particle depolarization, and water-vapor mixing ratio over Tsukuba, Appl. Opt., AO, 42, 7103–7116, https://doi.org/10.1364/AO.42.007103, 2003.

Shipley, S., Tracy, D., Eloranta, E., Trauger, J., Sroga, J., Roesler, F. and Weinman, J.: High Spectral Resolution Lidar to Measure Optical-Scattering Properties, Appl. Optics, 22(23), 3716–3724, doi:10.1364/AO.22.003716, 1983.

Shimizu, A., Nishizawa, T., Jin, J., Kim S.-W. Wang, Z., Batdorj, D., and Sugimoto, N., 2017: Evolution of a lidar network for tropospheric aerosol detection in East Asia. Opt. Eng., 56(3), 031219, doi: 10.1117/1.OE.56.3.031219.

Smirnov, A., Holben, B., Slutsker, I., Giles, D., McClain, C., Eck, T., Sakerin, S., Macke, A., Croot, P., Zibordi, G., Quinn, P., Sciare, J., Kinne, S., Harvey, M., Smyth, T., Piketh, S., Zielinski, T., Proshutinsky, A., Goes, J., Nelson, N., Larouche, P., Radionov, V., Goloub, P., Moorthy, K., Matarrese, R., Robertson, E., and Jourdin, F.: Maritime Aerosol Network as a component of Aerosol Robotic Network, J. Geophys. Res.-Atmos., 114, D06204, https://doi.org/10.1029/2008JD011257, 2009.

Stephens, G., Winker, D., Pelon, J., Trepte, C., Vane, D., Yuhas, C., L'Ecuyer, T., and Lebsock, M.: CloudSat and CALIPSO within the A-Train: Ten Years of Actively Observing the Earth System, Bull. Amer. Meteor. Soc., 99, 569–581, https://doi.org/10.1175/BAMS-D-16-0324.1, 2018.

Straume-Lindner, A. G., Parrinello, T., Von Bismarck, J., Bley, S., Wernham, D., Kanitz, T., Alvarez, E., Fischey, P., De Laurentis, M., Fehr, T., Ehlers, F., Duc Tran, V., Krisch, I., Reitebuch, O., and Renni, M.: ESA'S Wind Mission Aeolus - Overview, Status and Outlook, in: 2021 IEEE International Geoscience and Remote Sensing Symposium IGARSS, 2021 IEEE International Geoscience and Remote Sensing Symposium IGARSS, 755–758, https://doi.org/10.1109/IGARSS47720.2021.9554007, 2021.

Tackett, J. L., Winker, D. M., Getzewich, B. J., Vaughan, M. A., Young, S. A., and Kar, J.: CALIPSO lidar level 3 aerosol profile product: version 3 algorithm design, Atmos. Meas. Tech., 11, 4129–4152, https://doi.org/10.5194/amt-11-4129-2018, 2018.

Tan, D. G. H., Anderson, E., De Kloe, J., Marseille, G.-J., Stoffelen, A., Poli, P., Denneulin, M.-L., Dabas, A., Huber, D., Reitebuch, O., Flamant, P., Le Rille, O. and Nett, H.: The ADM-Aeolus wind

retrieval algorithms, Tellus Ser. A-Dyn. Meteorol. Oceanol., 60(2), 191–205, doi:10.1111/j.1600-0870.2007.00285.x, 2008.

Tesche, M., Ansmann, A., Müller, D., Althausen, D., Engelmann, R., Freudenthaler, V., and Groß, S.: Vertically resolved separation of dust and smoke over Cape Verde using multiwavelength Raman and polarization lidars during Saharan Mineral Dust Experiment 2008, 114, https://doi.org/10.1029/2009JD011862, 2009.

Tesche, M., Gross, S., Ansmann, A., Müller, D., Althausen, D., Freudenthaler, V., and Esselborn, M.: Profiling of Saharan dust and biomass-burning smoke with multiwavelength polarization Raman lidar at Cape Verde, 63, 649–676, https://doi.org/10.1111/j.1600-0889.2011.00548.x, 2011.

Toth, T. D., Campbell, J. R., Reid, J. S., Tackett, J. L., Vaughan, M. A., Zhang, J., and Marquis, J. W.: Minimum aerosol layer detection sensitivities and their subsequent impacts on aerosol optical thickness retrievals in CALIPSO level 2 data products, 11, 499–514, https://doi.org/10.5194/amt-11-499-2018, 2018.

Vaughan, M. A., Powell, K. A., Winker, D. M., Hostetler, C. A., Kuehn, R. E., Hunt, W. H., Getzewich, B. J., Young, S. A., Liu, Z., and McGill, M. J.: Fully Automated Detection of Cloud and Aerosol Layers in the CALIPSO Lidar Measurements, J. Atmos. Oceanic Technol., 26, 2034–2050, https://doi.org/10.1175/2009JTECHA1228.1, 2009.

Vaughan, M., Garnier, A., Josset, D., Avery, M., Lee, K.-P., Liu, Z., Hunt, W., Pelon, J., Hu, Y., Burton, S., Hair, J., Tackett, J. L., Getzewich, B., Kar, J., and Rodier, S.: CALIPSO lidar calibration at 1064 nm: version 4 algorithm, 12, 51–82, https://doi.org/10.5194/amt-12-51-2019, 2019.

Weinzierl, B., Sauer, D., Esselborn, M., Petzold, A., Veira, A., Rose, M., Mund, S., Wirth, M., Ansmann, A., Tesche, M., Gross, S., and Freudenthaler, V.: Microphysical and optical properties of dust and tropical biomass burning aerosol layers in the Cape Verde region—an overview of the airborne in situ and lidar measurements during SAMUM-2, Tellus B: Chemical and Physical Meteorology, 63, 589–618, https://doi.org/10.1111/j.1600-0889.2011.00566.x, 2011.

Welton, E. J., Campbell, J. R., Spinhirne, J. D., and Scott, V. S., 2001: Global monitoring of clouds and aerosols using a network of micro-pulse lidar systems. In Lidar Remote Sensing for Industry and Environmental Monitoring, U. N. Singh, T. Itabe, N. Sugimoto, (eds.), Proc. SPIE, vol. 4153, 151-158.

Wiegner, M., Groß, S., Freudenthaler, V., Schnell, F., and Gasteiger, J.: The May/June 2008 Saharan dust event over Munich: Intensive aerosol parameters from lidar measurements, 116, https://doi.org/10.1029/2011JD016619, 2011.

Winker, D. M., Vaughan, M. A., Omar, A., Hu, Y., Powell, K. A., Liu, Z., Hunt, W. H., and Young, S. A.: Overview of the CALIPSO Mission and CALIOP Data Processing Algorithms, J. Atmos. Ocean. Technol., 26, 2310–2323, https://doi.org/10.1175/2009JTECHA1281.1, 2009.

Winker, D. M., Pelon, J., Coakley, J. A., Ackerman, S. A., Charlson, R. J., Colarco, P. R., Flamant, P., Fu, Q., Hoff, R. M., Kittaka, C., Kubar, T. L., Le Treut, H., Mccormick, M. P., Mégie, G., Poole, L., Powell, K., Trepte, C., Vaughan, M. A., and Wielicki, B. A.: The CALIPSO MissionA Global 3D View of Aerosols and Clouds, Bull. Amer. Meteor. Soc., 91, 1211–1230, https://doi.org/10.1175/2010BAMS3009.1, 2010.

Yorks, J. E., McGill, M. J., Scott, V. S., Wake, S. W., Kupchock, A., Hlavka, D. L., Hart, W. D., and Selmer, P. A.: The Airborne Cloud-Aerosol Transport System: Overview and Description of the Instrument and Retrieval Algorithms, J. Atmos. Ocean. Tech., 31, 2482–2497, https://doi.org/10.1175/JTECH-D-14-00044.1, 2014.

Zeng, S., Vaughan, M., Liu, Z., Trepte, C., Kar, J., Omar, A., Winker, D., Lucker, P., Hu, Y., Getzewich, B., and Avery, M.: Application of high-dimensional fuzzy k-means cluster analysis to CALIOP/CALIPSO version 4.1 cloud–aerosol discrimination, 12, 2261–2285, https://doi.org/10.5194/amt-12-2261-2019, 2019.

[End of ESA-L2A+ DI01 - RBD.]